THE ASTROPHYSICAL JOURNAL SUPPLEMENT SERIES, 114:1–36, 1998 January


# *COBE*-DMR–NORMALIZED OPEN COLD DARK MATTER COSMOGONIES

KRZYSZTOF M. GÓRSKI,[1,2,3] BHARAT RATRA,[4,5] RADOSŁAW STOMPOR,[6,7] NAOSHI SUGIYAMA,[8] AND A. J. BANDAY[9]

*Received 1996 August 6; accepted 1997 July 18*

## ABSTRACT

Cut-sky orthogonal mode analyses of the *COBE*-DMR 53 and 90 GHz sky maps are used to determine the normalization of a variety of open cosmogonical models based on the cold dark matter scenario. To constrain the allowed cosmological parameter range for these open cosmogonies, the predictions of the DMR-normalized models are compared to various observational measures of cosmography and large-scale structure, viz., the age of the universe; small-scale dynamical estimates of the clustered-mass density parameter $\Omega_0$; constraints on the Hubble parameter $h$, the X-ray cluster baryonic-mass fraction $\Omega_B/\Omega_0$, and the matter power spectrum shape parameter; estimates of the mass perturbation amplitude; and constraints on the large-scale peculiar velocity field.

The open-bubble inflation model (Ratra & Peebles; Bucher, Goldhaber, & Turok; Yamamoto, Sasaki, & Tanaka) is consistent with current determinations of the 95% confidence level (c.l.) range of these observational constraints, provided $0.3 < \Omega_0 \lesssim 0.6$ ($\sim$95% c.l.). More specifically, for a range of $h$, the model is reasonably consistent with recent high-redshift estimates of the deuterium abundance that suggest $\Omega_B h^2 \sim 0.007$, provided $\Omega_0 \sim 0.35$; recent high-redshift estimates of the deuterium abundance that suggest $\Omega_B h^2 \sim 0.02$ favor $\Omega_0 \sim 0.5$, while the old nucleosynthesis value $\Omega_B h^2 = 0.0125$ requires $\Omega_0 \sim 0.4$.

Small shifts in the inferred *COBE*-DMR normalization amplitudes due to (1) the small differences between the galactic- and ecliptic-coordinate sky maps, (2) the inclusion or exclusion of the quadrupole moment in the analysis, (3) the faint high-latitude Galactic emission treatment, and (4) the dependence of the theoretical cosmic microwave background anisotropy angular spectral shape on the value of $h$ and $\Omega_B$ are explicitly quantified. Corresponding variations in the likelihood fits of models to the DMR data then imply that the DMR data alone do not possess sufficient discriminative power to prefer any values for $\Omega_0$, $h$, or $\Omega_B$ at the 95% c.l. for the models considered. At a lower c.l., and when the quadrupole moment is included in the analysis, the DMR data are most consistent with either $\Omega_0 \lesssim 0.1$ or $\Omega_0 \sim 0.7$ (depending on the model considered). However, when the quadrupole moment is excluded from the analysis, the DMR data are most consistent with $\Omega_0 \sim 0.35$–$0.5$ in all open models considered (with $0.1 \leq \Omega_0 \leq 1$), including the open-bubble inflation model. Earlier claims (Yamamoto & Bunn; Bunn & White) that the DMR data require a 95% c.l. lower bound on $\Omega_0$ ($\sim$0.3) are not supported by our (complete) analysis of the 4 year data: the DMR data alone cannot be used to constrain $\Omega_0$ meaningfully.

*Subject headings:* cosmic microwave background — cosmology: observations — galaxies: formation — large-scale structure of universe

## 1. INTRODUCTION

Quantum mechanical fluctuations during an early epoch of inflation provide a plausible mechanism to generate the energy-density perturbations responsible for observed cosmological structure. While it has been known for quite some time that inflation is consistent with open spatial hypersurfaces (Gott 1982; Guth & Weinberg 1983), attention was initially focused on models in which there are a very large number of $e$-foldings during inflation, resulting in almost exactly flat spatial hypersurfaces for the observable part of the present universe (Guth 1981; also see Kazanas 1980; Sato 1981a, 1981b). This was, perhaps, inevitable because of strong theoretical prejudice toward flat spatial hypersurfaces and their resulting simplicity. However, to get a very large number of $e$-foldings during inflation, it seems necessary that the inflation model have a small dimensionless parameter (J. R. Gott 1994, private communication; Banks et al. 1995), which would require an explanation.

Attempts to reconcile these "favored" flat spatial hypersurfaces with observational measures of a low value for the clustered-mass density parameter $\Omega_0$ have concentrated on models in which one postulates the presence of a cosmological constant $\Lambda$ (Peebles 1984). In the simplest flat-$\Lambda$ model, one assumes a scale-invariant (Harrison 1970; Peebles & Yu 1970; Zeldovich 1972) primordial power spectrum for Gaussian adiabatic energy-density pertur-

[1] Hughes STX Corporation, Code 685, LASP, NASA/GSFC, Greenbelt, MD 20771.
[2] Theoretical Astrophysics Center, Juliane Maries Vej 30, 2100 Copenhagen Ø, Denmark.
[3] Warsaw University Observatory, Aleje Ujazdowskie 4, 00-478 Warszawa, Poland.
[4] Center for Theoretical Physics, Massachusetts Institute of Technology, Cambridge, MA 02139.
[5] Department of Physics, Kansas State University, Manhattan, KS 66506.
[6] Department of Physics, University of Oxford, Keble Road, Oxford, OX1 3RH, UK.
[7] Copernicus Astronomical Center, Bartycka 18, 00-716 Warszawa, Poland.
[8] Department of Physics, Kyoto University, Kitashirakawa-Oiwakecho, Sakyo-ku, Kyoto 606, Japan.
[9] Max-Planck-Institut für Astrophysik, Karl-Schwarzschild-Strasse 1, 85740 Garching, Germany.

bations. Such a spectrum is generated by quantum mechanical fluctuations during an early epoch of inflation in a spatially flat model, provided that the inflaton potential is reasonably flat (Fischler, Ratra, & Susskind 1985, and references therein).[10] It has been demonstrated that these models are indeed consistent with current observational constraints (see, e.g., Stompor, Górski, & Banday 1995; Ostriker & Steinhardt 1995; Ratra et al. 1997; Liddle et al. 1996b; Ganga, Ratra, & Sugiyama 1996, hereafter GRS).

An alternative, more popular of late, is to accept that the spatial hypersurfaces are not flat. In this case, the radius of curvature for the open spatial sections introduces a new length scale (in addition to the Hubble length), which requires a generalization of the usual flat-space scale-invariant spectrum (Ratra & Peebles 1994, hereafter RP94). Such a spectrum is generated by quantum mechanical fluctuations during an epoch of inflation in an open-bubble model (RP94; Ratra & Peebles 1995, hereafter RP95; Bucher, Goldhaber, & Turok 1995, hereafter BGT; Lyth & Woszczyna 1995; Yamamoto, Sasaki, & Tanaka 1995, hereafter YST), provided that the inflaton potential inside the bubble is reasonably flat. Such Gaussian adiabatic open-bubble inflation models have also been shown to be consistent with current observational constraints (RP94; Kamionkowski et al. 1994; Górski et al. 1995, hereafter GRSB; Liddle et al. 1996a, hereafter LLRV; Ratra et al. 1997; GRS).

Inflation theory by itself is unable to predict the normalization amplitude for the energy-density perturbations. Currently, the least controversial and most robust method for the normalization of a cosmological model is to fix the amplitude of the model-predicted large-scale CMB spatial anisotropy by comparing it to the observed CMB anisotropy discovered by the *COBE*-DMR experiment (Smoot et al. 1992).

Previously, specific open cold dark matter (CDM) models have been examined in light of the *COBE*-DMR 2 year results (Bennett et al. 1994). GRSB investigated the CMB anisotropy angular spectra predicted by the open-bubble inflation model (RP94) and compared large-scale structure predictions of this DMR-normalized model to observational data.[11] Cayón et al. (1996) performed a related analysis for the open model with a flat-space scale-invariant spectrum (Wilson 1983; hereafter W83), and Yamamoto & Bunn (1996; hereafter YB) examined the effect of additional sources of quantum fluctuations (BGT; YST) in the open-bubble inflation model.

In this paper, we study the observational predictions for a number of open CDM models. In particular, we employ the power spectrum estimation technique devised by Górski (1994) for incomplete sky coverage to normalize the open models using the *COBE*-DMR 4 year data (Bennett et al. 1996). In § 2, we provide an overview of open-bubble inflation cosmogonies. In § 3, we discuss the various open models we consider, detail the various DMR data sets used in the analyses here, and present the DMR estimate of the CMB rms quadrupole anisotropy amplitude $Q_{\rm rms\text{-}PS}$ as a function of $\Omega_0$ for these open models. In § 4, we detail the computation of several cosmographic and large-scale structure statistics for the DMR-normalized open models. These statistics are confronted by various current observational constraints in § 5. Our results are summarized in § 6.

## 2. OPEN-BUBBLE INFLATION MODELS

The simplest open inflation model is that in which a single open-inflation bubble nucleates in a (possibly) spatially flat, inflating spacetime (Gott 1982; Guth & Weinberg 1983). In this model, the first epoch of inflation smooths away any pre-existing spatial inhomogeneities while simultaneously generating quantum mechanical zero-point fluctuations. Then, in a tunnelling event, an open-inflation bubble nucleates, and for a small enough nucleation probability the observable universe lies inside a single open-inflation bubble. Fluctuations of relevance to the late-time universe can be generated via three different quantum mechanical mechanisms: (1) they can be generated in the first epoch of inflation; (2) they can be generated during the tunnelling event (thus resulting in a slightly inhomogeneous initial hypersurface inside the bubble, or a slightly nonspherical bubble); and (3) they can be generated inside the bubble. The tunneling amplitude is largest for the most symmetrical solution (and deviations from symmetry lead to an exponential suppression), so it has usually been assumed that the nucleation process (mechanism [2]) does not lead to the generation of significant inhomogeneities. Quantum mechanical fluctuations generated during evolution inside the bubble (RP95) are significant. Assuming that the energy-density difference between the two epochs of inflation is negligible (and so the bubble wall is not significant), one may estimate the contribution to the perturbation spectrum after bubble nucleation from quantum mechanical fluctuations during the first epoch of inflation (BGT; YST). As discussed by Bucher & Turok (1995; hereafter BT) (also see YST; YB), the observable predictions of these simple open-bubble inflation models are almost completely insensitive to the details of the first epoch of inflation for the observationally viable range of $\Omega_0$. This is because the fluctuations generated during this epoch affect only the smallest wavenumber part of the energy-density perturbation power spectrum, which cannot contribute significantly to observable quantities because of the spatial curvature length "cutoff" in an open universe (see, e.g., W83; Kamionkowski & Spergel 1994; RP95). Inclusion of such fluctuations in the calculations alters the predictions for the present value of the rms linear mass fluctuations averaged over an $8\ h^{-1}$ Mpc sphere, $(\delta M/M)[8\ h^{-1}\ \mathrm{Mpc}]$, by $\sim 0.1\%$–$0.2\%$ (which is comparable to our computational accuracy).

Besides the open-bubble inflation model spectra, a variety of alternatives have also been considered. Predictions for the usual flat-space scale-invariant spectrum in an open model have been examined (W83; Abbott & Schaefer 1986; Gouda, Sugiyama, & Sasaki 1991; Sugiyama & Gouda 1992; Kamionkowski & Spergel 1994; Sugiyama & Silk 1994; Cayón et al. 1996). The possibility that the standard formulation of quantum mechanics is incorrect in an open universe and that allowance must be made for non–square-integrable basis functions has been investigated (Lyth & Woszczyna 1995), and other spectra have also been considered (see, e.g., W83; Abbott & Schaefer 1986;

[10] In inflation models, the small observed cosmic microwave background (CMB) anisotropy could be the consequence of the small ratio of the inflation epoch mass scale to the Planck mass (Ratra 1991, and references therein; also see Banks et al. 1995).

[11] Ratra et al. (1997) and GRS subsequently extended the analysis to smaller scales, comparing detailed CMB anisotropy predictions to observational data.

Kamionkowski & Spergel 1994). These spectra, being inconsistent with either standard quantum mechanics or the length scale set by spatial curvature, are of historical interest.

More recently, the open-bubble inflation scenario has been further elaborated on. YST have considered a very specific model for the nucleation of the open bubble in a spatially flat de Sitter spacetime and have demonstrated a possible additional contribution from a non–square-integrable basis function that depends on the form of the potential and on the assumed form of the quantum state prior to bubble nucleation.[12] However, since the non–square-integrable basis function contributes only on the very largest scales, the spatial curvature "cutoff" in an open universe makes almost all of the model predictions insensitive to this basis function, for the observationally viable range of $\Omega_0$ (YST; YB). For example, at $\Omega_0 \sim 0.4$–$0.5$ its effect is to change $(\delta M/M)[8\,h^{-1}\ \mathrm{Mpc}]$ by $\sim 0.8\%$–$1\%$.[13]

An additional possible effect determined for the specific model of an open-inflation bubble nucleating in a spatially flat de Sitter spacetime is that fluctuations of the bubble wall behave like a non–square-integrable basis function (Hamazaki et al. 1996; Garriga 1996; García-Bellido 1996; Yamamoto, Sasaki, & Tanaka 1996). While there are models in which these bubble-wall fluctuations are completely insignificant (Garriga 1996; Yamamoto et al. 1996), there is as yet no computation that accounts for both the bubble-wall fluctuations as well as those generated during the evolution inside the bubble (which are always present), so it is not yet known if bubble-wall fluctuations can give rise to an observationally significant effect. Also, again in this very specific model, the effects of a finite bubble size at nucleation seem to alter the zero bubble size predictions only by a very small amount (Yamamoto et al. 1996; Cohn 1996). Finally, we note that two-field open-bubble inflation models have also been considered (Linde 1995; Linde & Mezhlumian 1995; Yamamoto et al. 1996).

While there is no guarantee that there is a spatially flat de Sitter spacetime prior to bubble nucleation, these computations do illustrate the important point that the spatial curvature length "cutoff" in an open universe (see, e.g., RP95) does seem to ensure that what happens prior to bubble nucleation does not significantly affect the observable predictions for observationally viable single-field open-bubble inflation models. It is indeed reassuring that accounting only for the quantum mechanical fluctuations generated during the evolution inside the bubble (RP94) seems to be essentially all that is required to make observational predictions for the single-field open-bubble inflation models. That is, the observational predictions of the open-bubble inflation scenario seem to be as robust as those for the spatially flat inflation scenario.

[12] If the length scale set by the mass determined by the curvature of the inflaton potential in the first epoch of inflation is significantly smaller than the Hubble length, as is expected in reasonable particle physics models, there is no non–square-integrable basis function in the second epoch of inflation (YST).

[13] Hence, it seems that there is as yet no need to speculate about the quantum state prior to bubble nucleation. However, more recently it has been suggested that in certain two-field models (Linde & Mezhlumian 1995) the contribution of this non–square-integrable basis function might be enhanced by the ratio of the energy densities before and after bubble nucleation, and it has been suggested that if this ratio is large, it would be a problem for these two-field models (Sasaki & Tanaka 1996). However, this depends sensitively on the speculative properties of the prenucleation model and vacuum state.

## 3. CMB ANISOTROPY NORMALIZATION PROCEDURE

### 3.1. *Theoretical Spectra of Anisotropy*

We consider four open model energy-density perturbation power spectra: (1) the open-bubble inflation model spectrum, accounting only for fluctuations that are generated during the evolution inside the bubble (RP94); (2) the open-bubble inflation model spectrum, now also accounting for the fluctuations generated in the first epoch of inflation (BGT; YST); (3) the open-bubble inflation model spectrum, now also accounting for both the usual fluctuations generated in the first epoch of inflation and a contribution from a non–square-integrable basis function (YST); and (4) an open model with a flat-space scale-invariant spectrum (W83). In all cases we have ignored the possibility of tilt or primordial gravity waves, since it is unlikely that they can have a significant effect in viable open models.

With the eigenvalue of the spatial scalar Laplacian being $-(k^2+1)$, where $k$ $(0 < k < \infty)$ is the radial coordinate spatial wavenumber, the gauge-invariant fractional energy-density perturbation power spectrum of type (1) above is

$$P(k) = A\,\frac{(4+k^2)^2}{k(1+k^2)}\,T^2(k)\,, \tag{1}$$

where $T(k)$ is the transfer function and $A$ is the normalization amplitude.[14] In the simplest example, perturbations generated in the first epoch of inflation introduce an additional multiplicative factor, $\coth(\pi k)$, on the right-hand side of equation (1). For a discussion of the effects of the non–square-integrable basis function, see YST and YB. The energy-density power spectrum of type (4) above is

$$P(k) = AkT^2(k)\,, \tag{2}$$

and in this case one can also consider, e.g., $P(k) \propto (1+k^2)^{1/2}$ (W83), but because of the spatial curvature "cutoff" in an open model, the predictions are essentially indistinguishable.[15] At small $k$, the asymptotic expressions are $P(k) \propto k^{-1}$ (type 1), $P(k) \propto k^{-2}$ (type 2), and $P(k) \propto k$ (type 4).

Conventionally, the CMB fractional temperature perturbation, $\delta T/T$, is expressed as a function of angular position,

[14] In the literature, the primordial part of this open-bubble inflation model spectrum is occasionally called the "conformal" spectrum or the "scale-invariant" spectrum. These names are misleading: the open de Sitter spacetime inside the bubble is not conformal to spatially flat Minkowski spacetime (more precisely, it is conformal to the upper "Milne wedge" of Minkowski spacetime), which is why the primordial part of the spectrum of eq. (1) is manifestly non–scale-invariant. This spectrum is, however, the "natural" generalization of the flat-space scale-invariant spectrum to the open model, and it is the open-bubble inflation model spectrum accounting only for those fluctuations generated during the evolution inside the bubble. Note that Bunn & White (1997, hereafter BW, eq. [30]) generalize the primordial part of the spectrum of eq. (1) by multiplying it with $(k^2+1)^{(n-1)/2}$. As yet, only the specific $n = 1$ generalized spectrum (i.e., eq. [1]) is known to be a prediction of an open-bubble inflation model and therefore consistent with the presence of spatial curvature. It is premature to draw conclusions about open cosmogony on the basis of the $n \neq 1$ version of the spectrum considered by BW.

[15] It should be noted that such open model spectra are "unnatural"—they do not account properly for the additional length scale set by the radius of space curvature in an open universe. We include the case of eq. (2) here both for historical reasons and to provide a "straw man" to compare to the open-bubble inflation model.

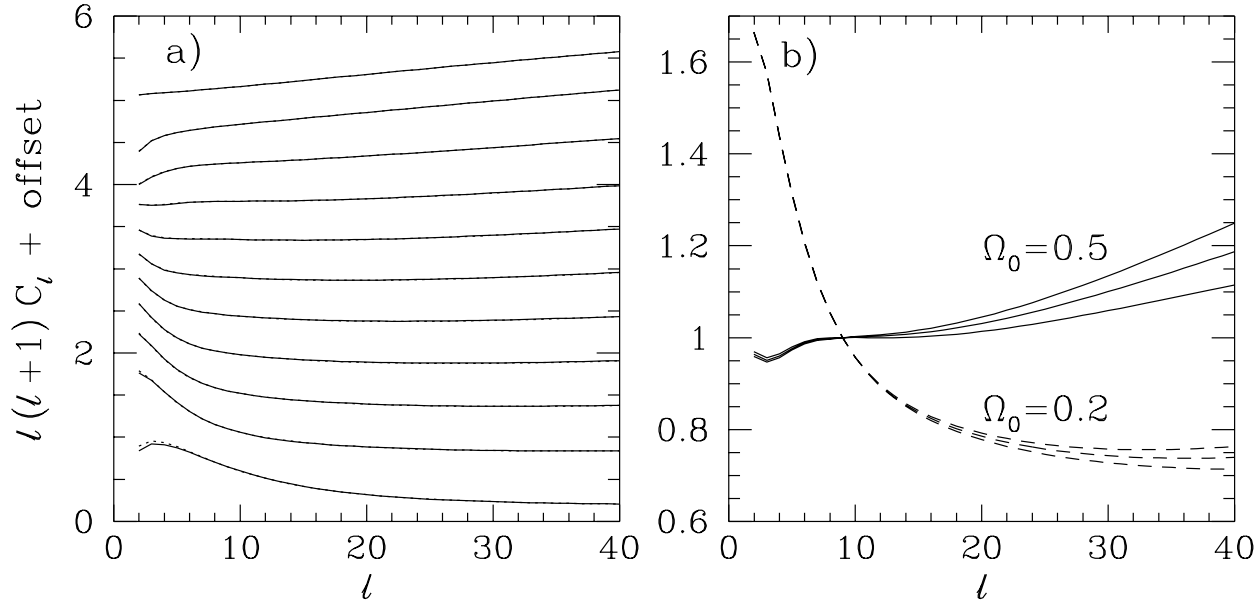


FIG. 1.—(*a*) CMB anisotropy multipole coefficients for the open-bubble inflation model, accounting only for fluctuations generated during the evolution inside the bubble (RP94; *solid lines*) and also accounting for fluctuations generated in the first epoch of inflation (BGT; YST, *dotted lines*—these overlap the solid lines, except at the lowest $\Omega_0$ and smallest $\ell$), for $\Omega_0 = 0.1$, 0.2, 0.25, 0.3, 0.35, 0.4, 0.45, 0.5, 0.6, 0.8, and 1.0, in ascending order. These are for $t_0 \simeq 12$ Gyr and $\Omega_B h^2 = 0.0125$. The coefficients are normalized relative to the $C_9$ amplitude, and different values of $\Omega_0$ are offset from each other to aid visualization. In (*b*) are the set of spectra for the open-bubble inflation model, accounting only for fluctuations generated during the evolution inside the bubble (RP94), with $\Omega_0 = 0.2$ and $\Omega_0 = 0.5$ for the three pairs of values $(t_0, \Omega_B h^2)$: ($\simeq$10.5 Gyr, =0.0055), ($\simeq$12 Gyr, =0.0125), and ($\simeq$13.5 Gyr, =0.0205). Spectra in the two sets are normalized to have the same $C_9$, and $\Omega_B h^2$ increases in ascending order on the right axis.

$(\theta, \phi)$, on the sky via the spherical harmonic decomposition,

$$\frac{\delta T}{T}(\theta, \phi) = \sum_{\ell=2}^{\infty} \sum_{m=-\ell}^{\ell} a_{\ell m} Y_{\ell m}(\theta, \phi) \, . \tag{3}$$

The CMB spatial anisotropy in a Gaussian model can then be characterized by the angular perturbation spectrum $C_\ell$, defined in terms of the ensemble average,

$$\langle a_{\ell m} a^*_{\ell' m'} \rangle = C_\ell \, \delta_{\ell \ell'} \, \delta_{m m'} \, . \tag{4}$$

The $C_\ell$'s used here were computed using two independent Boltzmann transfer codes developed by NS (see, e.g., Sugiyama 1995) and RS (see, e.g., Stompor 1994) which agree to $\sim$0.1%. The computations here assume a standard recombination thermal history and ignore the possibility of early reionization. The simplest open models (with the least possible number of free parameters) have yet to be ruled out by observational data (GRSB; Ratra et al. 1997; GRS; this paper), so there is insufficient motivation to expand the model parameter space by including the effect of early reionization, tilt or gravity waves.[16]

For the $P(k)$ of types (1), (2), and (4) above, we have evaluated the CMB anisotropy angular spectra for a range of $\Omega_0$ spanning the interval between 0.1 and 1.0, for a variety of values of $h$ (the Hubble parameter $H_0 = 100\ h$ km s$^{-1}$ Mpc$^{-1}$) and the baryonic-mass density parameter $\Omega_B$. The values of $h$ were selected to cover the lower part of the range of ages consistent with current requirements ($t_0 \simeq 10.5$ Gyr, 12 Gyr, or 13.5 Gyr, with $h$ as a function of $\Omega_0$ computed accordingly; see, for example, Jimenez et al. 1996; Chaboyer et al. 1996). The values of $\Omega_B$ were chosen to be consistent with current standard nucleosynthesis requirements ($\Omega_B h^2 = 0.0055$, 0.0125, or 0.0205; see, e.g., Copi, Schramm, & Turner 1995; Sarkar 1996). To render the problem tractable, $C_\ell$'s were determined for the central values of $t_0$ and $\Omega_B h^2$, and for the two combinations of these parameters that most perturb the $C_\ell$'s from those computed at the central values (i.e., for the smallest $t_0$ we used the smallest $\Omega_B h^2$, and for the largest $t_0$ we used the largest $\Omega_B h^2$). Specific parameter values are given in columns (1) and (2) of Tables 1–6, and representative anisotropy spectra can be seen in Figures 1 and 2. We therefore improve on our earlier analysis of the DMR 2 year data (GRSB) by considering a suitably broader range in the $(\Omega_B, h)$ parameter space.

The CMB anisotropy spectra for $P(k)$ of type (3) above were computed for a range of $\Omega_0$ spanning the interval between 0.1 and 0.9, for $h = 0.6$ and $\Omega_B = 0.035$. Specific parameter values are given in columns (1) and (2) of Table 7, and these spectra are shown in Figure 3. In Figure 4 we compare the various spectra considered here.

The differences in the low-$\ell$ shapes of the $C_\ell$'s in the various models (Figs. 1–4) are a consequence of three effects: (1) the shape of the energy-density perturbation power spectrum at low wavenumber; (2) the exponential suppression at the spatial curvature scale in an open model; and (3) the interplay between the "usual" (fiducial CDM) Sachs-Wolfe term and the "integrated" Sachs-Wolfe (hereafter SW) term in the expression for the CMB spatial anisotropy. The relative importance of these effects is determined by the value of $\Omega_0$ and leads to the nonmonotonic behavior of the large-scale $C_\ell$'s as a function of $\Omega_0$ seen in

[16] Note that the geometrical effect in an open universe moves the effects of early reionization on the CMB anisotropy to a smaller angular scale. As a result $Q_{\rm rms\text{-}PS}$ values determined from the DMR data here (assuming no early reionization) are unlikely to be very significantly affected by early reionization. However, since structure forms earlier in an open model, other effects of early reionization might be more significant in an open model. While it is possible to heuristically account for such effects, an accurate quantitative estimate must await a better understanding of structure formation.

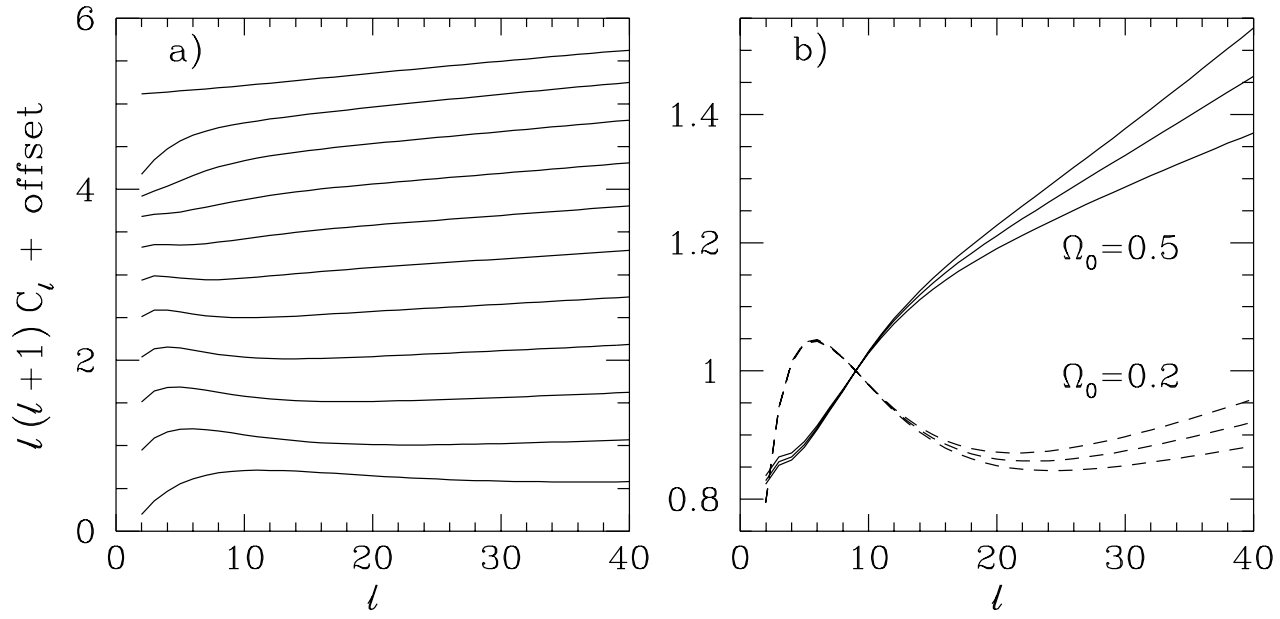


FIG. 2.—CMB spatial anisotropy multipole coefficients for the flat-space scale-invariant spectrum open model (W83). Conventions and parameter values are as in the legend of Fig. 1 (although only one set of spectra are shown in Fig. 2*a*).

Figures 1–4. More precisely, the contributions to the CMB anisotropy angular spectrum from the "usual" and "integrated" SW terms have a different $\ell$-dependence as well as a relative amplitude that is both $\Omega_0$ and $P(k)$ dependent.

On very large angular scales (small $\ell$'s), the dominant contribution to the "usual" SW term comes from a higher redshift (when the length scales are smaller) than does the dominant contribution to the "integrated" SW term (Hu & Sugiyama 1994, 1995). As a result, in an open model on very large angular scales, the "usual" SW term is cut off more sharply by the spatial curvature length scale than is the "integrated" SW term (Hu & Sugiyama 1994), i.e., on very large angular scales in an open model, the "usual" SW term has a larger (positive) effective index $n$ than the "integrated" SW term. On slightly smaller angular scales the "integrated" SW term is damped (i.e., it has a negative effective index $n$) while the "usual" SW term plateaus (Hu & Sugiyama 1994). As a consequence, going from the largest to slightly smaller angular scales, the "usual" term rises steeply and then flattens, while the "integrated" term

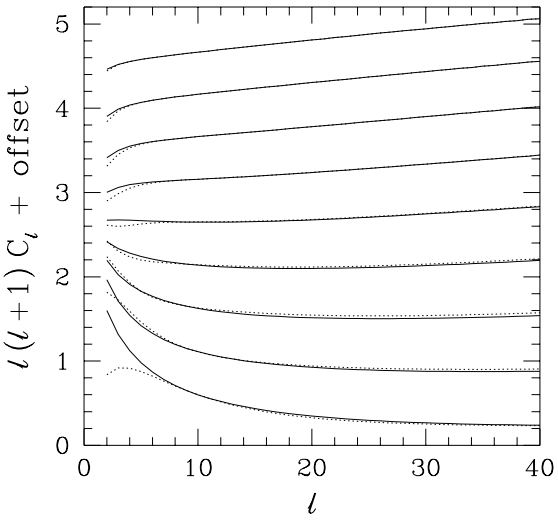


FIG. 3.—CMB spatial anisotropy multipole coefficients for the open-bubble inflation spectrum, also accounting for both fluctuations generated in the first epoch of inflation and that corresponding to a non–square-integrable basis function (YST, *solid lines*), and ignoring both these fluctuations (RP94, *dotted lines*). They are, in ascending order, for $\Omega_0 = 0.1$ to 0.9 in steps of 0.1, with $h = 0.6$ and $\Omega_B = 0.035$, normalized relative to the $C_9$ amplitude, and different values of $\Omega_0$ are offset from each other to aid visualization.

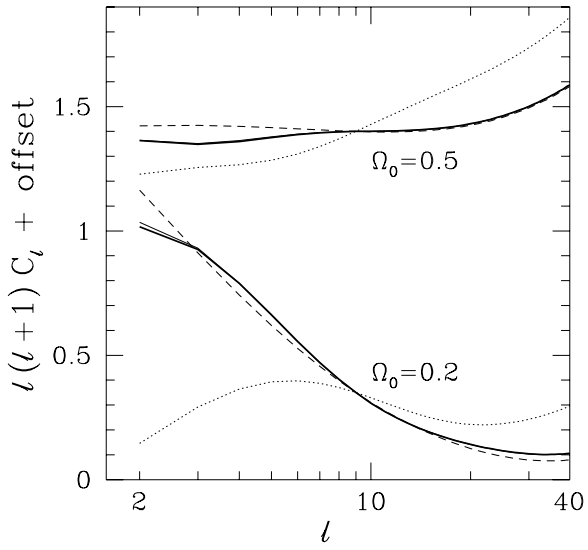


FIG. 4.—CMB spatial anisotropy multipole coefficients, as a function of $\ell$, for the various spectra considered in this paper, at $\Omega_0 = 0.2$ and 0.5 (vertically offset). Light solid and heavy solid lines show the open-bubble inflation cases accounting for (type [2] spectra above) and ignoring (type [1] spectra, at $\Omega_0 = 0.5$ these completely overlap the type [2] spectra) fluctuations generated in the first epoch of inflation. Dashed lines show the open-bubble inflation models, now also accounting for the contribution from the non–square-integrable basis function (type [3] spectra). Dotted lines show the flat-space scale-invariant spectrum open model spectra (type [4] spectra). All spectra are for $h = 0.6$ and $\Omega_B = 0.035$.

rises less steeply and then drops (i.e., it has a peak). The change in shape, as a function of $\ell$, of these two terms is both $\Omega_0$ and $P(k)$ dependent. These are the two dominant effects at $\ell \lesssim 15$–$20$; at higher $\ell$, other effects come into play.

More specifically, for $\Omega_0 > 0.8$, the curvature length scale cutoff and the precise large-scale form of the $P(k)$ considered here are relatively unimportant—the CMB anisotropy angular spectrum is quite similar to that for $\Omega_0 = 1$, and the dominant contribution is the "usual" SW term. For a $P(k)$ that does not diverge at low wavenumber, as with the flat-space scale-invariant spectrum in an open model, for $\Omega_0 \lesssim 0.8$ the exponential "cutoff" at the spatial curvature length dominates, and the lowest $\ell$ $C_\ell$'s are suppressed (Figs. 2 and 4). For this $P(k)$, as $\Omega_0$ is reduced, the "usual" term continues to be important on the largest angular scales down to $\Omega_0 \sim 0.4$–$0.5$. As $\Omega_0$ is reduced below $\sim 0.4$–$0.5$, the "integrated" term starts to dominate on the largest angular scales, and as $\Omega_0$ is further reduced the "integrated" term also starts to dominate on smaller angular scales. From Figure 2*a*, one will notice that the "integrated" SW term "peak" first makes an appearance at $\Omega_0 = 0.4$—the central line in the plot at $\ell(\ell + 1)C_\ell$ + offset $\sim 3$—and that as $\Omega_0$ is further reduced (in descending order along the curves shown) the "integrated" term "peak" moves to smaller angular scales. The $\Omega_0 \sim 0.4$ case is where the "integrated" term peaks at $\ell \sim 2$–$3$, and the damping of this term on smaller angular scales ($\ell \gtrsim 5$) is compensated for by the steep rise of the "usual" SW term—the two terms are of roughly equal magnitude at $\ell \sim 10$—and these effects result in the almost exactly scale-invariant spectrum at $\Omega_0 \sim 0.4$ (this case is more scale-invariant than fiducial CDM). A discussion of some of these features of the CMB anisotropy angular spectrum in the flat-space scale-invariant spectrum open model is given in Cayón et al. (1996).

Open-bubble inflation models have a $P(k)$ that diverges at low wavenumber (RP95; note that no physical quantity diverges), and this increases the low-$\ell$ $C_\ell$'s (Figs. 1 and 4) relative to those of the flat-space scale-invariant spectrum open model (Figs. 2 and 4). The $C_\ell$'s for low-$\Omega_0$ models increase more than the higher $\Omega_0$ ones, since, for a fixed wavenumber dependence of $P(k)$, the divergence is more prominent at lower $\Omega_0$ (RP94). The non–square-integrable basis function (YST) contributes even more power on large angular scales, and so, at low-$\ell$, the $C_\ell$'s of Figure 3 are slightly larger than those of Figure 1 (also see Fig. 4). Again, spectra at lower values of $\Omega_0$ are more significantly influenced.

As is clear from Figures 1 and 4, in an open-bubble inflation model, quantum mechanical zero-point fluctuations generated in the first epoch of inflation scarcely affect the $C_\ell$'s, although at the very lowest values of $\Omega_0$ the very lowest order $C_\ell$ coefficients are slightly modified. The effect is concentrated in this region of the parameter space since the fluctuations in the first inflation epoch contribute to, and increase, only the lowest wavenumber part of $P(k)$. In simple open-bubble inflation models, the precise value of this small effect is dependent on the model assumed for the first epoch of inflation (BT). Since the DMR data are most sensitive to multipole moments with $l \sim 8$–$10$, one expects the effect at $l \sim 2$–$3$ to be almost completely negligible (BT; also see YST; YB).

Figures 2–4 show that both the flat-space scale-invariant spectrum open model and the contribution from the non–square-integrable mode do lead to significantly different $C_\ell$'s (compared to those of Fig. 1).

### 3.2. *Data Selection and Power Spectrum Inference*

In this paper, we utilize the DMR 4 year 53 and 90 GHz sky maps in both galactic and ecliptic coordinates. We thus quantify explicitly the expected small shifts in the inferred normalization amplitudes due to the small differences between the galactic- and ecliptic-coordinate maps. The maps are co-added using inverse–noise-variance weights derived in each coordinate system. The least sensitive 31 GHz maps have been omitted from the analysis, since their contribution is minimal under such a weighting scheme. In particular, we find that the normalization of the fiducial CDM model is shifted by $-0.9\%$ when the 31 GHz data is included in the co-added sky map, with a correspondingly small improvement in the error.

The dominant source of emission in the DMR maps is due to the Galactic plane. We are unable to model this contribution to the sky temperature to sufficient accuracy to enable its subtraction; thus, we excise all pixels in which the Galactic-plane signal dominates the CMB. The geometry of the cut has been determined by using the DIRBE 140 $\mu$m map as a tracer of the strongest emission, as described completely in Banday et al. (1997). All pixels with Galactic latitude $|b| < 20^\circ$ are removed, together with regions toward Scorpius-Ophiucus and Taurus-Orion. There are 3881 surviving pixels in galactic coordinates and 3890 in ecliptic out of an initial 6144 in both coordinate frames. This extended (4 year data) Galactic plane cut has provided the biggest impact on the analysis of the DMR data (see Górski et al. 1996; hereafter G96).

The extent to which residual high-latitude Galactic emission can modify our results has been quantified in two ways. Since the spatial morphology of Galactic synchrotron, free-free and dust emission seems to be well described by a steeply falling power spectrum, the cosmological signal is predominantly compromised on the largest angular scales. As a simple test of Galactic contamination, we perform all computations both including and excluding the observed sky quadrupole. A more detailed approach (G96) notes that a large fraction of the Galactic signal can be accounted for by using the DIRBE 140 $\mu$m sky map (Reach et al. 1995) as a template for free-free and dust emission and the 408 MHz all-sky radio survey (Haslam et al. 1981) to describe synchrotron emission. A correlation analysis yields coupling coefficients for the two templates at each of the DMR frequencies. We have repeated our model analysis after correcting the co-added sky maps by the Galactic templates scaled by the coefficients derived in G96. In particular, we adopt those values derived under the assumption that the CMB anisotropy is well described by an $n = 1$ power-law model with normalization amplitude $Q_{\rm rms\text{-}PS} \sim 18$ $\mu$K.[17] One might make criticisms of either technique: excluding information from an analysis, in this case the quadrupole components, can obviously weaken any conclusions simply because statistical uncertainties will grow; at the same time,

[17] A more self-consistent analysis would simultaneously compute the $Q_{\rm rms\text{-}PS}$ and coupling coefficient amplitudes. In fact, we have investigated this for a subsample of the models considered here in which we varied $\Omega_0$ but fixed $h$ and $\Omega_B$. No statistically significant changes were found in the derived values of either $Q_{\rm rms\text{-}PS}$ or the coupling coefficients.

it is not clear whether the Galactic corrections applied are completely adequate. We believe that, given these uncertainties, our analysis is the most complete and conservative one that is possible.

The power spectrum analysis technique developed by Górski (1994) is implemented. Orthogonal basis functions for the Fourier decomposition of the sky maps are constructed that specifically include both pixelization effects and the Galactic cut. (These are linear combinations of the usual spherical harmonics with multipole $\ell \leq 30$.) The functions are coordinate system dependent. A likelihood analysis is then performed as described in Górski et al. (1994).

### 3.3. *Results of $Q_{\rm rms\text{-}PS}$ Fitting*

The results of the DMR likelihood analyses are summarized in Figures 5–20 and Tables 1–7 and 13.

Two representative sets of likelihood functions $L(Q_{\rm rms\text{-}PS}, \Omega_0)$ are shown in Figures 5 and 6. Figure 5 shows those derived from the ecliptic-frame sky maps, ignoring the correction for faint high-latitude foreground Galactic emission, and excluding the quadrupole moment from the analysis. Figure 6 shows the likelihood functions derived from the galactic-frame sky maps, accounting for the faint high-latitude foreground Galactic emission correction, and including the quadrupole moment in the analysis. Together, these two data sets span the maximum range of normalizations inferred from our analysis (the former providing the highest, and the latter the lowest $Q_{\rm rms\text{-}PS}$).

Tables 1–7 give the $Q_{\rm rms\text{-}PS}$ central values and 1 and 2 $\sigma$ ranges for spectra of type (1), (3), and (4) above, computed from the appropriate posterior probability density distribution function assuming a uniform prior. Each row in Tables 1–7 lists these values at a given $\Omega_0$ for the eight possible combinations of (1) galactic- or ecliptic-coordinate map; (2) faint high-latitude Galactic foreground emission correction accounted for or ignored; and (3) quadrupole included ($\ell_{\rm min} = 2$) or excluded ($\ell_{\rm min} = 3$). The corresponding ridge

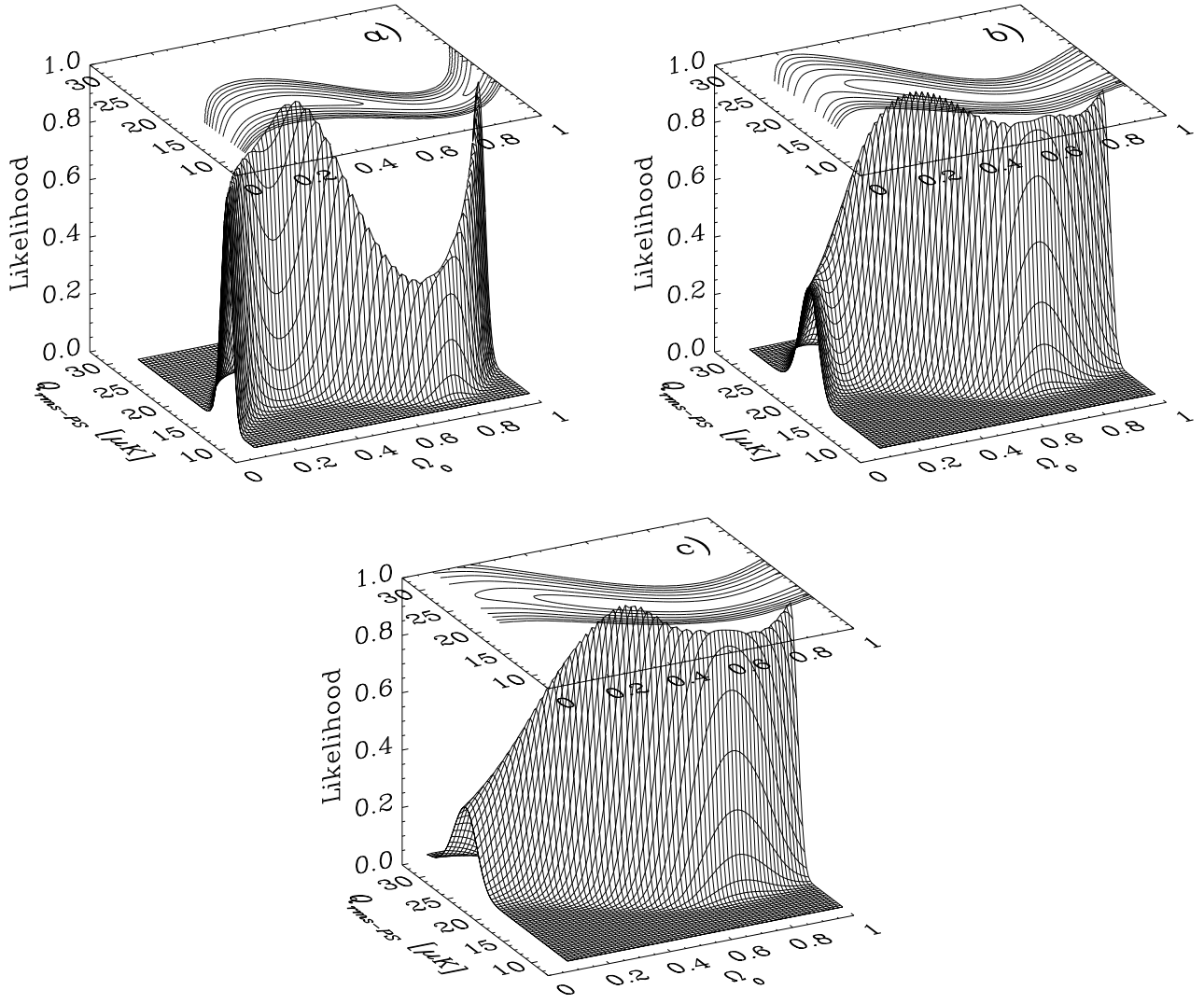


FIG. 5.—Likelihood functions $L(Q_{\rm rms\text{-}PS}, \Omega_0)$ (arbitrarily normalized to unity at the highest peak at $\Omega_0 \sim 0.4$) derived from a simultaneous analysis of the DMR 53 and 90 GHz ecliptic-frame data, ignoring the correction for faint high-latitude foreground Galactic emission, and excluding the quadrupole moment from the analysis. These are for the $h = 0.6, \Omega_B = 0.035$ models. Panel (*a*) is for the flat-space scale-invariant spectrum open model (W83), (*b*) is for the open-bubble inflation model accounting only for perturbations generated during the evolution inside the bubble (RP94), and (*c*) is for the open-bubble inflation model now also accounting for both the fluctuations generated in the first epoch of inflation and those corresponding to a non–square-integrable basis function (YST).

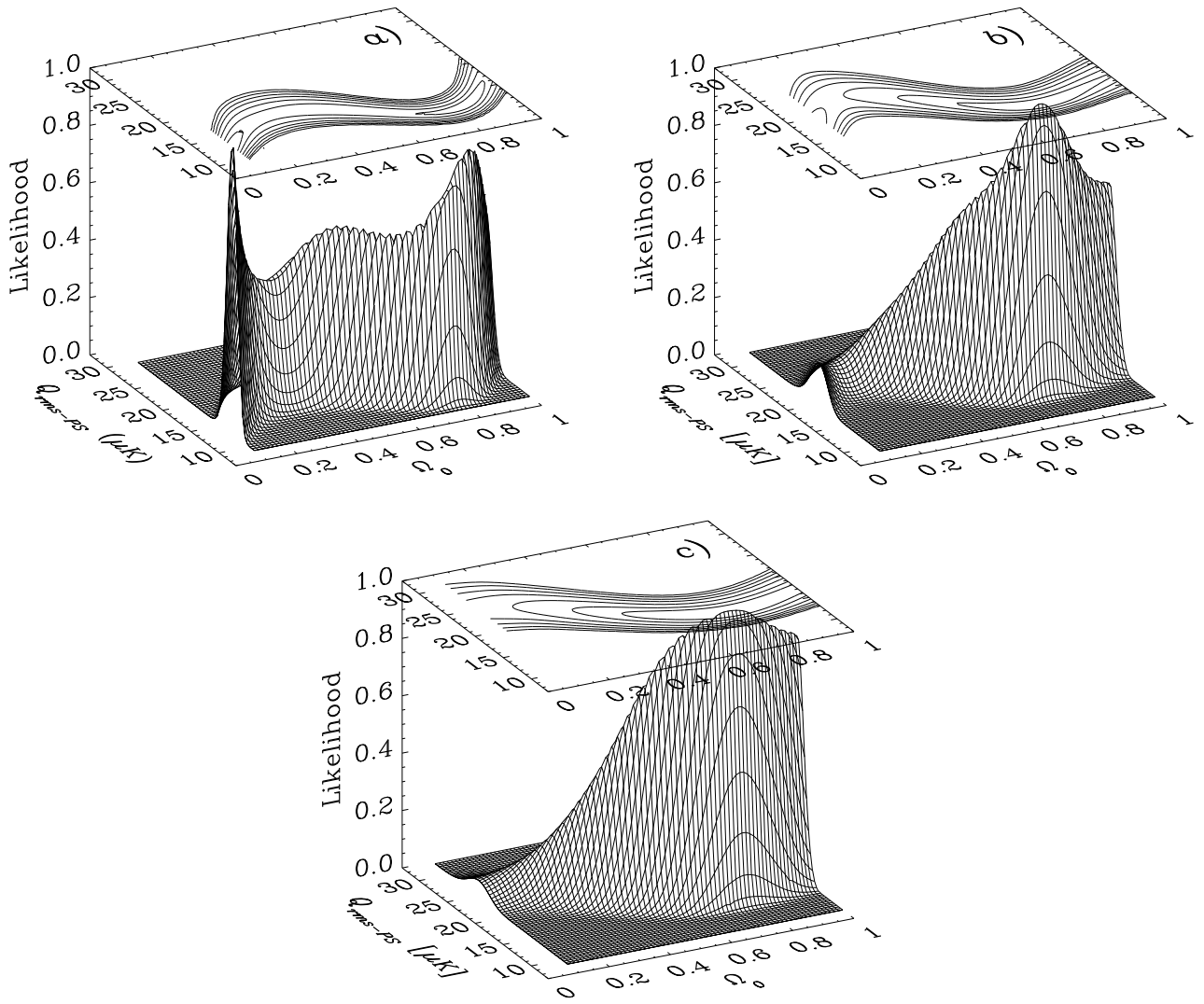


FIG. 6.—Likelihood functions $L(Q_{\text{rms-PS}}, \Omega_0)$ (arbitrarily normalized to unity at the highest peak near either $\Omega_0 \sim 0.1$ or 0.7), derived from a simultaneous analysis of the DMR 53 and 90 GHz galactic-frame data, accounting for the faint high-latitude foreground Galactic emission correction, and including the quadrupole moment in the analysis. Conventions and parameter values are as for Fig. 5.

lines of maximum likelihood $Q_{\text{rms-PS}}$ value as a function of $\Omega_0$ are shown in Figures 7–9 for some of the cosmological parameter values considered here.

Although we have computed these values for spectra of type (2) above (i.e., those accounting for perturbations generated in the first epoch of inflation), we record only a subset of them in column (4) of Table 13. These should be compared to columns (2) and (6) of Table 13, which show the maximal 2 $\sigma$ $Q_{\text{rms-PS}}$ range for spectra of types (1) and (3). While the differences in $Q_{\text{rms-PS}}$ between spectra (1) and (2) [cols. (2) and (4) of Table 13] are not totally insignificant, more importantly the differences between the $(\delta M/M)[8\ h^{-1}$ Mpc] values for the three spectra (cols. [3], [5], and [7] of Table 13) are observationally insignificant.

The entries in Tables 1–6 illustrate the shift in the inferred normalization amplitudes due to changes in $h$ and $\Omega_B$. These shifts are larger for models with a larger $\Omega_0$, since these models have CMB anisotropy spectra that rise somewhat more rapidly toward large $\ell$, so in these cases the DMR data are sensitive to somewhat smaller angular scales where the effects of varying $h$ and $\Omega_B h^2$ are more prominent. Figure 10 shows the effects that varying $t_0$ and $\Omega_B h^2$ have on some of the ridge lines of maximum likelihood $Q_{\text{rms-PS}}$ as a function of $\Omega_0$, and Figure 12 illustrates the effects on some of the conditional (fixed $\Omega_0$ slice) likelihood densities for $Q_{\text{rms-PS}}$. On the whole, for the CMB anisotropy spectra considered here, shifts in $h$ and $\Omega_B h^2$ have only a small effect on the inferred normalization amplitude.

The normalization amplitude is somewhat more sensitive to the differences between the galactic- and ecliptic-coordinate sky maps, to the foreground high-latitude Galactic emission treatment, and to the inclusion or exclusion of the $\ell = 2$ moment. See Figures 7–9. For the purpose of normalizing models, we choose for our 2 $\sigma$ c.l. bounds values from the likelihood fits that span the maximal range in the $Q_{\text{rms-PS}}$ normalizations. Specifically, for the lower 2 $\sigma$ bound, we adopt the value determined from the analysis of the galactic-coordinate maps accounting for the high-latitude Galactic emission correction and including the $\ell = 2$ moment in the analysis and for the upper 2 $\sigma$ value that determined from the analysis of the ecliptic-coordinate maps ignoring the Galactic emission correction and exclud-

TABLE 1

$Q_{\rm rms\text{-}PS}$ VALUES ($\mu$K) FOR THE $t_0 \simeq 10.5$ Gyr, $\Omega_B h^2 = 0.0055$ OPEN-BUBBLE INFLATION MODELS[a]

| | | ECLIPTIC FRAME | | | | GALACTIC FRAME | | | |
|---|---|---|---|---|---|---|---|---|---|
| $\Omega_0$ (1) | $h$ (2) | No GC[b] ($\ell_{\rm min} = 2$) (3) | No GC[b] ($\ell_{\rm min} = 3$) (4) | GC[b] ($\ell_{\rm min} = 2$) (5) | GC[b] ($\ell_{\rm min} = 3$) (6) | No GC[b] ($\ell_{\rm min} = 2$) (7) | No GC[b] ($\ell_{\rm min} = 3$) (8) | GC[b] ($\ell_{\rm min} = 2$) (9) | GC[b] ($\ell_{\rm min} = 3$) (10) |
| 0.1 ..... | 0.84 | $21.04^{22.61\ 24.32}_{19.51\ 18.12}$ | $21.56^{23.18\ 24.93}_{20.03\ 18.58}$ | $20.40^{21.99\ 23.61}_{18.86\ 17.51}$ | $20.85^{22.42\ 24.12}_{19.25\ 17.86}$ | $20.39^{21.92\ 23.63}_{18.91\ 17.52}$ | $20.90^{22.47\ 24.19}_{19.37\ 17.94}$ | $19.77^{21.31\ 22.97}_{18.33\ 16.96}$ | $20.20^{21.73\ 23.44}_{18.68\ 17.29}$ |
| 0.2 ..... | 0.79 | $24.28^{26.04\ 28.03}_{22.52\ 20.90}$ | $24.89^{26.72\ 28.72}_{23.10\ 21.44}$ | $23.58^{25.25\ 27.20}_{21.81\ 20.18}$ | $24.09^{25.89\ 27.83}_{22.33\ 20.70}$ | $23.49^{25.25\ 27.19}_{21.78\ 20.20}$ | $24.09^{25.90\ 27.84}_{22.33\ 20.71}$ | $22.80^{24.50\ 26.42}_{21.09\ 19.52}$ | $23.31^{25.11\ 27.01}_{21.59\ 20.02}$ |
| 0.25..... | 0.77 | $24.28^{26.04\ 27.94}_{22.56\ 20.94}$ | $24.84^{26.67\ 28.63}_{23.10\ 21.48}$ | $23.63^{25.25\ 27.10}_{21.85\ 20.27}$ | $24.10^{25.84\ 27.74}_{22.32\ 20.70}$ | $23.49^{25.25\ 27.15}_{21.82\ 20.25}$ | $24.09^{25.85\ 27.80}_{22.33\ 20.76}$ | $22.80^{24.50\ 26.38}_{21.14\ 19.60}$ | $23.31^{25.06\ 26.96}_{21.59\ 20.02}$ |
| 0.3 ..... | 0.75 | $23.63^{25.34\ 27.19}_{22.01\ 20.48}$ | $24.20^{25.91\ 27.82}_{22.50\ 20.97}$ | $22.96^{24.69\ 26.40}_{21.39\ 19.80}$ | $23.44^{25.21\ 27.00}_{21.83\ 20.24}$ | $22.89^{24.56\ 26.41}_{21.27\ 19.79}$ | $23.44^{25.16\ 27.01}_{21.78\ 20.25}$ | $22.24^{23.86\ 25.65}_{20.63\ 19.14}$ | $22.70^{24.42\ 26.22}_{21.08\ 19.56}$ |
| 0.35..... | 0.74 | $22.61^{24.19\ 25.94}_{21.04\ 19.60}$ | $23.10^{24.76\ 26.55}_{21.52\ 20.07}$ | $21.99^{23.52\ 25.29}_{20.45\ 19.01}$ | $22.43^{23.99\ 25.76}_{20.82\ 19.41}$ | $21.92^{23.49\ 25.20}_{20.39\ 18.95}$ | $22.43^{24.05\ 25.81}_{20.90\ 19.42}$ | $21.26^{22.84\ 24.54}_{19.77\ 18.37}$ | $21.73^{23.31\ 25.02}_{20.16\ 18.77}$ |
| 0.4 ..... | 0.73 | $21.36^{22.84\ 24.46}_{19.88\ 18.54}$ | $21.82^{23.35\ 25.01}_{20.37\ 18.96}$ | $20.77^{22.21\ 23.73}_{19.28\ 17.90}$ | $21.18^{22.66\ 24.26}_{19.68\ 18.27}$ | $20.71^{22.19\ 23.81}_{19.28\ 17.98}$ | $21.18^{22.70\ 24.32}_{19.74\ 18.35}$ | $20.11^{21.56\ 23.14}_{18.71\ 17.43}$ | $20.53^{22.01\ 23.63}_{19.09\ 17.75}$ |
| 0.45..... | 0.71 | $20.02^{21.36\ 22.89}_{18.63\ 17.43}$ | $20.46^{21.82\ 23.35}_{19.05\ 17.77}$ | $19.45^{20.81\ 22.29}_{18.11\ 16.95}$ | $19.78^{21.18\ 22.66}_{18.44\ 17.21}$ | $19.42^{20.76\ 22.29}_{18.07\ 16.87}$ | $19.83^{21.22\ 22.75}_{18.49\ 17.24}$ | $18.88^{20.20\ 21.69}_{17.56\ 16.37}$ | $19.19^{20.57\ 22.06}_{17.89\ 16.64}$ |
| 0.5 ..... | 0.70 | $18.68^{19.93\ 21.31}_{17.43\ 16.27}$ | $19.05^{20.37\ 21.78}_{17.81\ 16.62}$ | $18.21^{19.28\ 20.74}_{16.87\ 15.83}$ | $18.51^{19.65\ 21.11}_{17.15\ 16.05}$ | $18.12^{19.42\ 20.76}_{16.92\ 15.76}$ | $18.54^{19.79\ 21.18}_{17.24\ 16.13}$ | $17.60^{18.88\ 20.24}_{16.45\ 15.30}$ | $17.94^{19.19\ 20.57}_{16.69\ 15.53}$ |
| 0.6 ..... | 0.68 | $16.50^{17.61\ 18.81}_{15.39\ 14.37}$ | $16.84^{17.99\ 19.18}_{15.73\ 14.66}$ | $16.05^{17.05\ 18.38}_{14.86\ 13.95}$ | $16.31^{17.34\ 18.63}_{15.11\ 14.13}$ | $16.04^{17.15\ 18.31}_{14.97\ 13.95}$ | $16.36^{17.47\ 18.68}_{15.25\ 14.23}$ | $15.60^{16.66\ 17.86}_{14.54\ 13.56}$ | $15.85^{16.92\ 18.12}_{14.74\ 13.72}$ |
| 0.8 ..... | 0.65 | $15.76^{16.82\ 17.94}_{14.74\ 13.77}$ | $16.07^{17.13\ 18.28}_{15.00\ 14.02}$ | $15.40^{16.42\ 17.54}_{14.38\ 13.45}$ | $15.58^{16.65\ 17.76}_{14.52\ 13.60}$ | $15.30^{16.36\ 17.47}_{14.32\ 13.35}$ | $15.62^{16.69\ 17.84}_{14.60\ 13.63}$ | $14.92^{15.94\ 17.05}_{13.94\ 13.00}$ | $15.11^{16.18\ 17.29}_{14.09\ 13.17}$ |
| 1 ..... | 0.62 | $18.07^{19.28\ 20.57}_{16.87\ 15.76}$ | $18.41^{19.65\ 21.01}_{17.22\ 16.11}$ | $17.68^{18.89\ 20.00}_{16.48\ 15.26}$ | $17.91^{19.11\ 20.33}_{16.70\ 15.51}$ | $17.52^{18.72\ 20.06}_{16.36\ 15.30}$ | $17.89^{19.14\ 20.48}_{16.73\ 15.62}$ | $17.09^{18.28\ 19.52}_{15.94\ 14.83}$ | $17.33^{18.54\ 19.83}_{16.18\ 15.06}$ |

[a] For the open-bubble inflation model accounting only for fluctuations generated during the evolution inside the bubble (RP94). The tabulated $Q_{\rm rms\text{-}PS}$ values are determined from the conditional likelihood function at fixed $\Omega_0$. At each $\Omega_0$, the first of the five entries in each of cols. (3)–(10) is the maximum likelihood value, the first (vertical) pair delimits the 68.3% (1 $\sigma$) highest posterior density range, and the second (vertical) pair delimits the 95.5% (2 $\sigma$) highest posterior density range.

[b] Accounting for (GC) or ignoring (No GC) the correction for faint high-latitude foreground Galactic emission.

TABLE 2

$Q_{\rm rms\text{-}PS}$ VALUES ($\mu$K) FOR THE $t_0 \simeq 12$ Gyr, $\Omega_B h^2 = 0.0125$ OPEN-BUBBLE INFLATION MODELS[a]

| | | ECLIPTIC FRAME | | | | GALACTIC FRAME | | | |
|---|---|---|---|---|---|---|---|---|---|
| $\Omega_0$ (1) | $h$ (2) | No GC[b] ($\ell_{\rm min} = 2$) (3) | No GC[b] ($\ell_{\rm min} = 3$) (4) | GC[b] ($\ell_{\rm min} = 2$) (5) | GC[b] ($\ell_{\rm min} = 3$) (6) | No GC[b] ($\ell_{\rm min} = 2$) (7) | No GC[b] ($\ell_{\rm min} = 3$) (8) | GC[b] ($\ell_{\rm min} = 2$) (9) | GC[b] ($\ell_{\rm min} = 3$) (10) |
| 0.1 ..... | 0.73 | $21.04^{22.66\ 24.32}_{19.56\ 18.12}$ | $21.56^{23.18\ 24.93}_{20.03\ 18.58}$ | $20.40^{22.08\ 23.66}_{18.96\ 17.57}$ | $20.85^{22.53\ 24.18}_{19.37\ 17.94}$ | $20.39^{21.92\ 23.63}_{18.91\ 17.52}$ | $20.90^{22.47\ 24.23}_{19.37\ 17.98}$ | $19.77^{21.31\ 22.97}_{18.33\ 16.96}$ | $20.20^{21.78\ 23.49}_{18.72\ 17.33}$ |
| 0.2 ..... | 0.69 | $24.28^{26.04\ 27.98}_{22.52\ 20.90}$ | $24.89^{26.72\ 28.68}_{23.10\ 21.44}$ | $23.67^{25.25\ 27.10}_{21.81\ 20.22}$ | $24.10^{25.84\ 27.78}_{22.33\ 20.65}$ | $23.44^{25.25\ 27.19}_{21.78\ 20.20}$ | $24.09^{25.90\ 27.84}_{22.33\ 20.71}$ | $22.80^{24.50\ 26.38}_{21.09\ 19.56}$ | $23.26^{25.06\ 27.01}_{21.59\ 19.97}$ |
| 0.25..... | 0.67 | $24.23^{25.99\ 27.94}_{22.52\ 20.94}$ | $24.84^{26.63\ 28.59}_{23.10\ 21.48}$ | $23.58^{25.20\ 27.16}_{21.85\ 20.15}$ | $24.04^{25.79\ 27.79}_{22.33\ 20.68}$ | $23.44^{25.20\ 27.10}_{21.78\ 20.25}$ | $24.05^{25.81\ 27.75}_{22.33\ 20.71}$ | $22.80^{24.46\ 26.33}_{21.14\ 19.56}$ | $23.26^{25.02\ 26.96}_{21.59\ 20.02}$ |
| 0.3 ..... | 0.66 | $23.58^{25.30\ 27.15}_{21.96\ 20.44}$ | $24.16^{25.86\ 27.74}_{22.46\ 20.92}$ | $22.80^{24.65\ 26.51}_{21.39\ 19.81}$ | $23.32^{25.12\ 27.02}_{21.80\ 20.21}$ | $22.89^{24.51\ 26.31}_{21.22\ 19.74}$ | $23.40^{25.11\ 26.96}_{21.78\ 20.25}$ | $22.20^{23.82\ 25.61}_{20.58\ 19.09}$ | $22.66^{24.32\ 26.18}_{21.04\ 19.51}$ |
| 0.35..... | 0.65 | $22.56^{24.14\ 25.85}_{20.99\ 19.56}$ | $23.05^{24.67\ 26.46}_{21.48\ 20.03}$ | $21.94^{23.46\ 25.09}_{20.35\ 18.84}$ | $22.34^{23.95\ 25.65}_{20.80\ 19.29}$ | $21.87^{23.44\ 25.16}_{20.34\ 18.95}$ | $22.38^{23.95\ 25.71}_{20.81\ 19.37}$ | $21.22^{22.80\ 24.46}_{19.73\ 18.33}$ | $21.64^{23.26\ 24.97}_{20.16\ 18.72}$ |
| 0.4 ..... | 0.63 | $21.27^{22.75\ 24.37}_{19.83\ 18.49}$ | $21.73^{23.27\ 24.93}_{20.29\ 18.92}$ | $20.67^{22.16\ 23.75}_{19.22\ 17.80}$ | $21.04^{22.56\ 24.23}_{19.58\ 18.22}$ | $20.67^{22.10\ 23.68}_{19.23\ 17.94}$ | $21.13^{22.61\ 24.23}_{19.65\ 18.31}$ | $20.07^{21.52\ 23.05}_{18.67\ 17.35}$ | $20.44^{21.92\ 23.54}_{19.00\ 17.70}$ |
| 0.45..... | 0.62 | $19.93^{21.27\ 22.80}_{18.58\ 17.33}$ | $20.37^{21.73\ 23.27}_{18.96\ 17.73}$ | $19.36^{20.60\ 22.20}_{18.01\ 16.80}$ | $19.73^{21.01\ 22.61}_{18.34\ 17.14}$ | $19.32^{20.71\ 22.15}_{18.03\ 16.78}$ | $19.74^{21.13\ 22.61}_{18.40\ 17.15}$ | $18.79^{20.11\ 21.56}_{17.47\ 16.28}$ | $19.14^{20.48\ 21.96}_{17.80\ 16.59}$ |
| 0.5 ..... | 0.61 | $18.58^{19.83\ 21.22}_{17.33\ 16.18}$ | $18.96^{20.24\ 21.65}_{17.69\ 16.54}$ | $18.15^{19.36\ 20.66}_{16.90\ 15.62}$ | $18.41^{19.65\ 21.03}_{17.16\ 15.92}$ | $18.03^{19.28\ 20.67}_{16.82\ 15.71}$ | $18.44^{19.69\ 21.08}_{17.19\ 16.04}$ | $17.56^{18.79\ 20.11}_{16.37\ 15.22}$ | $17.84^{19.09\ 20.48}_{16.64\ 15.48}$ |
| 0.6 ..... | 0.60 | $16.45^{17.52\ 18.72}_{15.34\ 14.32}$ | $16.75^{17.86\ 19.09}_{15.64\ 14.62}$ | $16.06^{17.02\ 18.28}_{14.94\ 14.01}$ | $16.28^{17.32\ 18.54}_{15.17\ 14.15}$ | $15.94^{17.06\ 18.21}_{14.88\ 13.86}$ | $16.27^{17.38\ 18.58}_{15.20\ 14.19}$ | $15.51^{16.58\ 17.77}_{14.45\ 13.51}$ | $15.76^{16.87\ 18.03}_{14.69\ 13.68}$ |
| 0.8 ..... | 0.57 | $15.67^{16.69\ 17.80}_{14.60\ 13.68}$ | $15.98^{17.01\ 18.16}_{14.92\ 13.94}$ | $15.24^{16.28\ 17.29}_{14.18\ 13.23}$ | $15.46^{16.50\ 17.54}_{14.39\ 13.47}$ | $15.20^{16.22\ 17.38}_{14.19\ 13.31}$ | $15.48^{16.55\ 17.70}_{14.46\ 13.54}$ | $14.83^{15.81\ 16.92}_{13.81\ 12.92}$ | $15.02^{16.04\ 17.15}_{14.00\ 13.12}$ |
| 1 ..... | 0.54 | $17.89^{19.09\ 20.44}_{16.73\ 15.67}$ | $18.28^{19.48\ 20.84}_{17.09\ 15.98}$ | $17.45^{18.61\ 19.90}_{16.23\ 15.27}$ | $17.69^{18.90\ 20.23}_{16.47\ 15.49}$ | $17.38^{18.58\ 19.88}_{16.27\ 15.16}$ | $17.75^{18.95\ 20.25}_{16.59\ 15.48}$ | $16.96^{18.11\ 19.39}_{15.81\ 14.75}$ | $17.19^{18.40\ 19.69}_{16.04\ 14.97}$ |

[a] For the open-bubble inflation model accounting only for fluctuations generated during the evolution inside the bubble (RP94). At each $\Omega_0$, the first of the five entries in each of cols. (3)–(10) is the maximum likelihood value, the first (vertical) pair delimits the 68.3% (1 $\sigma$) highest posterior density range, and the second (vertical) pair delimits the 95.5% (2 $\sigma$) highest posterior density range.

[b] Accounting for (GC) or ignoring (No GC) the correction for faint high-latitude foreground Galactic emission.

TABLE 3

$Q_{\rm rms\text{-}PS}$ VALUES ($\mu$K) FOR THE $t_0 \simeq 13.5$ Gyr, $\Omega_B h^2 = 0.0205$ OPEN-BUBBLE INFLATION MODELS[a]

| | | ECLIPTIC FRAME | | | | GALACTIC FRAME | | | |
|---|---|---|---|---|---|---|---|---|---|
| $\Omega_0$ (1) | $h$ (2) | No GC[b] ($\ell_{\rm min} = 2$) (3) | No GC[b] ($\ell_{\rm min} = 3$) (4) | GC[b] ($\ell_{\rm min} = 2$) (5) | GC[b] ($\ell_{\rm min} = 3$) (6) | No GC[b] ($\ell_{\rm min} = 2$) (7) | No GC[b] ($\ell_{\rm min} = 3$) (8) | GC[b] ($\ell_{\rm min} = 2$) (9) | GC[b] ($\ell_{\rm min} = 3$) (10) |
| 0.1 ..... | 0.65 | $21.08^{22.66\ 24.37}_{19.56\ 18.17}$ | $21.56^{23.22\ 24.97}_{20.07\ 18.62}$ | $20.40^{22.04\ 23.71}_{18.91\ 17.62}$ | $20.89^{22.52\ 24.23}_{19.35\ 17.98}$ | $20.44^{21.92\ 23.63}_{18.91\ 17.52}$ | $20.90^{22.47\ 24.23}_{19.37\ 17.98}$ | $19.77^{21.31\ 22.97}_{18.33\ 16.96}$ | $20.25^{21.78\ 23.49}_{18.72\ 17.33}$ |
| 0.2 ..... | 0.61 | $24.23^{26.04\ 27.98}_{22.52\ 20.90}$ | $24.84^{26.67\ 28.68}_{23.05\ 21.44}$ | $23.53^{25.25\ 27.21}_{21.86\ 20.18}$ | $24.04^{25.84\ 27.84}_{22.34\ 20.65}$ | $23.44^{25.25\ 27.15}_{21.78\ 20.20}$ | $24.05^{25.85\ 27.84}_{22.33\ 20.71}$ | $22.76^{24.50\ 26.38}_{21.09\ 19.52}$ | $23.26^{25.06\ 27.01}_{21.59\ 19.97}$ |
| 0.25..... | 0.60 | $24.23^{25.99\ 27.89}_{22.52\ 20.90}$ | $24.80^{26.59\ 28.55}_{23.05\ 21.44}$ | $23.53^{25.25\ 27.15}_{21.86\ 20.22}$ | $24.04^{25.81\ 27.75}_{22.34\ 20.70}$ | $23.44^{25.20\ 27.06}_{21.78\ 20.20}$ | $24.00^{25.81\ 27.70}_{22.33\ 20.71}$ | $22.76^{24.46\ 26.33}_{21.09\ 19.56}$ | $23.26^{25.02\ 26.92}_{21.59\ 20.02}$ |
| 0.3 ..... | 0.59 | $23.54^{25.25\ 27.06}_{21.92\ 20.39}$ | $24.12^{25.82\ 27.70}_{22.41\ 20.88}$ | $22.76^{24.50\ 26.36}_{21.25\ 19.81}$ | $23.27^{25.01\ 26.92}_{21.69\ 20.21}$ | $22.84^{24.51\ 26.27}_{21.22\ 19.69}$ | $23.35^{25.06\ 26.92}_{21.73\ 20.20}$ | $22.16^{23.78\ 25.57}_{20.54\ 19.09}$ | $22.61^{24.28\ 26.13}_{20.99\ 19.51}$ |
| 0.35..... | 0.57 | $22.52^{24.09\ 25.81}_{20.94\ 19.51}$ | $23.01^{24.63\ 26.38}_{21.44\ 19.94}$ | $21.89^{23.37\ 25.15}_{20.30\ 18.97}$ | $22.29^{23.85\ 25.67}_{20.70\ 19.34}$ | $21.82^{23.40\ 25.06}_{20.30\ 18.86}$ | $22.33^{23.91\ 25.67}_{20.76\ 19.32}$ | $21.18^{22.71\ 24.37}_{19.69\ 18.28}$ | $21.59^{23.17\ 24.93}_{20.06\ 18.68}$ |
| 0.4 ..... | 0.56 | $21.22^{22.70\ 24.32}_{19.79\ 18.44}$ | $21.69^{23.18\ 24.80}_{20.20\ 18.88}$ | $20.51^{22.06\ 23.75}_{19.23\ 17.88}$ | $20.96^{22.46\ 24.15}_{19.56\ 18.25}$ | $20.62^{22.06\ 23.63}_{19.19\ 17.84}$ | $21.04^{22.52\ 24.14}_{19.60\ 18.26}$ | $19.99^{21.44\ 23.01}_{18.62\ 17.30}$ | $20.39^{21.82\ 23.44}_{18.95\ 17.66}$ |
| 0.45..... | 0.55 | $19.83^{21.22\ 22.70}_{18.54\ 17.29}$ | $20.29^{21.65\ 23.18}_{18.92\ 17.64}$ | $19.26^{20.62\ 22.16}_{17.96\ 16.81}$ | $19.58^{21.03\ 22.53}_{18.30\ 17.11}$ | $19.28^{20.62\ 22.06}_{17.98\ 16.73}$ | $19.69^{21.04\ 22.56}_{18.35\ 17.10}$ | $18.75^{20.03\ 21.48}_{17.43\ 16.24}$ | $19.05^{20.44\ 21.87}_{17.75\ 16.55}$ |
| 0.5 ..... | 0.55 | $18.54^{19.79\ 21.13}_{17.29\ 16.13}$ | $18.92^{20.20\ 21.61}_{17.64\ 16.49}$ | $18.01^{19.20\ 20.57}_{16.81\ 15.69}$ | $18.34^{19.58\ 20.94}_{17.11\ 15.95}$ | $17.98^{19.23\ 20.57}_{16.78\ 15.62}$ | $18.35^{19.60\ 21.04}_{17.15\ 15.99}$ | $17.47^{18.71\ 20.03}_{16.28\ 15.17}$ | $17.80^{19.05\ 20.39}_{16.59\ 15.44}$ |
| 0.6 ..... | 0.53 | $16.36^{17.43\ 18.63}_{15.25\ 14.28}$ | $16.66^{17.77\ 18.96}_{15.56\ 14.54}$ | $15.92^{16.97\ 18.24}_{14.78\ 13.96}$ | $16.14^{17.23\ 18.46}_{14.99\ 14.11}$ | $15.90^{16.96\ 18.12}_{14.83\ 13.81}$ | $16.22^{17.29\ 18.49}_{15.11\ 14.09}$ | $15.43^{16.54\ 17.69}_{14.41\ 13.47}$ | $15.67^{16.78\ 17.94}_{14.60\ 13.63}$ |
| 0.8 ..... | 0.50 | $15.57^{16.59\ 17.70}_{14.56\ 13.63}$ | $15.86^{16.92\ 18.03}_{14.83\ 13.90}$ | $15.21^{16.19\ 17.30}_{14.19\ 13.24}$ | $15.39^{16.41\ 17.52}_{14.32\ 13.42}$ | $15.11^{16.13\ 17.24}_{14.14\ 13.21}$ | $15.39^{16.45\ 17.56}_{14.42\ 13.44}$ | $14.75^{15.73\ 16.84}_{13.77\ 12.87}$ | $14.93^{15.94\ 17.06}_{13.91\ 13.03}$ |
| 1 ..... | 0.48 | $17.80^{18.95\ 20.25}_{16.64\ 15.53}$ | $18.16^{19.35\ 20.67}_{16.96\ 15.86}$ | $17.30^{18.46\ 19.66}_{16.12\ 15.00}$ | $17.59^{18.76\ 20.04}_{16.37\ 15.25}$ | $17.29^{18.44\ 19.74}_{16.18\ 15.11}$ | $17.61^{18.81\ 20.11}_{16.45\ 15.39}$ | $16.84^{17.99\ 19.22}_{15.73\ 14.66}$ | $17.10^{18.26\ 19.56}_{15.94\ 14.88}$ |

[a] For the open-bubble inflation model accounting only for fluctuations generated during the evolution inside the bubble (RP94). At each $\Omega_0$, the first of the five entries in each of cols. (3)–(10) is the maximum likelihood value, the first (vertical) pair delimits the 68.3% (1 $\sigma$) highest posterior density range, and the second (vertical) pair delimits the 95.5% (2 $\sigma$) highest posterior density range.

[b] Accounting for (GC) or ignoring (No GC) the correction for faint high-latitude foreground Galactic emission.

TABLE 4

$Q_{\rm rms\text{-}PS}$ VALUES ($\mu$K) FOR THE $t_0 \simeq 10.5$ Gyr, $\Omega_B h^2 = 0.0055$ FLAT-SPACE SCALE-INVARIANT SPECTRUM OPEN MODELS[a]

| | | ECLIPTIC FRAME | | | | GALACTIC FRAME | | | |
|---|---|---|---|---|---|---|---|---|---|
| $\Omega_0$ (1) | $h$ (2) | No GC[b] ($\ell_{\rm min} = 2$) (3) | No GC[b] ($\ell_{\rm min} = 3$) (4) | GC[b] ($\ell_{\rm min} = 2$) (5) | GC[b] ($\ell_{\rm min} = 3$) (6) | No GC[b] ($\ell_{\rm min} = 2$) (7) | No GC[b] ($\ell_{\rm min} = 3$) (8) | GC[b] ($\ell_{\rm min} = 2$) (9) | GC[b] ($\ell_{\rm min} = 3$) (10) |
| 0.1 ..... | 0.84 | $13.73^{14.62\ 15.63}_{12.78\ 11.96}$ | $14.08^{14.99\ 16.01}_{13.11\ 12.25}$ | $13.29^{14.24\ 15.18}_{12.40\ 11.58}$ | $13.60^{14.52\ 15.52}_{12.64\ 11.82}$ | $13.47^{14.36\ 15.43}_{12.57\ 11.77}$ | $13.79^{14.74\ 15.80}_{12.90\ 12.06}$ | $13.06^{13.97\ 14.99}_{12.20\ 11.39}$ | $13.35^{14.26\ 15.32}_{12.44\ 11.63}$ |
| 0.2 ..... | 0.79 | $17.14^{18.35\ 19.67}_{15.98\ 14.88}$ | $17.57^{18.80\ 20.14}_{16.39\ 15.26}$ | $16.69^{17.83\ 19.13}_{15.52\ 14.41}$ | $17.02^{18.25\ 19.55}_{15.87\ 14.75}$ | $16.70^{17.92\ 19.23}_{15.57\ 14.50}$ | $17.15^{18.38\ 19.70}_{15.98\ 14.88}$ | $16.22^{17.41\ 18.69}_{15.10\ 14.02}$ | $16.57^{17.83\ 19.12}_{15.46\ 14.37}$ |
| 0.25..... | 0.77 | $18.17^{19.40\ 20.76}_{16.90\ 15.72}$ | $18.59^{19.88\ 21.27}_{17.30\ 16.12}$ | $17.68^{18.82\ 20.14}_{16.35\ 15.17}$ | $18.02^{19.26\ 20.63}_{16.72\ 15.53}$ | $17.66^{18.93\ 20.35}_{16.49\ 15.34}$ | $18.11^{19.39\ 20.83}_{16.88\ 15.70}$ | $17.14^{18.37\ 19.77}_{15.96\ 14.83}$ | $17.50^{18.80\ 20.23}_{16.32\ 15.16}$ |
| 0.3 ..... | 0.75 | $18.67^{20.00\ 21.37}_{17.43\ 16.22}$ | $19.12^{20.47\ 21.86}_{17.84\ 16.60}$ | $18.10^{19.47\ 20.79}_{16.92\ 15.72}$ | $18.51^{19.88\ 21.22}_{17.26\ 16.05}$ | $18.15^{19.46\ 20.83}_{16.95\ 15.81}$ | $18.57^{19.94\ 21.32}_{17.36\ 16.20}$ | $17.62^{18.91\ 20.25}_{16.44\ 15.31}$ | $18.00^{19.33\ 20.68}_{16.79\ 15.65}$ |
| 0.35..... | 0.74 | $18.83^{20.05\ 21.42}_{17.54\ 16.37}$ | $19.23^{20.52\ 21.92}_{17.94\ 16.76}$ | $18.31^{19.47\ 20.88}_{17.03\ 15.87}$ | $18.66^{19.88\ 21.27}_{17.35\ 16.19}$ | $18.27^{19.56\ 20.91}_{17.06\ 15.85}$ | $18.70^{20.00\ 21.41}_{17.47\ 16.24}$ | $17.73^{19.02\ 20.36}_{16.55\ 15.36}$ | $18.10^{19.40\ 20.75}_{16.87\ 15.68}$ |
| 0.4 ..... | 0.73 | $18.55^{19.78\ 21.12}_{17.27\ 16.12}$ | $18.96^{20.20\ 21.59}_{17.67\ 16.49}$ | $18.01^{19.23\ 20.51}_{16.74\ 15.60}$ | $18.38^{19.59\ 20.95}_{17.07\ 15.90}$ | $18.03^{19.30\ 20.60}_{16.83\ 15.68}$ | $18.44^{19.72\ 21.04}_{17.21\ 16.03}$ | $17.51^{18.75\ 20.04}_{16.33\ 15.20}$ | $17.87^{19.12\ 20.44}_{16.65\ 15.48}$ |
| 0.45..... | 0.71 | $17.93^{19.14\ 20.43}_{16.76\ 15.68}$ | $18.32^{19.55\ 20.84}_{17.14\ 16.01}$ | $17.47^{18.65\ 19.92}_{16.29\ 15.25}$ | $17.74^{18.98\ 20.25}_{16.59\ 15.50}$ | $17.44^{18.66\ 19.92}_{16.31\ 15.23}$ | $17.83^{19.08\ 20.36}_{16.69\ 15.58}$ | $16.98^{18.16\ 19.39}_{15.85\ 14.77}$ | $17.25^{18.49\ 19.74}_{16.15\ 15.04}$ |
| 0.5 ..... | 0.70 | $17.12^{18.18\ 19.42}_{15.97\ 14.93}$ | $17.46^{18.59\ 19.82}_{16.33\ 15.26}$ | $16.71^{17.59\ 18.95}_{15.46\ 14.53}$ | $16.96^{17.93\ 19.28}_{15.72\ 14.75}$ | $16.68^{17.79\ 18.95}_{15.58\ 14.55}$ | $17.07^{18.13\ 19.35}_{15.88\ 14.89}$ | $16.22^{17.30\ 18.48}_{15.15\ 14.13}$ | $16.51^{17.58\ 18.80}_{15.36\ 14.36}$ |
| 0.6 ..... | 0.68 | $15.01^{15.94\ 17.01}_{14.06\ 13.15}$ | $15.31^{16.28\ 17.35}_{14.34\ 13.43}$ | $14.63^{15.46\ 16.54}_{13.61\ 12.74}$ | $14.85^{15.73\ 16.82}_{13.84\ 12.93}$ | $14.69^{15.63\ 16.65}_{13.73\ 12.83}$ | $15.01^{15.92\ 16.97}_{13.98\ 13.09}$ | $14.29^{15.20\ 16.22}_{13.32\ 12.46}$ | $14.52^{15.44\ 16.49}_{13.54\ 12.64}$ |
| 0.8 ..... | 0.65 | $12.53^{13.33\ 14.23}_{11.76\ 11.03}$ | $12.79^{13.59\ 14.51}_{11.98\ 11.23}$ | $12.22^{12.99\ 13.92}_{11.47\ 10.73}$ | $12.38^{13.18\ 14.11}_{11.60\ 10.86}$ | $12.23^{13.07\ 13.93}_{11.48\ 10.78}$ | $12.49^{13.33\ 14.23}_{11.73\ 10.98}$ | $11.93^{12.73\ 13.59}_{11.18\ 10.48}$ | $12.08^{12.92\ 13.80}_{11.32\ 10.61}$ |
| 1 ..... | 0.62 | $18.09^{19.29\ 20.57}_{16.90\ 15.76}$ | $18.43^{19.66\ 21.00}_{17.24\ 16.12}$ | $17.70^{18.90\ 20.00}_{16.50\ 15.26}$ | $17.92^{19.13\ 20.33}_{16.72\ 15.51}$ | $17.51^{18.65\ 20.05}_{16.32\ 15.29}$ | $17.88^{19.06\ 20.46}_{16.69\ 15.61}$ | $17.08^{18.21\ 19.50}_{15.90\ 14.83}$ | $17.33^{18.46\ 19.81}_{16.14\ 15.06}$ |

[a] For the flat-space scale-invariant spectrum open model (W83). The tabulated $Q_{\rm rms\text{-}PS}$ values are determined from the conditional likelihood function at fixed $\Omega_0$. At each $\Omega_0$, the first of the five entries in each of cols. (3)–(10) is the maximum likelihood value, the first (vertical) pair delimits the 68.3% (1 $\sigma$) highest posterior density range, and the second (vertical) pair delimits the 95.5% (2 $\sigma$) highest posterior density range.

[b] Accounting for (GC) or ignoring (No GC) the correction for faint high-latitude foreground Galactic emission.

TABLE 5

$Q_{\rm rms\text{-}PS}$ VALUES ($\mu$K) FOR THE $t_0 \simeq 12$ Gyr, $\Omega_B h^2 = 0.0125$ FLAT-SPACE SCALE-INVARIANT SPECTRUM OPEN MODELS[a]

| | | ECLIPTIC FRAME | | | | GALACTIC FRAME | | | |
|---|---|---|---|---|---|---|---|---|---|
| $\Omega_0$ (1) | $h$ (2) | No GC[b] ($\ell_{\rm min} = 2$) (3) | No GC[b] ($\ell_{\rm min} = 3$) (4) | GC[b] ($\ell_{\rm min} = 2$) (5) | GC[b] ($\ell_{\rm min} = 3$) (6) | No GC[b] ($\ell_{\rm min} = 2$) (7) | No GC[b] ($\ell_{\rm min} = 3$) (8) | GC[b] ($\ell_{\rm min} = 2$) (9) | GC[b] ($\ell_{\rm min} = 3$) (10) |
| 0.1 ..... | 0.73 | $13.67^{14.63\ 15.61}_{12.79\ 11.95}$ | $14.02^{14.99\ 16.01}_{13.11\ 12.25}$ | $13.24^{14.21\ 15.18}_{12.37\ 11.59}$ | $13.54^{14.53\ 15.52}_{12.66\ 11.82}$ | $13.46^{14.38\ 15.36}_{12.59\ 11.76}$ | $13.79^{14.74\ 15.75}_{12.90\ 12.06}$ | $13.06^{13.97\ 14.94}_{12.20\ 11.39}$ | $13.33^{14.29\ 15.27}_{12.47\ 11.63}$ |
| 0.2 ..... | 0.69 | $17.14^{18.35\ 19.65}_{15.98\ 14.88}$ | $17.57^{18.80\ 20.14}_{16.39\ 15.26}$ | $16.71^{17.83\ 19.05}_{15.52\ 14.40}$ | $17.02^{18.22\ 19.51}_{15.85\ 14.73}$ | $16.70^{17.92\ 19.19}_{15.57\ 14.49}$ | $17.16^{18.38\ 19.65}_{15.98\ 14.85}$ | $16.22^{17.41\ 18.64}_{15.10\ 14.02}$ | $16.57^{17.79\ 19.06}_{15.44\ 14.34}$ |
| 0.25..... | 0.67 | $18.13^{19.35\ 20.79}_{16.83\ 15.74}$ | $18.59^{19.82\ 21.27}_{17.24\ 16.12}$ | $17.63^{18.78\ 20.23}_{16.34\ 15.21}$ | $17.99^{19.21\ 20.67}_{16.68\ 15.57}$ | $17.64^{18.88\ 20.28}_{16.40\ 15.33}$ | $18.09^{19.35\ 20.76}_{16.82\ 15.70}$ | $17.14^{18.32\ 19.71}_{15.90\ 14.83}$ | $17.50^{18.74\ 20.15}_{16.25\ 15.18}$ |
| 0.3 ..... | 0.66 | $18.61^{19.95\ 21.33}_{17.37\ 16.16}$ | $19.07^{20.41\ 21.81}_{17.78\ 16.55}$ | $18.00^{19.39\ 20.80}_{16.88\ 15.68}$ | $18.43^{19.80\ 21.23}_{17.23\ 16.00}$ | $18.17^{19.40\ 20.81}_{16.89\ 15.76}$ | $18.57^{19.86\ 21.32}_{17.32\ 16.16}$ | $17.62^{18.86\ 20.25}_{16.39\ 15.26}$ | $18.00^{19.26\ 20.70}_{16.75\ 15.59}$ |
| 0.35..... | 0.65 | $18.72^{20.02\ 21.36}_{17.48\ 16.26}$ | $19.12^{20.47\ 21.86}_{17.89\ 16.65}$ | $18.20^{19.46\ 20.77}_{16.95\ 15.72}$ | $18.53^{19.84\ 21.20}_{17.30\ 16.07}$ | $18.21^{19.50\ 20.87}_{17.00\ 15.87}$ | $18.64^{19.92\ 21.35}_{17.39\ 16.24}$ | $17.67^{18.96\ 20.31}_{16.49\ 15.36}$ | $18.02^{19.33\ 20.71}_{16.83\ 15.70}$ |
| 0.4 ..... | 0.63 | $18.45^{19.64\ 21.02}_{17.18\ 16.08}$ | $18.86^{20.09\ 21.49}_{17.57\ 16.44}$ | $17.89^{19.12\ 20.51}_{16.62\ 15.57}$ | $18.24^{19.48\ 20.89}_{16.96\ 15.87}$ | $18.00^{19.16\ 20.52}_{16.73\ 15.64}$ | $18.38^{19.60\ 21.00}_{17.10\ 15.99}$ | $17.46^{18.64\ 19.98}_{16.22\ 15.15}$ | $17.79^{19.00\ 20.38}_{16.53\ 15.44}$ |
| 0.45..... | 0.62 | $17.83^{19.03\ 20.32}_{16.69\ 15.55}$ | $18.21^{19.45\ 20.74}_{17.03\ 15.90}$ | $17.35^{18.49\ 19.79}_{16.23\ 15.07}$ | $17.66^{18.83\ 20.15}_{16.51\ 15.35}$ | $17.40^{18.57\ 19.86}_{16.22\ 15.17}$ | $17.77^{20.28\ 20.28}_{16.57\ 15.50}$ | $16.92^{18.05\ 19.34}_{15.74\ 14.72}$ | $17.23^{18.38\ 19.70}_{16.03\ 14.98}$ |
| 0.5 ..... | 0.61 | $17.00^{18.09\ 19.33}_{15.88\ 14.89}$ | $17.35^{18.48\ 19.71}_{16.22\ 15.20}$ | $16.57^{17.63\ 18.84}_{15.40\ 14.44}$ | $16.82^{17.93\ 19.16}_{15.67\ 14.67}$ | $16.57^{17.63\ 18.91}_{15.48\ 14.51}$ | $16.93^{18.01\ 19.29}_{15.80\ 14.81}$ | $16.12^{17.19\ 18.43}_{15.04\ 14.08}$ | $16.38^{17.48\ 18.74}_{15.29\ 14.30}$ |
| 0.6 ..... | 0.60 | $14.92^{15.87\ 16.91}_{13.97\ 13.06}$ | $15.20^{16.17\ 17.24}_{14.24\ 13.32}$ | $14.56^{15.44\ 16.51}_{13.62\ 12.72}$ | $14.77^{15.69\ 16.75}_{13.81\ 12.87}$ | $14.58^{15.57\ 16.57}_{13.65\ 12.75}$ | $14.89^{15.86\ 16.91}_{13.94\ 13.03}$ | $14.18^{15.15\ 16.17}_{13.27\ 12.41}$ | $14.41^{15.40\ 16.40}_{13.48\ 12.56}$ |
| 0.8 ..... | 0.57 | $12.48^{13.23\ 14.12}_{11.64\ 10.91}$ | $12.73^{13.49\ 14.40}_{11.87\ 11.12}$ | $12.17^{12.92\ 13.73}_{11.33\ 10.58}$ | $12.33^{13.07\ 13.94}_{11.47\ 10.73}$ | $12.17^{12.95\ 13.83}_{11.43\ 10.67}$ | $12.41^{13.21\ 14.09}_{11.65\ 10.85}$ | $11.87^{12.63\ 13.49}_{11.12\ 10.37}$ | $12.02^{12.79\ 13.67}_{11.26\ 10.50}$ |
| 1 ..... | 0.54 | $17.87^{19.12\ 20.39}_{16.72\ 15.64}$ | $18.26^{19.50\ 20.79}_{17.08\ 15.96}$ | $17.43^{18.63\ 19.85}_{16.22\ 15.24}$ | $17.67^{18.92\ 20.18}_{16.47\ 15.46}$ | $17.34^{18.57\ 19.83}_{16.25\ 15.13}$ | $17.71^{18.94\ 20.20}_{16.57\ 15.45}$ | $16.92^{18.10\ 19.34}_{15.79\ 14.72}$ | $17.15^{18.39\ 19.64}_{16.02\ 14.94}$ |

[a] For the flat-space scale-invariant spectrum open model (W83). At each $\Omega_0$, the first of the five entries in each of cols. (3)–(10) is the maximum likelihood value, the first (vertical) pair delimits the 68.3% (1 $\sigma$) highest posterior density range, and the second (vertical) pair delimits the 95.5% (2 $\sigma$) highest posterior density range.

[b] Accounting for (GC) or ignoring (No GC) the correction for faint high-latitude foreground Galactic emission.

TABLE 6

$Q_{\rm rms\text{-}PS}$ VALUES ($\mu$K) FOR THE $t_0 \simeq 13.5$ Gyr, $\Omega_B h^2 = 0.0205$ FLAT-SPACE SCALE-INVARIANT SPECTRUM OPEN MODELS[a]

| | | ECLIPTIC FRAME | | | | GALACTIC FRAME | | | |
|---|---|---|---|---|---|---|---|---|---|
| $\Omega_0$ (1) | $h$ (2) | No GC[b] ($\ell_{\rm min} = 2$) (3) | No GC[b] ($\ell_{\rm min} = 3$) (4) | GC[b] ($\ell_{\rm min} = 2$) (5) | GC[b] ($\ell_{\rm min} = 3$) (6) | No GC[b] ($\ell_{\rm min} = 2$) (7) | No GC[b] ($\ell_{\rm min} = 3$) (8) | GC[b] ($\ell_{\rm min} = 2$) (9) | GC[b] ($\ell_{\rm min} = 3$) (10) |
| 0.1 ..... | 0.65 | $13.70^{14.63\ 15.61}_{12.79\ 11.95}$ | $14.02^{14.99\ 16.01}_{13.11\ 12.25}$ | $13.28^{14.23\ 15.20}_{12.39\ 11.57}$ | $13.58^{14.54\ 15.53}_{12.66\ 11.81}$ | $13.47^{14.32\ 15.36}_{12.53\ 11.77}$ | $13.79^{14.70\ 15.76}_{12.85\ 12.08}$ | $13.06^{13.91\ 14.94}_{12.14\ 11.39}$ | $13.35^{14.23\ 15.27}_{12.41\ 11.63}$ |
| 0.2 ..... | 0.61 | $17.09^{18.29\ 19.60}_{15.93\ 14.83}$ | $17.51^{18.75\ 20.09}_{16.33\ 15.20}$ | $16.60^{17.76\ 19.02}_{15.43\ 14.34}$ | $16.96^{18.17\ 19.48}_{15.79\ 14.66}$ | $16.72^{17.87\ 19.19}_{15.53\ 14.50}$ | $17.15^{18.31\ 19.66}_{15.93\ 14.87}$ | $16.22^{17.35\ 18.64}_{15.04\ 14.02}$ | $16.59^{17.75\ 19.08}_{15.40\ 14.34}$ |
| 0.25..... | 0.60 | $18.09^{19.31\ 20.72}_{16.83\ 15.66}$ | $18.53^{19.77\ 21.22}_{17.24\ 16.06}$ | $17.59^{18.76\ 20.17}_{16.34\ 15.16}$ | $17.95^{19.17\ 20.61}_{16.69\ 15.50}$ | $17.58^{18.86\ 20.20}_{16.40\ 15.26}$ | $18.02^{19.31\ 20.70}_{16.82\ 15.64}$ | $17.08^{18.32\ 19.66}_{15.90\ 14.77}$ | $17.45^{18.72\ 20.10}_{16.26\ 15.10}$ |
| 0.3 ..... | 0.59 | $18.56^{19.84\ 21.27}_{17.32\ 16.17}$ | $19.02^{20.31\ 21.76}_{17.73\ 16.55}$ | $17.94^{19.24\ 20.71}_{16.79\ 15.70}$ | $18.37^{19.66\ 21.14}_{17.15\ 16.01}$ | $18.11^{19.36\ 20.77}_{16.86\ 15.70}$ | $18.51^{19.80\ 21.26}_{17.26\ 16.09}$ | $17.57^{18.80\ 20.20}_{16.33\ 15.20}$ | $17.94^{19.20\ 20.64}_{16.69\ 15.54}$ |
| 0.35..... | 0.57 | $18.64^{19.92\ 21.29}_{17.37\ 16.24}$ | $19.07^{20.36\ 21.76}_{17.78\ 16.60}$ | $18.14^{19.32\ 20.75}_{16.84\ 15.79}$ | $18.48^{19.71\ 21.16}_{17.17\ 16.07}$ | $18.14^{19.48\ 20.83}_{16.95\ 15.79}$ | $18.58^{19.90\ 21.33}_{17.33\ 16.18}$ | $17.62^{18.91\ 20.25}_{16.44\ 15.31}$ | $17.96^{19.29\ 20.69}_{16.75\ 15.62}$ |
| 0.4 ..... | 0.56 | $18.34^{19.55\ 20.95}_{17.13\ 16.01}$ | $18.75^{19.98\ 21.38}_{17.51\ 16.39}$ | $17.78^{19.00\ 20.43}_{16.65\ 15.51}$ | $18.15^{19.37\ 20.77}_{16.96\ 15.82}$ | $17.88^{19.12\ 20.41}_{16.71\ 15.57}$ | $18.26^{19.55\ 20.85}_{17.10\ 15.93}$ | $17.35^{18.59\ 19.88}_{16.22\ 15.10}$ | $17.70^{18.94\ 20.23}_{16.53\ 15.38}$ |
| 0.45..... | 0.55 | $17.75^{18.94\ 20.20}_{16.63\ 15.53}$ | $18.16^{19.34\ 20.63}_{16.98\ 15.85}$ | $17.24^{18.37\ 19.72}_{16.12\ 15.10}$ | $17.55^{18.76\ 20.05}_{16.41\ 15.35}$ | $17.29^{18.47\ 19.75}_{16.18\ 15.11}$ | $17.66^{18.84\ 20.20}_{16.52\ 15.45}$ | $16.81^{17.94\ 19.23}_{15.69\ 14.67}$ | $17.10^{18.31\ 19.58}_{15.97\ 14.92}$ |
| 0.5 ..... | 0.55 | $16.89^{18.05\ 19.20}_{15.84\ 14.84}$ | $17.24^{18.43\ 19.61}_{16.17\ 15.15}$ | $16.44^{17.57\ 18.69}_{15.42\ 14.43}$ | $16.73^{17.87\ 19.00}_{15.68\ 14.65}$ | $16.53^{17.60\ 18.82}_{15.43\ 14.44}$ | $16.89^{17.96\ 19.22}_{15.77\ 14.76}$ | $16.06^{17.14\ 18.32}_{14.99\ 14.02}$ | $16.36^{17.43\ 18.63}_{15.26\ 14.24}$ |
| 0.6 ..... | 0.53 | $14.86^{15.81\ 16.84}_{13.91\ 13.04}$ | $15.15^{16.12\ 17.14}_{14.18\ 13.27}$ | $14.45^{15.40\ 16.49}_{13.48\ 12.68}$ | $14.67^{15.63\ 16.71}_{13.68\ 12.85}$ | $14.54^{15.43\ 16.46}_{13.61\ 12.72}$ | $14.84^{15.73\ 16.79}_{13.86\ 12.95}$ | $14.13^{15.04\ 16.06}_{13.22\ 12.36}$ | $14.35^{15.26\ 16.31}_{13.40\ 12.52}$ |
| 0.8 ..... | 0.50 | $12.39^{13.17\ 14.04}_{11.60\ 10.86}$ | $12.63^{13.43\ 14.29}_{11.82\ 11.07}$ | $12.10^{12.85\ 13.70}_{11.31\ 10.58}$ | $12.24^{13.03\ 13.89}_{11.44\ 10.70}$ | $12.11^{12.90\ 13.77}_{11.37\ 10.64}$ | $12.35^{13.15\ 14.03}_{11.59\ 10.85}$ | $11.82^{12.57\ 13.43}_{11.07\ 10.37}$ | $11.96^{12.75\ 13.63}_{11.20\ 10.50}$ |
| 1 ..... | 0.48 | $17.80^{18.94\ 20.21}_{16.65\ 15.52}$ | $18.16^{19.34\ 20.63}_{16.98\ 15.85}$ | $17.30^{18.46\ 19.62}_{16.13\ 14.99}$ | $17.59^{18.75\ 20.00}_{16.38\ 15.25}$ | $17.27^{18.40\ 19.75}_{16.13\ 15.11}$ | $17.59^{18.77\ 20.12}_{16.41\ 15.39}$ | $16.81^{17.94\ 19.23}_{15.69\ 14.67}$ | $17.08^{18.22\ 19.57}_{15.90\ 14.88}$ |

[a] For the flat-space scale-invariant spectrum open model (W83). At each $\Omega_0$, the first of the five entries in each of cols. (3)–(10) is the maximum likelihood value, the first (vertical) pair delimits the 68.3% (1 $\sigma$) highest posterior density range, and the second (vertical) pair delimits the 95.5% (2 $\sigma$) highest posterior density range.

[b] Accounting for (GC) or ignoring (No GC) the correction for faint high-latitude foreground Galactic emission.

TABLE 7

$Q_{\rm rms\text{-}PS}$ VALUES ($\mu$K) FOR THE $h = 0.6$, $\Omega_B = 0.035$ OPEN-BUBBLE INFLATION MODELS[a]

| | | ECLIPTIC FRAME | | | | GALACTIC FRAME | | | |
|---|---|---|---|---|---|---|---|---|---|
| $\Omega_0$ (1) | $t_0$ (2) | No GC[b] ($\ell_{\rm min} = 2$) (3) | No GC[b] ($\ell_{\rm min} = 3$) (4) | GC[b] ($\ell_{\rm min} = 2$) (5) | GC[b] ($\ell_{\rm min} = 3$) (6) | No GC[b] ($\ell_{\rm min} = 2$) (7) | No GC[b] ($\ell_{\rm min} = 3$) (8) | GC[b] ($\ell_{\rm min} = 2$) (9) | GC[b] ($\ell_{\rm min} = 3$) (10) |
| 0.1..... | 14.6 | $26.45^{28.49\ 30.62}_{24.56\ 22.75}$ | $27.15^{29.19\ 31.41}_{25.20\ 23.40}$ | $25.71^{27.71\ 29.74}_{23.77\ 21.95}$ | $26.27^{28.32\ 30.48}_{24.37\ 22.50}$ | $25.57^{27.56\ 29.69}_{23.72\ 21.96}$ | $26.27^{28.31\ 30.48}_{24.37\ 22.56}$ | $24.83^{26.73\ 28.81}_{22.94\ 21.22}$ | $25.39^{27.38\ 29.56}_{23.54\ 21.73}$ |
| 0.2..... | 13.8 | $25.39^{27.29\ 29.32}_{23.58\ 21.92}$ | $26.04^{27.94\ 30.06}_{24.19\ 22.47}$ | $24.59^{26.50\ 28.54}_{22.78\ 21.32}$ | $25.19^{27.10\ 29.19}_{23.33\ 21.75}$ | $24.60^{26.45\ 28.44}_{22.84\ 21.13}$ | $25.20^{27.10\ 29.19}_{23.40\ 21.73}$ | $23.86^{25.67\ 27.66}_{22.10\ 20.48}$ | $24.42^{26.27\ 28.31}_{22.61\ 20.94}$ |
| 0.3..... | 13.2 | $23.40^{25.11\ 26.92}_{21.78\ 20.25}$ | $23.95^{25.67\ 27.56}_{22.29\ 20.76}$ | $22.64^{24.37\ 26.22}_{21.13\ 19.54}$ | $23.15^{24.88\ 26.78}_{21.55\ 20.00}$ | $22.70^{24.37\ 26.13}_{21.08\ 19.60}$ | $23.21^{24.93\ 26.78}_{21.59\ 20.06}$ | $22.01^{23.65\ 25.44}_{20.44\ 18.95}$ | $22.47^{24.14\ 25.99}_{20.85\ 19.37}$ |
| 0.4..... | 12.7 | $21.13^{22.66\ 24.28}_{19.74\ 18.40}$ | $21.64^{23.17\ 24.79}_{20.16\ 18.77}$ | $20.47^{22.11\ 23.63}_{19.24\ 17.90}$ | $20.93^{22.53\ 24.09}_{19.57\ 18.19}$ | $20.53^{21.96\ 23.58}_{19.09\ 17.80}$ | $20.99^{22.52\ 24.09}_{19.56\ 18.21}$ | $19.93^{21.36\ 22.94}_{18.54\ 17.24}$ | $20.34^{21.82\ 23.40}_{18.91\ 17.56}$ |
| 0.5..... | 12.3 | $19.09^{20.39\ 21.78}_{17.80\ 16.55}$ | $19.46^{20.81\ 22.24}_{18.17\ 16.92}$ | $18.64^{19.83\ 21.27}_{17.29\ 16.08}$ | $18.93^{20.20\ 21.59}_{17.61\ 16.31}$ | $18.49^{19.79\ 21.18}_{17.24\ 16.08}$ | $18.91^{20.20\ 21.64}_{17.61\ 16.45}$ | $17.98^{19.23\ 20.67}_{16.73\ 15.62}$ | $18.31^{19.60\ 20.99}_{17.06\ 15.85}$ |
| 0.6..... | 11.9 | $17.33^{18.54\ 19.83}_{16.18\ 15.20}$ | $17.75^{18.95\ 20.20}_{16.55\ 15.44}$ | $16.64^{18.02\ 19.38}_{15.65\ 14.87}$ | $17.06^{18.33\ 19.67}_{15.91\ 15.04}$ | $16.96^{18.07\ 19.32}_{15.81\ 14.69}$ | $17.24^{18.44\ 19.74}_{16.13\ 15.02}$ | $16.50^{17.61\ 18.81}_{15.34\ 14.23}$ | $16.78^{17.89\ 19.14}_{15.57\ 14.46}$ |
| 0.7..... | 11.6 | $16.36^{17.47\ 18.72}_{15.34\ 14.46}$ | $16.69^{17.84\ 19.09}_{15.67\ 14.74}$ | $15.90^{17.01\ 18.26}_{14.88\ 14.09}$ | $16.13^{17.29\ 18.54}_{15.11\ 14.28}$ | $16.04^{17.10\ 18.26}_{14.93\ 13.91}$ | $16.36^{17.47\ 18.63}_{15.25\ 14.19}$ | $15.57^{16.64\ 17.80}_{14.46\ 13.54}$ | $15.81^{16.92\ 18.07}_{14.69\ 13.72}$ |
| 0.8..... | 11.3 | $16.27^{17.38\ 18.63}_{15.30\ 14.42}$ | $16.55^{17.70\ 18.95}_{15.57\ 14.65}$ | $15.92^{16.87\ 18.22}_{14.90\ 14.11}$ | $16.13^{17.15\ 18.47}_{15.10\ 14.26}$ | $15.90^{17.01\ 18.12}_{14.83\ 13.81}$ | $16.27^{17.33\ 18.49}_{15.16\ 14.09}$ | $15.44^{16.50\ 17.66}_{14.37\ 13.44}$ | $15.71^{16.78\ 17.94}_{14.60\ 13.63}$ |
| 0.9..... | 11.1 | $16.82^{17.98\ 19.23}_{15.76\ 14.83}$ | $17.19^{18.35\ 19.65}_{16.08\ 15.11}$ | $16.30^{17.45\ 18.71}_{15.30\ 14.42}$ | $16.61^{17.72\ 19.02}_{15.53\ 14.60}$ | $16.50^{17.61\ 18.77}_{15.39\ 14.32}$ | $16.82^{17.94\ 19.14}_{15.71\ 14.60}$ | $16.04^{17.15\ 18.31}_{14.93\ 13.91}$ | $16.31^{17.38\ 18.58}_{15.16\ 14.09}$ |

[a] For the open-bubble inflation model accounting for fluctuations generated during the evolution inside the bubble (RP94), as well as those that come into the bubble from the first epoch of inflation (BGT; YST) and those that correspond to a non–square integrable basis function (YST). At each $\Omega_0$, the first of the five entries in each of cols. (3)–(10) is the maximum likelihood value, the first (vertical) pair delimits the 68.3% (1 $\sigma$) highest posterior density range, and the second (vertical) pair delimits the 95.5% (2 $\sigma$) highest posterior density range.

[b] Accounting for (GC) or ignoring (No GC) the correction for faint high-latitude foreground Galactic emission.

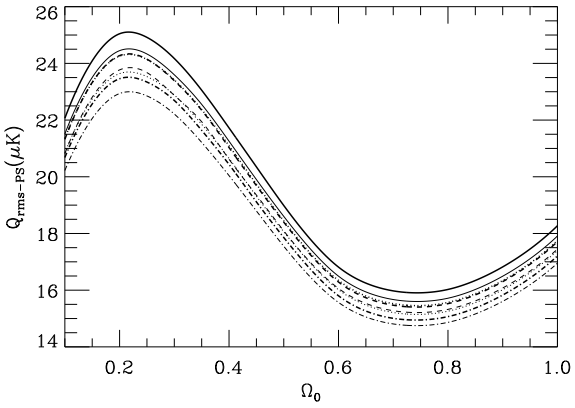


FIG. 7.—Ridge lines of the maximum likelihood $Q_{rms\text{-}PS}$ value as a function of $\Omega_0$, for the open-bubble inflation model accounting only for fluctuations generated during the evolution inside the bubble (type [1] spectra), for the eight different DMR data sets considered here, and for $t_0 \simeq 12$ Gyr, $\Omega_B h^2 = 0.0125$. Heavy lines correspond to the case when the quadrupole moment is excluded from the analysis, while light lines account for the quadrupole moment. These are for the ecliptic-frame sky maps, accounting for (*dashed lines*) and ignoring (*solid lines*) the faint high-latitude foreground Galactic emission correction, and for the galactic-frame maps, accounting for (*dot-dashed lines*) and ignoring (*dotted lines*) this Galactic emission correction. The general features of this figure are consistent with that derived from the DMR two-year data (GRSB, Fig. 2).

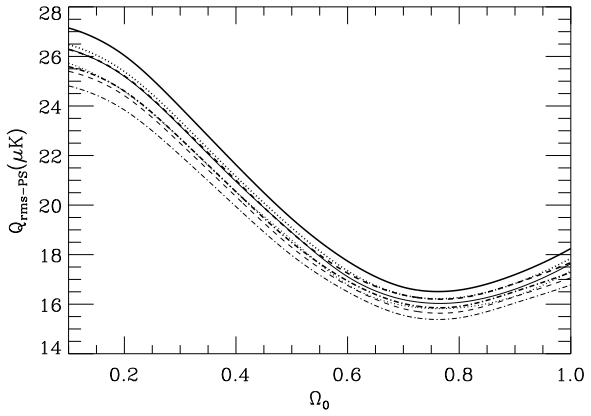


FIG. 9.—Ridge lines of the maximum likelihood $Q_{rms\text{-}PS}$ value as a function of $\Omega_0$, for the open-bubble inflation model now also accounting for both the fluctuations generated in the first epoch of inflation (BGT; YST) and those from a non–square-integrable basis function (YST), for the eight different DMR data sets considered here, and for $h = 0.6$, $\Omega_B = 0.035$. Heavy lines correspond to the cases where the faint high-latitude foreground Galactic emission correction is ignored, while light lines account for this Galactic emission correction. These are from the ecliptic frame analyses, accounting for (*dotted lines*) or ignoring (*solid lines*) the quadrupole moment; and from the galactic-frame analyses, accounting for (*dot-dashed lines*) or ignoring (*dashed lines*) the quadrupole moment. The general features of this figure are consistent with that derived from the DMR two-year data (YB, Fig. 2).

ing the $\ell = 2$ moment from the analysis. These values are recorded in columns (5) and (8) of Tables 9–12 and columns (2), (4), and (6) of Table 13.[18]

Figure 11 compares the ridge lines of maximum likelihood $Q_{rms\text{-}PS}$ value, as a function of $\Omega_0$, for the four different CMB anisotropy angular spectra considered here, and Figure 13 compares some of the conditional (fixed $\Omega_0$ slice) likelihood densities for $Q_{rms\text{-}PS}$ for these four CMB anisotropy angular spectra.

[18] Since different grids (in $Q_{rms\text{-}PS}$) were used in the likelihood analyses of the various model spectra, and different interpolation methods were used in the determination of the $Q_{rms\text{-}PS}$ values, there are small (but insignificant) differences in the quoted $Q_{rms\text{-}PS}$ values for some identical models in these tables.

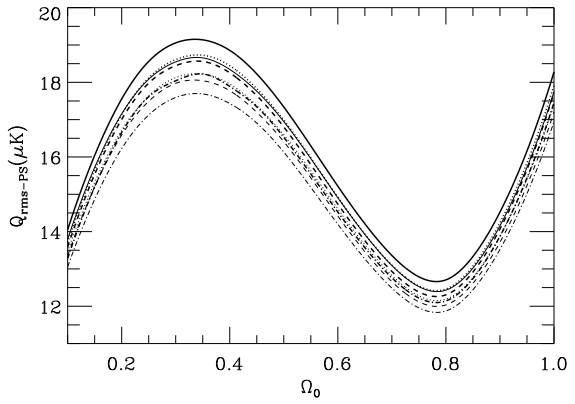


FIG. 8.—Ridge lines of the maximum likelihood $Q_{rms\text{-}PS}$ value as a function of $\Omega_0$, for the flat-space scale-invariant spectrum open model (type [4] spectra), for the eight different DMR data sets, and for $t_0 \simeq 12$ Gyr, $\Omega_B h^2 = 0.0125$. Heavy lines correspond to the ecliptic-frame analyses, while light lines are from the galactic-frame analyses. These are for the cases ignoring the faint high-latitude Galactic emission correction, and either including (*dotted lines*) or excluding (*solid lines*) the quadrupole moment; and accounting for this Galactic emission correction, and either including (*dot-dashed lines*) or excluding (*dashed lines*) the quadrupole moment. The general features of this figure are roughly consistent with that derived from the DMR two-year data (Cayón et al. 1996, Fig. 3).

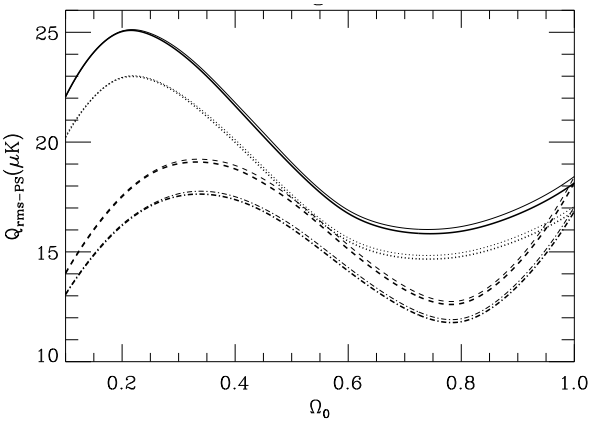


FIG. 10.—Ridge lines of the maximum likelihood $Q_{rms\text{-}PS}$ value as a function of $\Omega_0$, for the two extreme DMR data sets, and two different CMB anisotropy angular spectra, showing the effects of varying $t_0$ and $\Omega_B h^2$. Heavy lines are for $t_0 \simeq 13.5$ Gyr and $\Omega_B h^2 = 0.0205$, while light lines are for $t_0 \simeq 10.5$ Gyr and $\Omega_B h^2 = 0.0055$. Two of the four pairs of lines are for the open-bubble inflation model accounting only for fluctuations generated during the evolution inside the bubble (type [1] spectra), either from the ecliptic-frame analysis without the faint high-latitude Galactic emission correction and ignoring the quadrupole moment in the analysis (*solid lines*), or from the galactic-frame analysis accounting for this Galactic emission correction and including the quadrupole moment in the analysis (*dotted lines*). The other two of the four pairs of lines are for the flat-space scale-invariant spectrum open model (type [4] spectra), either from the ecliptic-frame analysis without the faint high-latitude Galactic emission correction and ignoring the quadrupole moment in the analysis (*dashed lines*), or from the galactic-frame analysis accounting for this Galactic emission correction and including the quadrupole moment in the analysis (*dot-dashed lines*). Given the other uncertainties, the effects of varying $t_0$ and $\Omega_B h^2$ are fairly negligible.

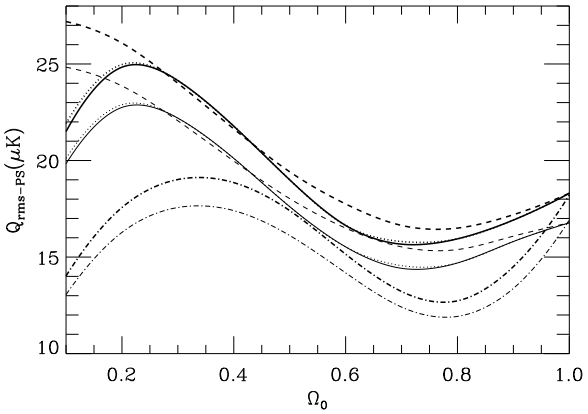


FIG. 11.—Ridge lines of the maximum likelihood $Q_{rms\text{-}PS}$ value as a function of $\Omega_0$, for the two extreme DMR data sets, for the four CMB anisotropy angular spectra models considered here, and for $h = 0.6, \Omega_B = 0.035$. Heavy lines are from the ecliptic-frame sky maps ignoring the faint high-latitude foreground Galactic emission correction and excluding the quadrupole moment from the analysis, while light lines are from the galactic-frame sky maps accounting for this Galactic emission correction and including the quadrupole moment in the analysis. Solid, dotted, and dashed lines show the open-bubble inflation cases, accounting only for the fluctuations generated during the evolution inside the bubble (type [1] spectra, *solid lines*), also accounting for the fluctuations generated in the first epoch of inflation (type [2] spectra, *dotted lines*—these overlap the solid lines except for $\Omega_0 \lesssim 0.2$ and $\Omega_0 \sim 0.7$), and finally also accounting for the fluctuations corresponding to the non–square-integrable basis function (type [3] spectra, *dashed lines*). Dot-dashed lines correspond to the flat-space scale-invariant spectrum open model (type [4] spectra).

Approximate fitting formulae may be derived to describe the above two extreme 2 $\sigma$ limits. For the open-bubble inflation model (RP94; BGT; YST), not including a contribution from a non–square-integrable basis function, we have

$$Q_{rms\text{-}PS}(\Omega_0)/\mu K \simeq 19^{+3.50}_{-3.25} + (4.95^{+1.1}_{-1.2} - \Omega_0) \times \sin\left[2\pi\{1 + 0.25(1.1 - \Omega_0)\}\{\Omega_0 - 0.05\}\right], \quad (5)$$

which is good to better than $\sim 5\%$ for all values of $\Omega_0$ (and to better than $\sim 2\%$ over the observationally viable range of $0.3 \lesssim \Omega \lesssim 0.6$). For those models including a contribution from the non–square-integrable basis function (YST), we have

$$Q_{rms\text{-}PS}(\Omega_0)/\mu K \simeq 21^{+3.7}_{-4.0} + (5.55^{+1.1}_{-1.1} - \Omega_0) \times \cos\left[1.25\pi\{1 + 0.25(1.1 - \Omega_0)\}\{\Omega_0 - 0.05\}\right], \quad (6)$$

mostly good to better than $\sim 2\%$. The flat-space scale-invariant spectrum open model fitting formula is

$$Q_{rms-PS}(\Omega_0)/\mu K \simeq 15^{+2.95}_{-2.50} + (3.25^{+0.6}_{-0.8}) \times \sin\left[2\pi(1 + 0.25\Omega_0)(\Omega_0 + 0.05) - 1.25\right], \quad (7)$$

generally good to better than $\sim 4\%$, except near $\Omega_0 \sim 0.1$ and $\Omega_0 \sim 1$, where the deviations are larger. Further details about these fitting formulae may be found in Stompor (1997).

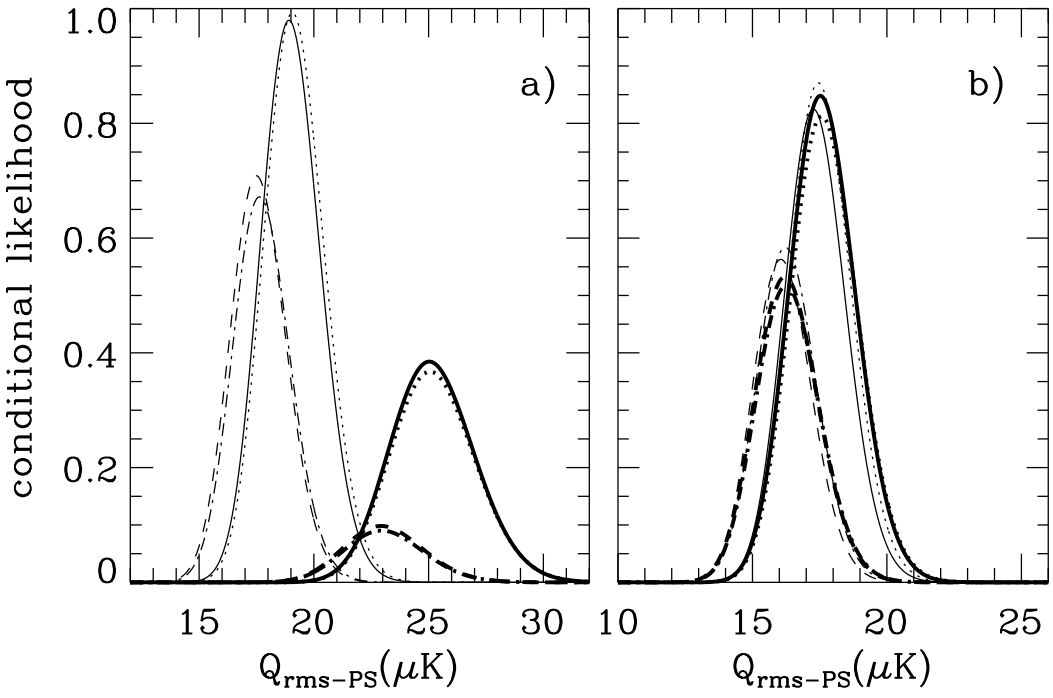


FIG. 12.—Conditional likelihood densities for $Q_{rms\text{-}PS}$, derived from $L(Q_{rms\text{-}PS}, \Omega_0)$ (which are normalized to be unity at the peak, for each DMR data set, CMB anisotropy angular spectrum, and set of model parameter values). Panel (*a*) is for the open-bubble inflation model accounting only for fluctuations generated during the evolution inside the bubble (type [1] spectra), while panel (*b*) is for the flat-space scale-invariant spectrum open model (type [4] spectra). The heavy lines are for $\Omega_0 = 0.2$, while the light lines are for $\Omega_0 = 0.5$. Two of the four pairs of lines in each panel correspond to the results from the analysis of the galactic-frame maps accounting for the faint high-latitude foreground Galactic emission correction and with the quadrupole moment included in the analysis, either for $t_0 \simeq 10.5$ Gyr and $\Omega_B h^2 = 0.0055$ (*dot-dashed lines*), or for $t_0 \simeq 13.5$ Gyr and $\Omega_B h^2 = 0.0205$ (*dashed lines*). The other two pairs of lines in each panel correspond to the results from the analysis of the ecliptic-frame maps ignoring this Galactic emission correction and with the quadrupole moment excluded from the analysis, either for $t_0 \simeq 10.5$ Gyr and $\Omega_B h^2 = 0.0055$ (*dotted lines*), or for $t_0 \simeq 13.5$ Gyr and $\Omega_B h^2 = 0.0205$ (*solid lines*). Given the other uncertainties, the effects of varying $t_0$ and $\Omega_B h^2$ are fairly negligible.

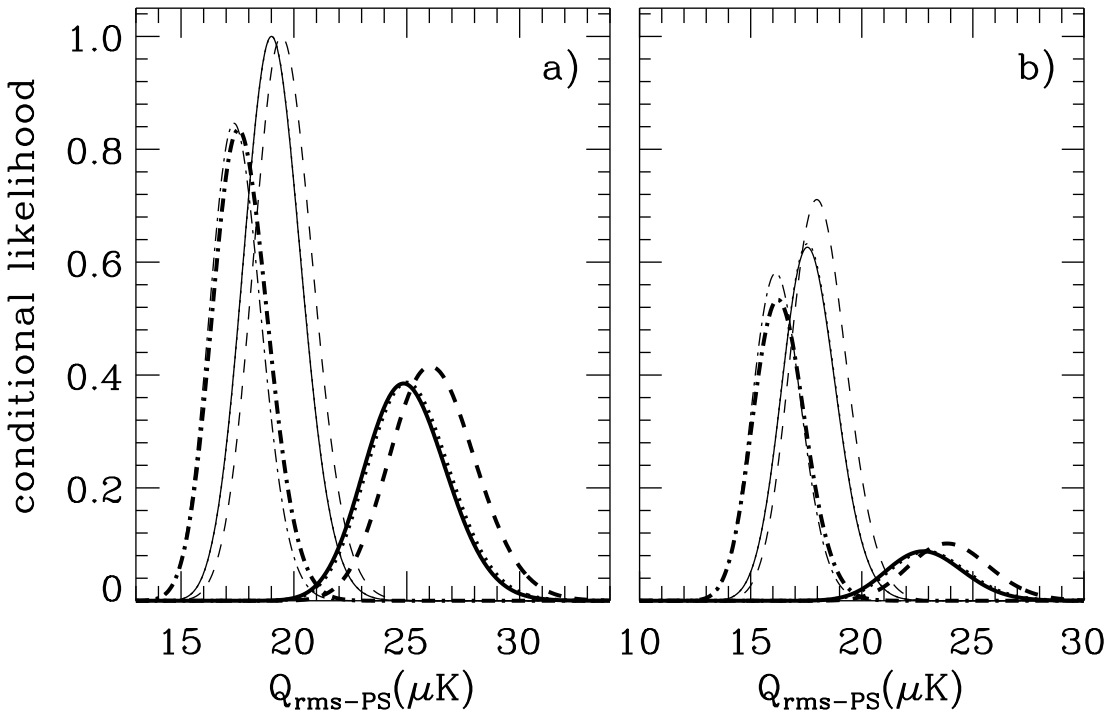


FIG. 13.—Conditional likelihood densities for $Q_{\text{rms-PS}}$ normalized as in the legend for Fig. 12. Panel (*a*) is from the analysis of the ecliptic-frame maps ignoring the faint high-latitude foreground Galactic emission correction and excluding the quadrupole moment from the analysis, while panel (*b*) is from the analysis of the galactic-frame maps accounting for this Galactic emission correction and including the quadrupole moment in the analysis. These are for $h = 0.6$ and $\Omega_B = 0.035$. The heavy lines are for $\Omega_0 = 0.2$ and the light lines are for $\Omega_0 = 0.5$. There are eight lines (four pairs) in each panel, although in each panel two pairs almost identically overlap. Solid, dotted, and dashed lines show the open-bubble inflation cases, accounting only for the fluctuations generated during the evolution inside the bubble (type [1] spectra, *solid lines*), also accounting for the fluctuations generated in the first epoch of inflation (type [2] spectra, *dotted lines*—these almost identically overlap the solid lines), and finally also accounting for the fluctuations corresponding to the non–square-integrable basis function (type [3] spectra, *dashed lines*). Dot-dashed lines correspond to the flat-space scale-invariant spectrum open model (type [4] spectra).

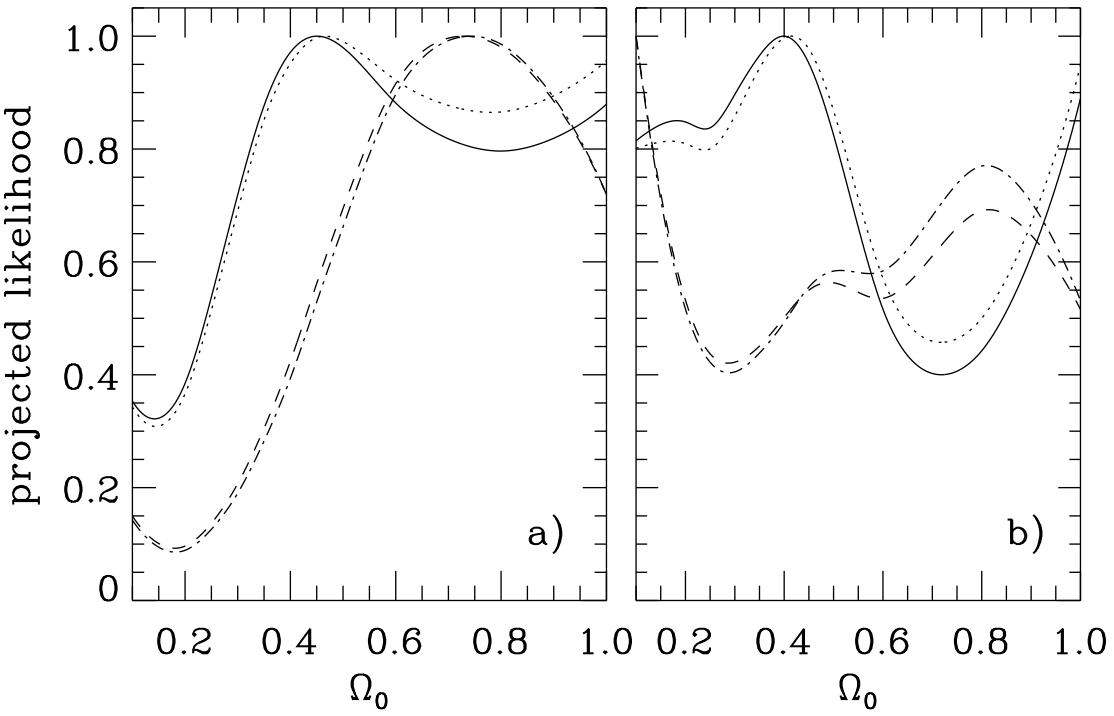


FIG. 14.—Projected likelihood densities for $\Omega_0$ derived from $L(Q_{\text{rms-PS}}, \Omega_0)$ (normalized as in the legend of Fig. 12). Panel (*a*) is for the open-bubble inflation model accounting only for the fluctuations generated during the evolution inside the bubble (type [1] spectra), and panel (*b*) is for the flat-space scale-invariant spectrum open model (type [4] spectra). Two of the curves in each panel correspond to the results from the analysis of the galactic-frame maps accounting for the faint high-latitude Galactic emission correction and with the quadrupole moment included in the analysis, for $t_0 \simeq 10.5$ Gyr and $\Omega_B h^2 = 0.0055$ (*dot-dashed lines*) and for $t_0 \simeq 13.5$ Gyr and $\Omega_B h^2 = 0.0205$ (*dashed lines*). The other two curves in each panel are from the analysis of the ecliptic-frame maps ignoring the Galactic emission correction and excluding the quadrupole moment from the analysis, for $t_0 \simeq 10.5$ Gyr and $\Omega_B h^2 = 0.0055$ (*dotted lines*) and for $t_0 \simeq 13.5$ Gyr and $\Omega_B h^2 = 0.0205$ (*solid lines*).

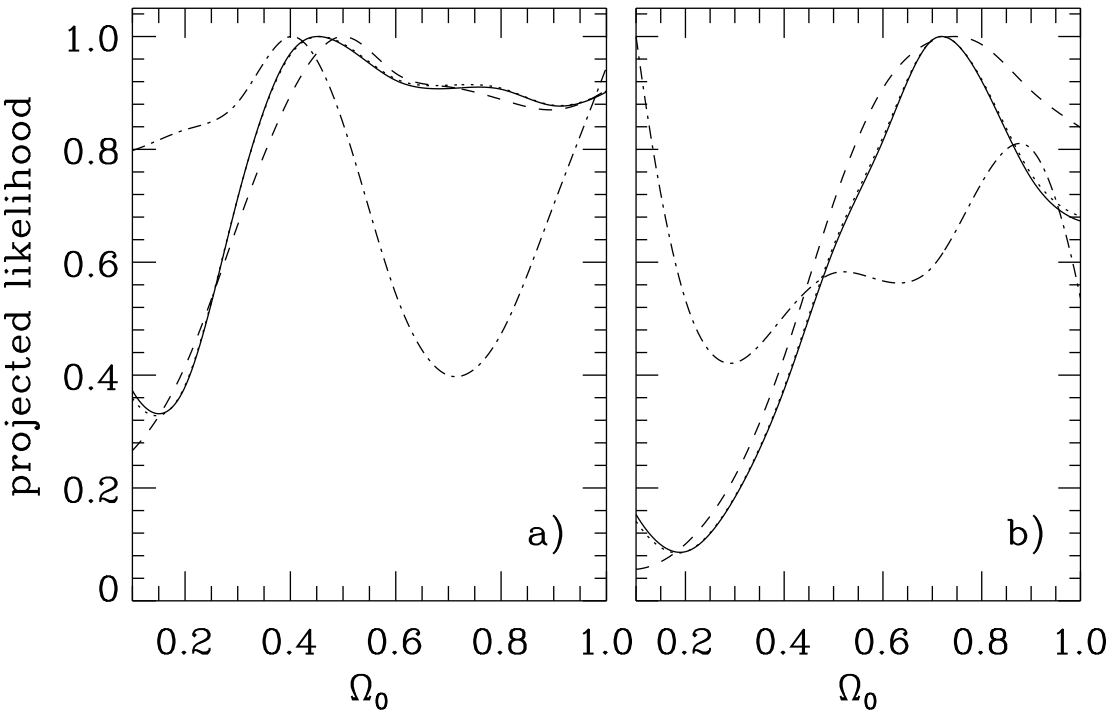


FIG. 15.—Projected likelihood densities for $\Omega_0$ derived from $L(Q_{\text{rms-PS}}, \Omega_0)$ (normalized as in the legend of Fig. 12). Panel (*a*) is from the analysis of the ecliptic-frame sky maps ignoring the faint high-latitude foreground Galactic emission correction and excluding the quadrupole moment from the analysis. Panel (*b*) is from the analysis of the galactic-frame sky maps accounting for this Galactic emission correction and including the quadrupole moment in the analysis. There are four curves in each panel, although in each panel two of them almost overlap. Solid, dotted, and dashed lines show the open-bubble inflation cases, accounting only for the fluctuations generated during the evolution inside the bubble (type [1] spectra, *solid lines*), also accounting for the fluctuations generated in the first epoch of spatially flat inflation (type [2] spectra, *dotted lines*—these almost exactly overlap the solid lines), and finally also accounting for the fluctuations corresponding to the non–square-integrable basis function (type [3] spectra, *dashed lines*). Dot-dashed lines correspond to the flat-space scale-invariant spectrum open model (type [4] spectra). These are for $h = 0.6$ and $\Omega_B = 0.035$.

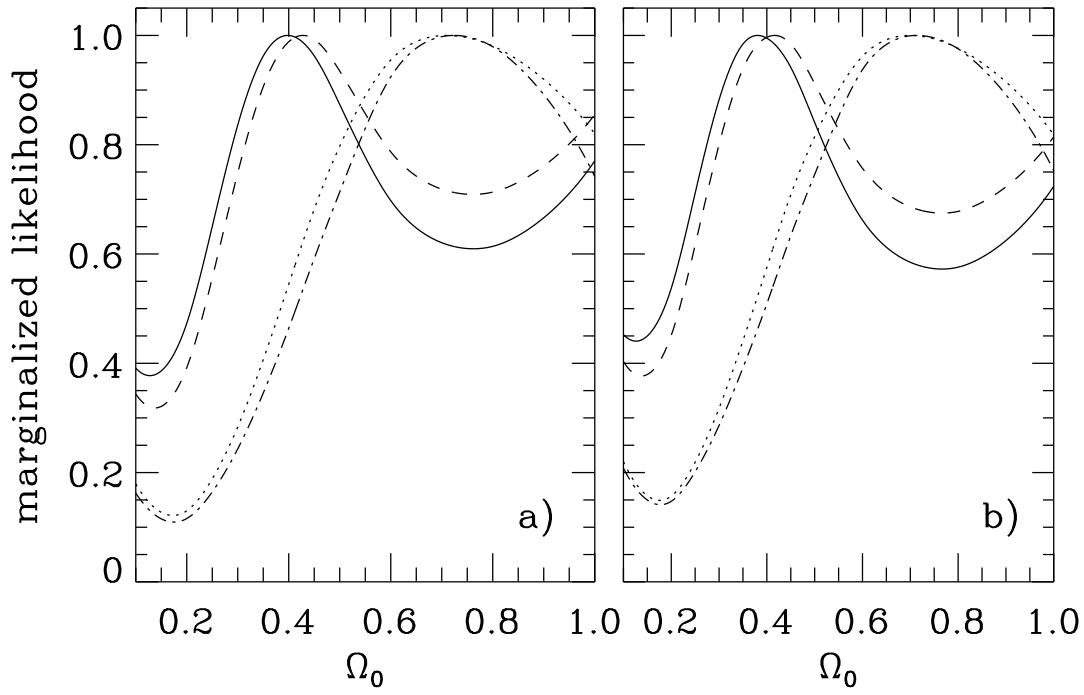


FIG. 16.—Marginal likelihood densities $[\propto \int dQ_{\text{rms-PS}}\, L(Q_{\text{rms-PS}}, \Omega_0)]$ for $\Omega_0$, normalized to unity at the peak, for the open-bubble inflation model accounting only for fluctuations generated during the evolution inside the bubble (RP94), for the eight different DMR data sets, and for $t_0 \simeq 12$ Gyr, $\Omega_B h^2 = 0.0125$. Panel (a) is from the ecliptic-frame analyses, and panel (*b*) is from the galactic-frame analyses. Two of the four lines in each panel are from the analysis without the faint high-latitude foreground Galactic emission correction, either accounting for (*dot-dashed lines*) or ignoring (*solid lines*) the quadrupole moment. The other two lines in each panel are from the analysis with this Galactic emission correction, either accounting for (*dotted lines*) or ignoring (*dashed lines*) the quadrupole moment.

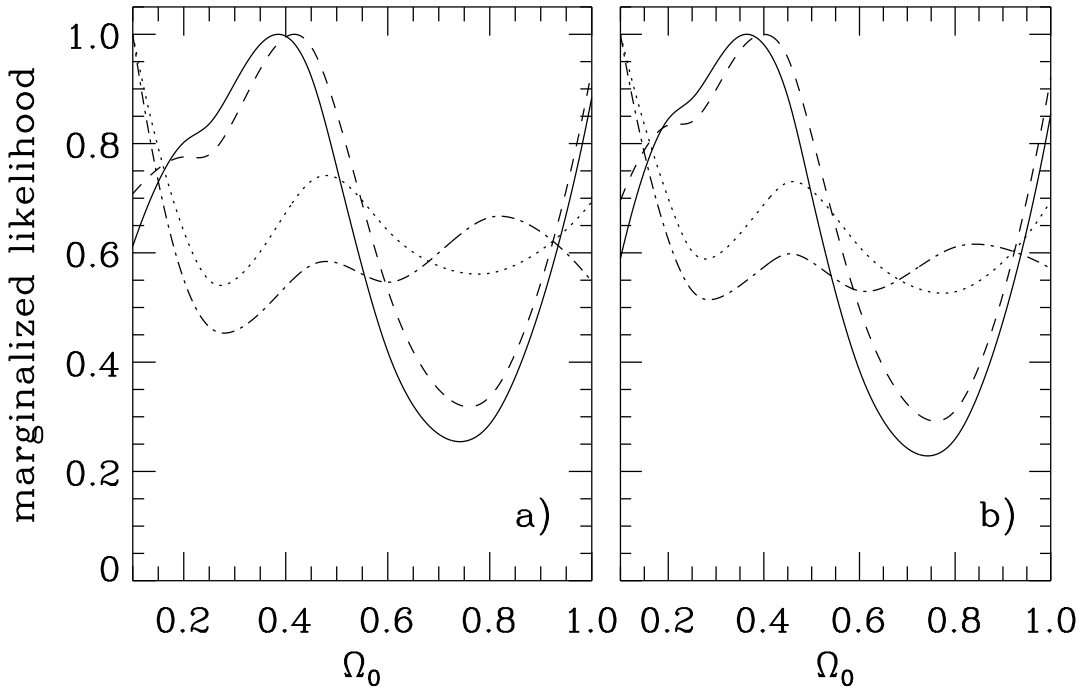


FIG. 17.—Marginal likelihood densities for $\Omega_0$, for the flat-space scale-invariant spectrum open model (W83). Conventions and parameter values are as in the legend of Fig. 16.

The approximate fitting formulae (5)–(7) provide a convenient, portable normalization of the open models. It is important, however, to note that they have been derived using the $Q_{\text{rms-PS}}$ values determined for a given $h$ and $\Omega_B$ and hence do not account for the additional uncertainty (which could be as large as $\sim 2\%$) owing to allowed variations in these parameters. We emphasize that in our analysis here we make use of the actual $Q_{\text{rms-PS}}$ values derived from the likelihood analyses, not these fitting formulae.

Figures 14 and 15 show projected likelihood densities for $\Omega_0$ for some of the models and DMR data sets considered here. Note that the general features of the projected likelihood densities for the open-bubble inflation model accounting only for the fluctuations generated during the evolution

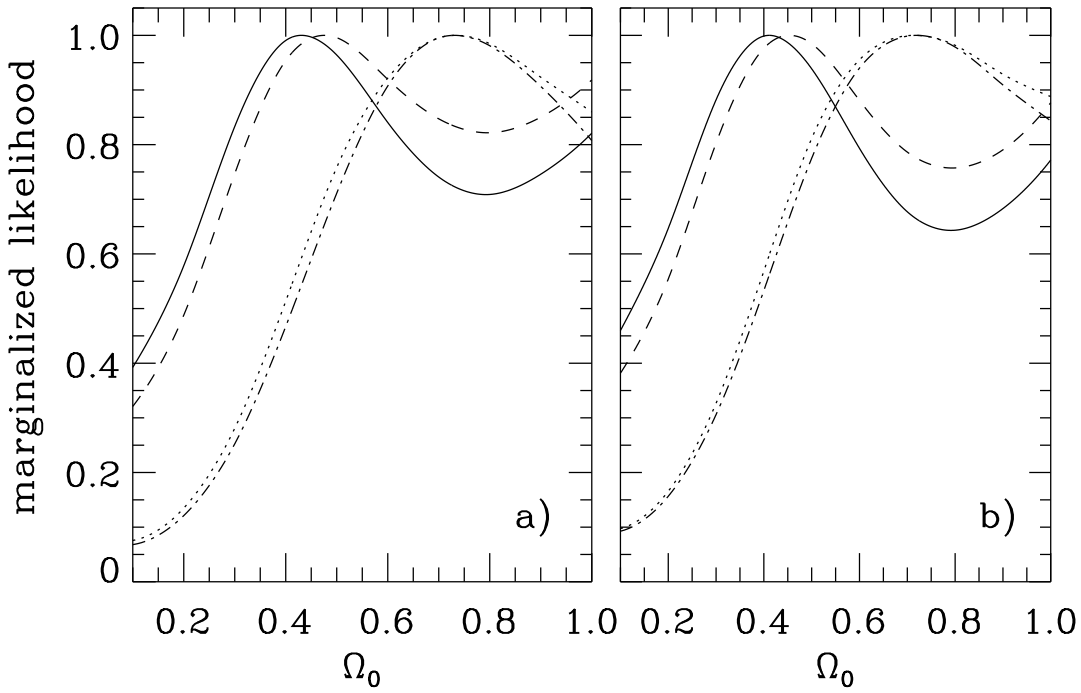


FIG. 18.—Marginal likelihood densities for $\Omega_0$, for the open-bubble inflation model now also accounting for both the fluctuations generated in the first spatially flat epoch of inflation and those that correspond to the non–square-integrable basis function (YST), computed for $h = 0.6$ and $\Omega_B = 0.035$. Conventions are as in the legend of Fig. 16.

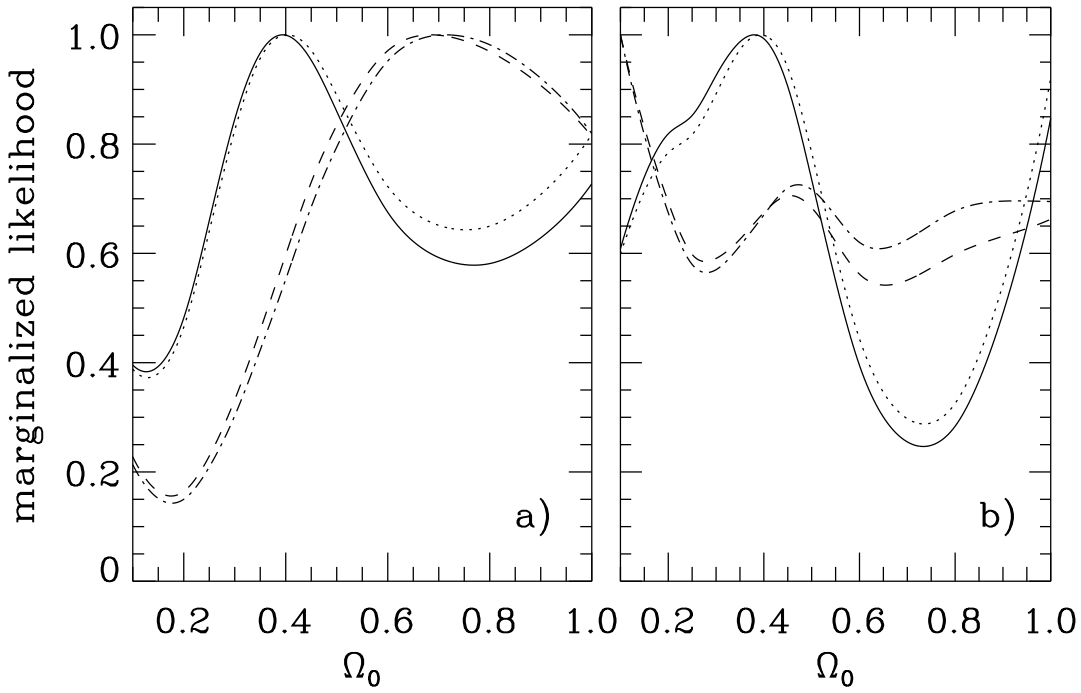


FIG. 19.—Marginal likelihood densities for $\Omega_0$ (normalized as in the legend of Fig. 16). Panel (*a*) is for the open-bubble inflation model accounting only for the fluctuations generated during the evolution inside the bubble (RP94), while panel (*b*) is for the flat-space scale-invariant spectrum open model (W83). Two of the lines in each panel are the results from the analysis of the galactic-frame data sets accounting for the faint high-latitude foreground Galactic emission correction and with the quadrupole moment included in the analysis, for $t_0 \simeq 10.5$ Gyr and $\Omega_B h^2 = 0.0055$ (*dot-dashed lines*), and for $t_0 \simeq 13.5$ Gyr and $\Omega_B h^2 = 0.0205$ (*dashed lines*). The other two lines in each panel are the results from the analysis of the ecliptic-frame data sets ignoring this Galactic emission correction and with the quadrupole moment excluded from the analysis, for $t_0 \simeq 10.5$ Gyr and $\Omega_B h^2 = 0.0055$ (*dotted lines*), and for $t_0 \simeq 13.5$ Gyr and $\Omega_B h^2 = 0.0205$ (*solid lines*).

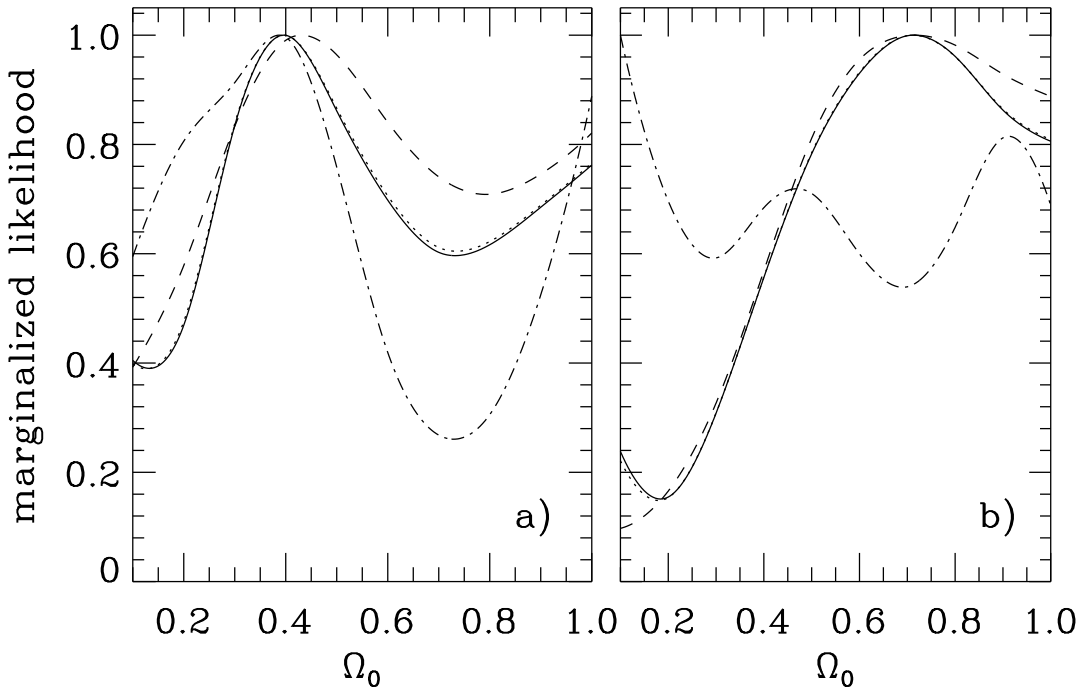


FIG. 20.—Marginal likelihood densities for $\Omega_0$ (normalized as in the caption of Fig. 16), computed for $h = 0.6$ and $\Omega_B = 0.035$. Panel (*a*) is from the analysis of the ecliptic-frame sky maps ignoring the faint high-latitude foreground Galactic emission correction and excluding the quadrupole moment from the analysis. Panel (*b*) is from the analysis of the galactic-frame sky maps accounting for this Galactic emission correction and including the quadrupole moment in the analysis. There are four lines in each panel, although in each panel two of the lines almost overlap. Solid, dotted, and dashed curves are the open-bubble inflation cases, accounting only for the fluctuations generated during the evolution inside the bubble (RP94; *solid lines*), also accounting for the fluctuations generated in the first epoch of spatially flat inflation (BGT; YST, *dotted lines*—these almost identically overlap the solid lines), and finally also accounting for the fluctuations corresponding to the non–square-integrable basis function (YST; *dashed lines*). Dot-dashed curves correspond to the flat-space scale-invariant spectrum open model (W83).

TABLE 8

GAUGE-INVARIANT FRACTIONAL ENERGY-DENSITY PERTURBATION POWER SPECTRUM NORMALIZATION FACTOR $Ah^4$ [a]

| $\Omega_0$ (1) | Inflation Model[b] $Ah^4$ ($10^5$ Mpc$^4$) (2) | Inflation Model[c] $Ah^4$ ($10^5$ Mpc$^4$) (3) | Scale-Invariant Model[d] $Ah^4$ ($10^5$ Mpc$^4$) (4) |
|---|---|---|---|
| 0.1 ..... | 1.49 | 1.42 | 7.00 |
| 0.2 ..... | 1.36 | 1.34 | 3.94 |
| 0.25..... | 1.44 | 1.43 | 3.52 |
| 0.3 ..... | 1.58 | 1.58 | 3.34 |
| 0.35..... | 1.78 | 1.78 | 3.31 |
| 0.4 ..... | 2.03 | 2.03 | 3.40 |
| 0.45..... | 2.34 | 2.34 | 3.60 |
| 0.5 ..... | 2.69 | 2.68 | 3.89 |
| 0.6 ..... | 3.37 | 3.35 | 4.80 |
| 0.8 ..... | 3.26 | 3.24 | 5.59 |
| 1 ..... | 2.03 | 2.03 | 2.03 |

[a] Normalized to $Q_{\text{rms-PS}} = 10\ \mu$K and scale like $(Q_{\text{rms-PS}}/10\ \mu\text{K})^2$. These are computed for $t_0 \simeq 12$ Gyr and $\Omega_B h^2 = 0.0125$, and over the range of these parameters considered here only the third significant figure in the numerical value for $A$ depends (weakly) on the values of these parameters.

[b] For the open-bubble inflation model, accounting only for fluctuations generated during the evolution inside the bubble (RP94).

[c] For the open-bubble inflation model, now also accounting for fluctuations generated in the first epoch of inflation (BGT; YST).

[d] For the flat-space scale-invariant spectrum open model (W83).

inside the bubble (spectrum [1] above) are consistent with those derived from the DMR two-year data (GRSB, Fig. 3). However, since we compute only down to $\Omega_0 = 0.1$ here, only the rise to the prominent peak at very low $\Omega_0$ (GRSB) is seen. BW show in the middle left-hand panel of their Figure 11 the likelihood density for $\Omega_0$ for the same open-bubble inflation model, the general features of which are consistent with those derived here.

Figures 16–20 show marginal likelihood densities for $\Omega_0$ for some of the models and DMR data sets considered here. For the open-bubble inflation model accounting only for the fluctuations generated during the evolution inside the bubble (RP94), the DMR 2 year data galactic-frame (quadrupole moment excluded and included) marginal likelihoods are shown in Figure 3 of GRSB and are in general concord with those shown in Figure 16 here (although, again, only the rise to the prominent low-$\Omega_0$ peak is seen here). Note that now, especially for the quadrupole-excluded case, the peaks and troughs are more prominent (although still not greatly statistically significant). Furthermore, comparing the solid line of Figure 16*b* here to the heavy dotted line of Figure 3 of GRSB, one notices that the intermediate-$\Omega_0$ peak is now at $\Omega_0 \lesssim 0.4$, instead of at $\Omega_0 \sim 0.5$ for the DMR 2 year data.

For the open-bubble inflation model now also accounting for both the fluctuations generated in the first spatially flat epoch of inflation (BGT; YST) and those from the non–square-integrable basis function (YST), the DMR 2 year data ecliptic-frame quadrupole-included marginal likelihood (shown as the solid line in Fig. 3 of YB) is in general agreement with the dot-dashed line of Figure 18*a*. However, YB did not compute for the case in which the quadrupole moment was excluded from the analysis and so did not find the peak at $\Omega_0 \sim 0.4$–$0.45$ in Figure 18.

Given the shapes of the marginal likelihoods in Figures 16–20, it is not at all clear if it is meaningful to derive limits on $\Omega_0$ without making use of other (prior) information. As an example, it is not at all clear what to use for the integration range in $\Omega_0$. Focusing on Figure 20*a* (which is similar to the other quadrupole excluded cases), the only conclusion seems to be that $\Omega_0 \sim 0.4$ is the value most consistent with the DMR data (at least among those models with $0.1 \leq \Omega_0 \leq 1$—some of the models have another peak at $\Omega_0 < 0.1$; GRSB). However, when the quadrupole moment is included in the analysis (as in Fig. 20*b*), the open-bubble inflation model peaks are at $\Omega_0 \sim 0.7$ (at least in the range $0.1 \leq \Omega_0 \leq 1$; GRSB), while the flat-space scale-invariant spectrum open model peak is at $\Omega_0 \lesssim 0.1$. At the 95% c.l., no value of $\Omega_0$ over the range considered, 0.1–1, is excluded. (The YB and BW[19] claims of a lower limit on $\Omega_0$ from the DMR data alone are not supported here.)

## 4. COMPUTATION OF LARGE-SCALE STRUCTURE STATISTICS

The $P(k)$ (e.g., eqs. [1] and [2]) were determined from a numerical integration of the linear perturbation theory equations of motion. As before, the computations were performed with two independent numerical codes. For some of the model parameter values considered here, the results of the two computations were compared and found to be in agreement to $\sim 0.3\%$.

Table 8 lists the $P(k)$ normalization amplitudes $A$ (e.g., eqs. [1] and [2]) when $Q_{\text{rms-PS}} = 10\ \mu$K. Examples of the power spectra normalized to $Q_{\text{rms-PS}}$ derived from the mean of the DMR 4 year data analysis extreme upper and lower $2\ \sigma$ limits discussed above are shown in Figure 21. One will notice, from Figure 21*e*, the good agreement between the open-bubble inflation spectra.

[19] BW have recently considered the DMR 4 year data in the context of the open-bubble inflation model accounting only for the fluctuations generated during the evolution inside the bubble (RP94). In the analysis, they use an analytic approximation to the CMB anisotropy angular spectra, consider the ecliptic-frame maps exclusively, do not attempt to correct for faint high-latitude Galactic foreground emission, and do not examine the consequences of exclusion of the quadrupole from the analysis. Many of their conclusions are specifically dependent on these selections.

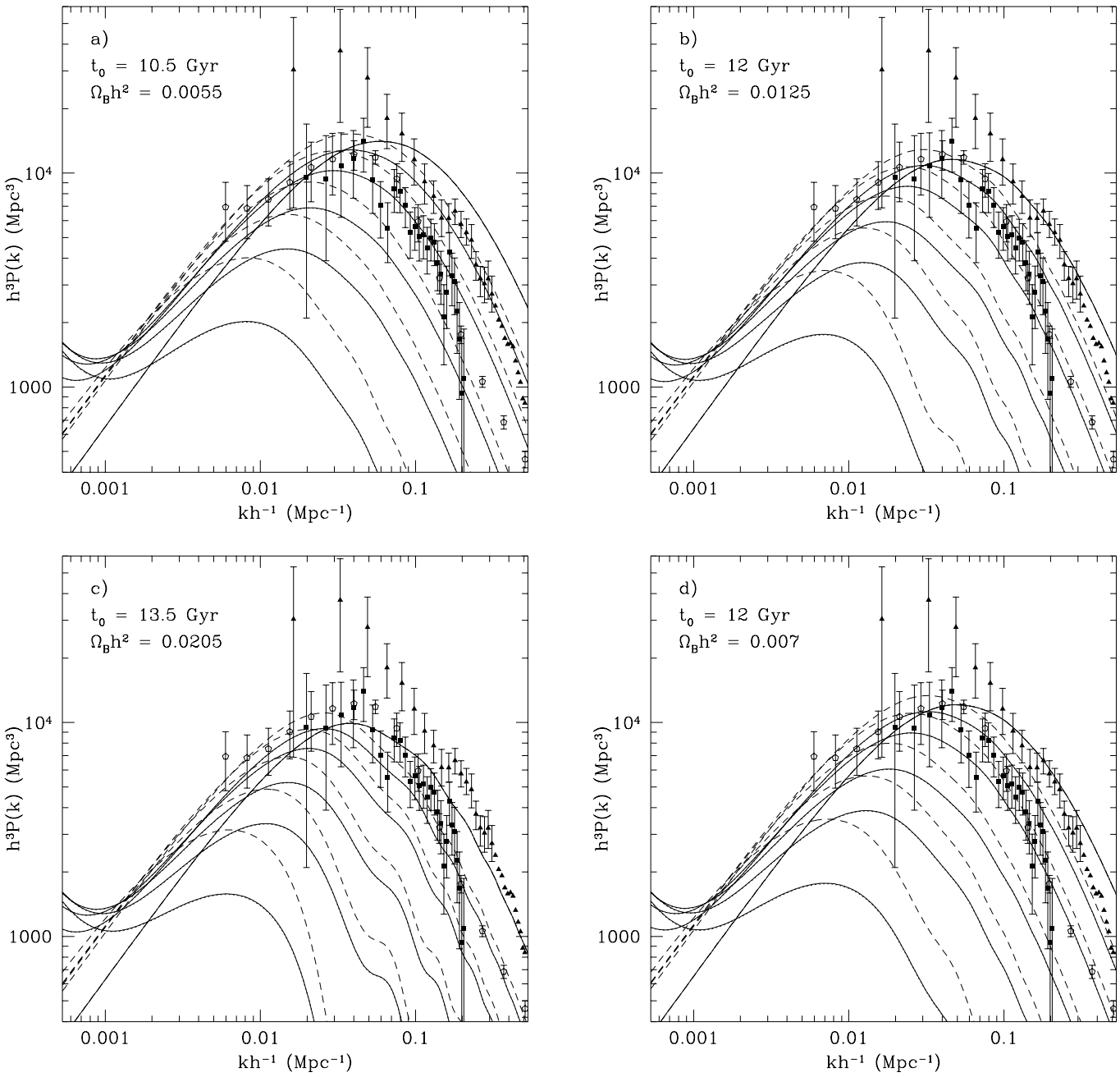


FIG. 21.—Fractional energy-density perturbation power spectra $P(k)$ as a function of wavenumber $k$. These are normalized to the mean of the extreme upper and lower 2 $\sigma$ $Q_{\rm rms\text{-}PS}$ values (as discussed in § 3.3). Panels (*a*)–(*d*) correspond to the four different sets of ($t_0$, $\Omega_B h^2$) of Tables 9–12, and each panel shows power spectra for three different models at six values of $\Omega_0$. Solid lines show the open-bubble inflation model $P(k)$ accounting only for fluctuations generated during the evolution inside the bubble (RP95); dotted lines are for the open-bubble inflation model now also accounting for fluctuations generated in the first epoch of inflation (BGT; YST); and dashed lines are for the flat-space scale-invariant spectrum open model (W83). Starting near the center of the lower horizontal axis, and moving counterclockwise, the spectra shown correspond to $\Omega_0 = 0.1$, 0.2, 0.3, 0.45, 0.6, and 1. Note that at $\Omega_0 = 1$, all three model spectra are identical and so overlap; also note that at a given $\Omega_0$, the open-bubble inflation model $P(k)$ accounting for the fluctuations generated in the first epoch of inflation (BGT; YST, *dotted lines*) essentially overlap those where this source of fluctuations is ignored (RP95; *solid lines*). Panel (*a*) corresponds to $t_0 \simeq 10.5$ Gyr and $\Omega_B h^2 = 0.0055$; (*b*) to $t_0 \simeq 12$ Gyr and $\Omega_B h^2 = 0.0125$; (*c*) to $t_0 \simeq 13.5$ Gyr and $\Omega_B h^2 = 0.205$; and (*d*) to $t_0 \simeq 12$ Gyr and $\Omega_B h^2 = 0.007$ (normalized using the results of the DMR analysis of the $t_0 \simeq 10.5$ Gyr, $\Omega_B h^2 = 0.0055$ models). Panel (*e*) shows the three $h = 0.6$, $\Omega_B = 0.035$ open-bubble inflation spectra of Table 13 at five different values of $\Omega_0$. The spectra are for the open-bubble inflation model accounting only for fluctuations generated during the evolution inside the bubble (RP95; *solid lines*), also accounting for fluctuations generated in the first epoch of inflation (BGT; YST, *dotted lines*), and also accounting for the contribution from the non–square-integrable basis function (YST; *dashed lines*). Starting near the center of the lower horizontal axis and moving counterclockwise, the models correspond to $\Omega_0 = 0.1$, 0.2, 0.3, 0.5, and 0.9. Note that at a given $\Omega_0$, the three spectra essentially overlap, especially for observationally viable values of $\Omega_0 \gtrsim 0.3$. The solid triangles represent the redshift-space da Costa et al. (1994) SSRS2 + CfA2 (130 $h^{-1}$ Mpc depth) optical galaxies data (and were very kindly provided to us by C. Park). The solid squares represent the [$P(k) = 8000(h^{-1}$ Mpc$)^3$ weighting] redshift-space results of the Tadros & Efstathiou (1995) analysis of the *IRAS* QDOT and 1.2 Jy infrared galaxy data. The hollow pentagons represent the real-space results of the Baugh & Efstathiou (1993) analysis of the APM optical galaxy data (and were very kindly provided to us by C. Baugh). It should be noted that the plotted model mass (not galaxy) power spectra do not account for any bias of galaxies with respect to mass. They also do not account for nonlinear or redshift-space–distortion (when relevant) corrections nor for the survey window functions. It should also be noted that the observational data error bars are determined under the assumption of a specific cosmological model and a specific evolution scenario, i.e., they do not necessarily account for these additional sources of uncertainty (e.g., Gaztañaga 1995). We emphasize that, because of the different assumptions, the different observed galaxy power spectra shown on the plots are defined somewhat differently and so cannot be directly quantitatively compared to each other.

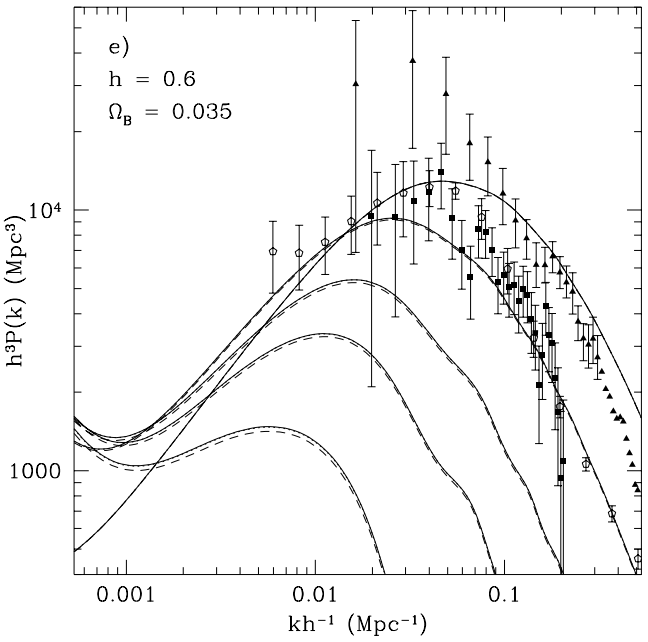


FIG. 21—*Continued*

When normalized to the two extreme 2 $\sigma$ $Q_{\rm rms\text{-}PS}$ limits (e.g., cols. [5] and [8] of Table 10), the $P(k)$ normalization factor (eq. [1] and Table 8) for the open-bubble inflation model (RP94; BGT; YST) may be summarized by, for the lower 2 $\sigma$ limit,

$$\frac{h^4 A(\Omega_0)}{10^5\ \mathrm{Mpc}^4} \simeq 4.3 + 1.95 \sin\left[1.07\pi(\Omega_0 - 0.1)^{0.85}\right], \quad (8)$$

and for the upper 2 $\sigma$ limit,

$$\frac{h^4 A(\Omega_0)}{10^5\ \mathrm{Mpc}^4} \simeq 9.3 + 3.35 \sin\left[1.13\pi(\Omega_0 - 0.1)^{0.78}\right]. \quad (9)$$

These fits are good to $\sim$1% for $0.1 \le \Omega_0 \le 1$. Note, however, that they are derived using the $Q_{\rm rms\text{-}PS}$ values determined for given $t_0$ and $\Omega_B h^2$ and hence do not account for the additional uncertainty introduced by allowed variations in these parameters (which could affect the power spectrum normalization amplitude by as much as $\sim$3%–4%). From Figure 21*e*, and given the uncertainties, we see that the fitting formulae of equations (8) and (9) provide an adequate summary for all the open-bubble inflation model spectra.

The extreme $\pm 2\ \sigma$ $P(k)$ normalization factor (eq. [2] and Table 8) for the flat-space scale-invariant spectrum open model (W83) may be summarized by, for the lower 2 $\sigma$ limit,

$$\frac{h^4 A(\Omega_0)}{10^5\ \mathrm{Mpc}^4} \simeq 4.85 + 2.9 \cos\left[0.9\pi\,|\,\Omega_0 - 0.325\,|^{1.25}\right], \quad (10)$$

and for the upper 2 $\sigma$ limit,

$$\frac{h^4 A(\Omega_0)}{10^5\ \mathrm{Mpc}^4} \simeq 11 + 5 \cos\left[0.85\pi\,|\,\Omega_0 - 0.2\,|^{1.2}\right]. \quad (11)$$

These fits are good to better than $\sim$2% for $0.2 \le \Omega_0 \le 1$; again, they are derived from $Q_{\rm rms\text{-}PS}$ values determined at given $t_0$ and $\Omega_B h^2$.

Given the uncertainties involved in the normalization procedure (born of both statistical and other arguments), it is not yet possible to quote a unique DMR normalization amplitude (G96). As a "central" value for the $P(k)$ normalization factor, we currently advocate the mean of equations (8) and (9) or equations (10) and (11) as required. We emphasize, however, that it is incorrect to draw conclusions about model viability based solely on this "central" value.

In conjunction with numerically determined transfer functions, the fits of equations (8)–(11) allow for a determination of $(\delta M/M)[8\ h^{-1}\ \mathrm{Mpc}]$, accurate to a few percent. Here the mean square linear mass fluctuation averaged over a sphere of coordinate radius $\bar{\chi}$ is

$$\left\langle \left[\frac{\delta M}{M}(\bar{\chi})\right]^2 \right\rangle = \frac{2}{\pi^2[\sinh(\bar{\chi})\cosh(\bar{\chi}) - \bar{\chi}]^2} \int_0^\infty \frac{dk}{(1+k^2)^2} \times [\cosh(\bar{\chi})\sin(k\bar{\chi}) - k\sinh(\bar{\chi})\cos(k\bar{\chi})]^2 P(k), \quad (12)$$

which, on small scales, reduces to the usual flat-space expression $[9/2\pi^2]\int_0^\infty dk\, k^2 P(k)[\sin(k\bar{\chi}) - k\bar{\chi}\cos(k\bar{\chi})]^2/(k\bar{\chi})^6$.

If instead use is made of the Bardeen et al. (1986; hereafter BBKS) analytic fit to the transfer function using the parameterization of equation (13) below (Sugiyama 1995) and numerically determined values for $A$, the resultant $(\delta M/M)[8\ h^{-1}\ \mathrm{Mpc}]$ values are accurate to better than $\sim$5% (except for large baryon-fraction, $\Omega_B/\Omega_0 \gtrsim 0.4$, models where the error could be as large as $\sim$7%). Use of the analytic fits of equations (8)–(11) for $A$ (instead of the numerically determined values) slightly increases the error, while use of the BBKS transfer function fit parameterized by an earlier version of equation (13) below, $S = \Omega_0 h \exp[-\Omega_B(1+\Omega_0)/\Omega_0]$, results in $(\delta M/M)[8\ h^{-1}\ \mathrm{Mpc}]$ values that could be off by as much as $\sim$7%–10%. Nevertheless, as has been demonstrated by LLRV, the approximate analytic fit to the transfer function greatly simplifies the computation and allows for rapid demarcation of the favored part of cosmological parameter space.

Numerical values for some cosmographic and large-scale structure statistics for the models considered here are recorded in Tables 9–15. We emphasize that when comparing to observational data, we make use of numerically determined large-scale structure predictions, not those derived using an approximate analytic fitting formula.

Tables 9–12 give the predictions for the open-bubble inflation model accounting only for the perturbations generated during the evolution inside the bubble (RP94) and for the flat-space scale-invariant spectrum open model (W83). Each of these tables corresponds to a different pair of $(t_0,\ \Omega_B h^2)$ values. The first two columns in these tables record $\Omega_0$ and $h$, and the third column is the cosmological baryonic-matter fraction $\Omega_B/\Omega_0$. The fourth column gives the value of the matter power spectrum scaling parameter (Sugiyama 1995),

$$S = \Omega_0 h e^{-\Omega_B(\sqrt{2h}+\Omega_0)/\Omega_0}, \quad (13)$$

which is used to parameterize approximate analytic fits to the power spectra derived from numerical integration of the perturbation equations. The quantities listed in columns (1)–(4) of these tables are sensitive only to the global parameters of the cosmological model.

Columns (5) and (8) of Tables 9–12 give the DMR data 2 $\sigma$ range of $Q_{\rm rms\text{-}PS}$ that is used to normalize the perturbations in the models considered here. The numerical values in Table 12 are for $t_0 \simeq 12$ Gyr, $\Omega_B h^2 = 0.007$. We

TABLE 9

NUMERICAL VALUES FOR THE $t_0 \simeq 10.5$ Gyr, $\Omega_B h^2 = 0.0055$ MODELS

| | | | | INFLATION MODEL[a] | | | SCALE-INVARIANT MODEL[b] | | |
|---|---|---|---|---|---|---|---|---|---|
| $\Omega_0$ (1) | $h$ (2) | $\frac{\Omega_B}{\Omega_0}$ (3) | $S$ (4) | $Q_{\text{rms-PS}}$ ($\mu$K) (5) | $\left.\frac{\delta M}{M}\right\|_{8\,h^{-1}\,\text{Mpc}}$ (6) | $\beta_I$ (7) | $Q_{\text{rms-PS}}$ ($\mu$K) (8) | $\left.\frac{\delta M}{M}\right\|_{8\,h^{-1}\,\text{Mpc}}$ (9) | $\beta_I$ (10) |
| 0.1 ..... | 0.84 | 0.078 | **0.075** | 16.98–24.96 | **0.105–0.154** | **0.034–0.050** | 11.39–16.01 | **0.152–0.213** | **0.050–0.070** |
| 0.2 ..... | 0.79 | 0.044 | **0.15** | 19.56–28.64 | **0.282–0.413** | **0.14–0.20** | 14.02–20.14 | **0.343–0.493** | 0.17–0.24 |
| 0.25..... | 0.77 | 0.037 | **0.18** | 19.62–28.58 | **0.379–0.552** | 0.21–0.31 | 14.83–21.27 | **0.446–0.641** | 0.25–0.36 |
| 0.3 ..... | 0.75 | **0.033** | 0.21 | 19.18–27.82 | **0.474–0.688** | 0.30–0.43 | 15.31–21.86 | 0.549–0.784 | 0.35–0.49 |
| 0.35..... | 0.74 | **0.029** | 0.25 | 18.40–26.56 | 0.575–0.830 | 0.40–0.57 | 15.36–21.92 | 0.655–0.934 | 0.45–0.65 |
| 0.4 ..... | 0.73 | **0.026** | **0.28** | 17.42–25.04 | 0.674–0.968 | 0.51–0.73 | 15.20–21.59 | 0.760–1.08 | 0.57–0.81 |
| 0.45..... | 0.71 | **0.024** | **0.31** | 16.38–23.40 | 0.756–1.08 | 0.61–0.87 | 14.77–20.84 | **0.845–1.19** | 0.68–0.96 |
| 0.5 ..... | 0.70 | **0.022** | **0.34** | 15.32–21.80 | **0.843–1.20** | 0.72–1.0 | 14.13–19.82 | **0.936–1.31** | 0.80–1.1 |
| **0.6** ..... | 0.68 | **0.020** | **0.39** | 13.56–19.22 | **0.966–1.41** | **0.95–1.4** | 12.46–17.35 | **1.09–1.52** | **1.0–1.5** |
| **0.8** ..... | 0.65 | **0.016** | **0.50** | 13.04–18.32 | **1.22–1.72** | **1.4–2.0** | 10.48–14.51 | **1.29–1.78** | **1.5–2.0** |
| **1** ..... | 0.62 | **0.014** | **0.60** | 14.86–21.02 | **1.31–1.86** | **1.7–2.4** | 14.83–21.00 | **1.31–1.85** | **1.7–2.4** |

[a] For the open-bubble inflation model, accounting only for fluctuations generated during the evolution inside the bubble (RP94). Two standard deviation range.

[b] For the flat-space scale-invariant spectrum open model (W83). Two standard deviation range.

TABLE 10

NUMERICAL VALUES FOR THE $t_0 \simeq 12$ Gyr, $\Omega_B h^2 = 0.0125$ MODELS

| | | | | INFLATION MODEL[a] | | | SCALE-INVARIANT MODEL[b] | | |
|---|---|---|---|---|---|---|---|---|---|
| $\Omega_0$ (1) | $h$ (2) | $\frac{\Omega_B}{\Omega_0}$ (3) | $S$ (4) | $Q_{\text{rms-PS}}$ ($\mu$K) (5) | $\left.\frac{\delta M}{M}\right\|_{8\,h^{-1}\,\text{Mpc}}$ (6) | $\beta_I$ (7) | $Q_{\text{rms-PS}}$ ($\mu$K) (8) | $\left.\frac{\delta M}{M}\right\|_{8\,h^{-1}\,\text{Mpc}}$ (9) | $\beta_I$ (10) |
| 0.1 ..... | 0.73 | **0.23** | **0.054** | 16.98–24.98 | **0.0663–0.0976** | **0.022–0.032** | 11.39–16.01 | **0.0965–0.136** | **0.032–0.044** |
| 0.2 ..... | 0.69 | 0.13 | **0.12** | 19.56–28.64 | **0.204–0.298** | **0.10–0.15** | 14.02–20.14 | **0.248–0.357** | **0.12–0.18** |
| 0.25..... | 0.67 | 0.11 | **0.14** | 19.60–28.54 | **0.279–0.406** | **0.16–0.23** | 14.83–21.27 | **0.330–0.473** | 0.19–0.27 |
| 0.3 ..... | 0.66 | 0.096 | **0.17** | 19.14–27.76 | **0.362–0.525** | 0.23–0.33 | 15.26–21.81 | **0.419–0.599** | 0.26–0.38 |
| 0.35..... | 0.65 | 0.085 | 0.20 | 18.36–26.48 | **0.445–0.642** | 0.31–0.44 | 15.36–21.86 | 0.508–0.723 | 0.35–0.50 |
| 0.4 ..... | 0.63 | 0.079 | 0.22 | 17.38–24.94 | 0.514–0.738 | 0.39–0.55 | 15.15–21.49 | 0.580–0.823 | 0.44–0.62 |
| 0.45..... | 0.62 | 0.072 | 0.25 | 16.32–23.28 | 0.591–0.844 | 0.48–0.68 | 14.72–20.74 | 0.661–0.931 | 0.53–0.75 |
| 0.5 ..... | 0.61 | 0.067 | 0.27 | 15.26–21.68 | 0.663–0.942 | 0.57–0.81 | 14.08–19.71 | 0.736–1.03 | 0.63–0.88 |
| **0.6** ..... | 0.60 | 0.058 | **0.33** | 13.50–19.10 | **0.807–1.14** | 0.77–1.1 | 12.41–17.24 | **0.884–1.23** | **0.85–1.2** |
| **0.8** ..... | 0.57 | **0.048** | **0.42** | 12.98–18.20 | **1.00–1.41** | **1.1–1.6** | 10.37–14.40 | **1.05–1.46** | **1.2–1.7** |
| **1** ..... | 0.54 | **0.043** | **0.49** | 14.74–20.84 | **1.08–1.52** | **1.4–2.0** | 14.72–20.79 | **1.08–1.52** | **1.4–2.0** |

[a] For the open-bubble inflation model, accounting only for fluctuations generated during the evolution inside the bubble (RP94). Two standard deviation range.

[b] For the flat-space scale-invariant spectrum open model (W83). Two standard deviation range.

TABLE 11

NUMERICAL VALUES FOR THE $t_0 \simeq 13.5$ Gyr, $\Omega_B h^2 = 0.0205$ MODELS

| | | | | INFLATION MODEL[a] | | | SCALE-INVARIANT MODEL[b] | | |
|---|---|---|---|---|---|---|---|---|---|
| $\Omega_0$ (1) | $h$ (2) | $\frac{\Omega_B}{\Omega_0}$ (3) | $S$ (4) | $Q_{\text{rms-PS}}$ ($\mu$K) (5) | $\left.\frac{\delta M}{M}\right\|_{8\,h^{-1}\,\text{Mpc}}$ (6) | $\beta_I$ (7) | $Q_{\text{rms-PS}}$ ($\mu$K) (8) | $\left.\frac{\delta M}{M}\right\|_{8\,h^{-1}\,\text{Mpc}}$ (9) | $\beta_I$ (10) |
| 0.1 ..... | 0.65 | **0.49** | **0.036** | 17.00–24.98 | **0.0353–0.0519** | **0.012–0.017** | 11.39–16.01 | **0.0515–0.0724** | **0.017–0.024** |
| 0.2 ..... | 0.61 | **0.28** | **0.085** | 19.56–28.60 | **0.135–0.197** | **0.067–0.098** | 14.02–20.09 | **0.165–0.236** | **0.082–0.12** |
| 0.25..... | 0.60 | **0.23** | **0.11** | 19.58–28.50 | **0.198–0.288** | **0.11–0.16** | 14.77–21.22 | **0.233–0.335** | **0.13–0.19** |
| 0.3 ..... | 0.59 | **0.20** | **0.13** | 19.12–27.70 | **0.264–0.382** | 0.17–0.24 | 15.20–21.76 | **0.305–0.436** | 0.19–0.28 |
| 0.35..... | 0.57 | 0.18 | **0.15** | 18.32–26.40 | **0.321–0.462** | 0.22–0.32 | 15.31–21.76 | **0.366–0.520** | 0.25–0.36 |
| 0.4 ..... | 0.56 | 0.16 | **0.18** | 17.32–24.86 | **0.385–0.552** | 0.29–0.41 | 15.10–21.38 | **0.434–0.615** | 0.33–0.46 |
| 0.45..... | 0.55 | 0.15 | 0.20 | 16.28–23.20 | 0.447–0.638 | 0.36–0.51 | 14.67–20.63 | 0.500–0.703 | 0.40–0.57 |
| 0.5 ..... | 0.55 | 0.14 | 0.22 | 15.20–21.60 | 0.520–0.740 | 0.45–0.63 | 14.02–19.61 | 0.578–0.808 | 0.50–0.69 |
| **0.6** ..... | 0.53 | 0.12 | 0.26 | 13.46–19.02 | 0.626–0.885 | 0.60–0.85 | 12.36–17.14 | 0.686–0.951 | 0.66–0.91 |
| **0.8** ..... | **0.50** | 0.10 | **0.33** | 12.92–18.08 | **0.790–1.11** | **0.90–1.3** | 10.37–14.29 | **0.830–1.14** | **0.94–1.3** |
| **1** ..... | **0.48** | 0.089 | **0.40** | 14.64–20.68 | **0.878–1.24** | **1.1–1.6** | 14.67–20.63 | **0.880–1.24** | **1.1–1.6** |

[a] For the open-bubble inflation model, accounting only for fluctuations generated during the evolution inside the bubble (RP94). Two standard deviation range.

[b] For the flat-space scale-invariant spectrum open model (W83). Two standard deviation range.

TABLE 12

NUMERICAL VALUES FOR THE $t_0 \simeq 12$ Gyr, $\Omega_B h^2 = 0.007$ MODELS[a]

| | | | | INFLATION MODEL[b] | | | SCALE-INVARIANT MODEL[c] | | |
|---|---|---|---|---|---|---|---|---|---|
| $\Omega_0$ (1) | $h$ (2) | $\frac{\Omega_B}{\Omega_0}$ (3) | $S$ (4) | $Q_{\text{rms-PS}}$ ($\mu$K) (5) | $\left.\frac{\delta M}{M}\right\|_{8\,h^{-1}\,\text{Mpc}}$ (6) | $\beta_I$ (7) | $Q_{\text{rms-PS}}$ ($\mu$K) (8) | $\left.\frac{\delta M}{M}\right\|_{8\,h^{-1}\,\text{Mpc}}$ (9) | $\beta_I$ (10) |
| 0.1 ..... | 0.73 | 0.13 | **0.061** | 16.98–24.96 | **0.0795–0.117** | **0.026–0.038** | 11.39–16.01 | **0.116–0.163** | **0.038–0.053** |
| 0.2 ..... | 0.69 | 0.074 | **0.12** | 19.56–28.64 | **0.226–0.331** | **0.11–0.16** | 14.02–20.14 | **0.275–0.396** | **0.14–0.20** |
| 0.25..... | 0.67 | 0.062 | **0.15** | 19.62–28.58 | **0.305–0.444** | 0.17–0.25 | 14.83–21.27 | **0.360–0.517** | 0.20–0.29 |
| 0.3 ..... | 0.66 | 0.054 | **0.18** | 19.18–27.82 | **0.391–0.568** | 0.25–0.36 | 15.31–21.86 | **0.454–0.648** | 0.29–0.41 |
| 0.35..... | 0.65 | 0.047 | 0.21 | 18.40–26.56 | 0.477–0.689 | 0.33–0.48 | 15.36–21.92 | 0.543–0.775 | 0.38–0.54 |
| 0.4 ..... | 0.63 | **0.044** | 0.24 | 17.42–25.04 | 0.549–0.789 | 0.41–0.59 | 15.20–21.59 | 0.620–0.881 | 0.47–0.66 |
| 0.45..... | 0.62 | **0.040** | 0.26 | 16.38–23.40 | 0.629–0.898 | 0.51–0.72 | 14.77–20.84 | 0.703–0.992 | 0.57–0.80 |
| 0.5 ..... | 0.61 | **0.038** | **0.29** | 15.32–21.80 | 0.703–1.00 | 0.60–0.86 | 14.13–19.82 | 0.780–1.09 | 0.67–0.94 |
| **0.6** ..... | 0.60 | **0.032** | **0.34** | 13.56–19.22 | **0.849–1.20** | **0.81–1.2** | 12.46–17.35 | **0.930–1.30** | **0.89–1.2** |
| **0.8** ..... | 0.57 | **0.027** | **0.43** | 13.04–18.32 | **1.05–1.47** | **1.2–1.7** | 10.48–14.51 | **1.10–1.53** | **1.3–1.7** |
| **1** ..... | 0.54 | **0.024** | **0.51** | 14.86–21.02 | **1.13–1.59** | **1.5–2.1** | 14.83–21.00 | **1.12–1.59** | **1.5–2.1** |

[a] Normalized to $Q_{\text{rms-PS}}$ for the $t_0 \simeq 10.5$ Gyr, $\Omega_B h^2 = 0.0055$ models.

[b] For the open-bubble inflation model, accounting only for fluctuations generated during the evolution inside the bubble (RP94). Two standard deviation range.

[c] For the flat-space scale-invariant spectrum open model (W83). Two standard deviation range.

TABLE 13

NUMERICAL VALUES FOR THE $h = 0.6$, $\Omega_B = 0.035$ OPEN-BUBBLE INFLATION MODELS

| $\Omega_0$ (1) | $Q_{\text{rms-PS}}$[a] ($\mu$K) (2) | $\left.\frac{\delta M}{M}\right\|_{8\,h^{-1}\,\text{Mpc}}$[a] (3) | $Q_{\text{rms-PS}}$[b] ($\mu$K) (4) | $\left.\frac{\delta M}{M}\right\|_{8\,h^{-1}\,\text{Mpc}}$[b] (5) | $Q_{\text{rms-PS}}$[c] ($\mu$K) (6) | $\left.\frac{\delta M}{M}\right\|_{8\,h^{-1}\,\text{Mpc}}$[c] (7) |
|---|---|---|---|---|---|---|
| 0.1..... | 16.96–24.93 | 0.0422–0.0620 | 17.24–25.34 | 0.0422–0.0620 | 21.22–31.41 | 0.0412–0.0610 |
| 0.2..... | 19.56–28.68 | 0.159–0.233 | 19.65–28.81 | 0.158–0.232 | 20.48–30.06 | 0.156–0.230 |
| 0.3..... | 19.14–27.75 | 0.311–0.450 | 19.14–27.75 | 0.310–0.450 | 18.95–27.56 | 0.306–0.445 |
| 0.4..... | 17.38–24.88 | 0.478–0.684 | 17.33–24.88 | 0.476–0.684 | 17.24–24.79 | 0.471–0.678 |
| 0.5..... | 15.25–21.69 | 0.647–0.921 | 15.25–21.69 | 0.647–0.920 | 15.62–22.24 | 0.642–0.914 |
| 0.6..... | 13.49–19.05 | 0.805–1.14 | 13.54–19.09 | 0.805–1.14 | 14.23–20.20 | 0.796–1.13 |
| 0.7..... | 12.80–17.89 | 0.953–1.33 | 12.84–17.94 | 0.952–1.33 | 13.54–19.09 | 0.940–1.33 |
| 0.8..... | 12.98–18.17 | 1.06–1.49 | 12.98–18.21 | 1.06–1.49 | 13.44–18.95 | 1.06–1.49 |
| 0.9..... | 13.72–19.37 | 1.15–1.62 | 13.72–19.37 | 1.14–1.62 | 13.91–19.65 | 1.15–1.62 |

[a] For the open-bubble inflation model, accounting only for fluctuations generated during the evolution inside the bubble (RP94). Two standard deviation range.

[b] For the open-bubble inflation model, now also accounting for fluctuations generated in the first epoch of inflation (BGT; YST). Two standard deviation range.

[c] For the open-bubble inflation model, now also accounting for both the fluctuations generated in the first epoch of inflation as well as those that correspond to a non-square-integrable basis function (YST). Two standard deviation range.

TABLE 14

APPROXIMATE FITTING FORMULAE FOR $(\delta M/M)[8\ h^{-1}\ \text{Mpc}]$[a]

| | | | INFLATION MODEL[b] | SCALE-INVARIANT MODEL[c] |
|---|---|---|---|---|
| $t_0$ (Gyr) (1) | $\Omega_B h^2$ (2) | Limit (3) | $\left.\frac{\delta M}{M}\right\|_{8\,h^{-1}\,\text{Mpc}}$ (4) | $\left.\frac{\delta M}{M}\right\|_{8\,h^{-1}\,\text{Mpc}}$ (5) |
| $\simeq 10.5$..... | 0.0055 | $+2\,\sigma$ | $1.92 \sin [0.5\pi(\Omega_0 - 0.065)]$ | $1.88 \sin [0.55\pi(\Omega_0 - 0.05)]$ |
| $\simeq 10.5$..... | 0.0055 | $-2\,\sigma$ | $1.34 \sin [0.5\pi(\Omega_0 - 0.065)]$ | $1.31 \sin [0.55\pi(\Omega_0 - 0.05)]$ |
| $\simeq 12$..... | 0.0125 | $+2\,\sigma$ | $1.52 \sin [0.5\pi(\Omega_0 - 0.075)]$ | $1.52 \sin [0.55\pi(\Omega_0 - 0.065)]$ |
| $\simeq 12$..... | 0.0125 | $-2\,\sigma$ | $1.08 \sin [0.5\pi(\Omega_0 - 0.080)]$ | $1.08 \sin [0.55\pi(\Omega_0 - 0.065)]$ |
| $\simeq 13.5$..... | 0.0205 | $+2\,\sigma$ | $1.23 \sin [0.495\pi(\Omega_0 - 0.095)]$ | $1.25 \sin [0.525\pi(\Omega_0 - 0.085)]$ |
| $\simeq 13.5$..... | 0.0205 | $-2\,\sigma$ | $0.87 \sin [0.495\pi(\Omega_0 - 0.100)]$ | $0.89 \sin [0.525\pi(\Omega_0 - 0.085)]$ |
| $\simeq 12$..... | 0.007 | $+2\,\sigma$ | $1.61 \sin [0.5\pi(\Omega_0 - 0.070)]$ | $1.59 \sin [0.55\pi(\Omega_0 - 0.055)]$ |
| $\simeq 12$..... | 0.007 | $-2\,\sigma$ | $1.14 \sin [0.5\pi(\Omega_0 - 0.075)]$ | $1.13 \sin [0.55\pi(\Omega_0 - 0.060)]$ |

[a] For the $\pm 2\,\sigma$ entries of cols. (6) and (9) of Tables 9–12. The fits are good to better than $\sim 3\%$ for $0.2 \leq \Omega_0 \leq 1$.

[b] For the open-bubble inflation model, accounting only for fluctuations generated during the evolution inside the bubble (RP94).

[c] For the flat-space scale-invariant spectrum open model (W83).

TABLE 15

NUMERICAL VALUES FOR A "CENTRAL" $(\delta M/M)[8\ h^{-1}\ \mathrm{Mpc}]$ VALUE[a]

| | INFLATION MODEL[b] | | | | SCALE-INVARIANT MODEL[c] | | | |
|---|---|---|---|---|---|---|---|---|
| $\Omega_0$ (1) | $t_0 \simeq 10.5$ $\Omega_B h^2 = 0.0055$ (2) | $t_0 \simeq 12$ $\Omega_B h^2 = 0.0125$ (3) | $t_0 \simeq 13.5$ $\Omega_B h^2 = 0.0205$ (4) | $t_0 \simeq 12$ $\Omega_B h^2 = 0.007$ (5) | $t_0 \simeq 10.5$ $\Omega_B h^2 = 0.0055$ (6) | $t_0 \simeq 12$ $\Omega_B h^2 = 0.0125$ (7) | $t_0 \simeq 13.5$ $\Omega_B h^2 = 0.0205$ (8) | $t_0 \simeq 12$ $\Omega_B h^2 = 0.007$ (9) |
| 0.1 ..... | 0.129 | 0.0820 | 0.0436 | 0.0982 | 0.183 | 0.116 | 0.0620 | 0.139 |
| 0.2 ..... | 0.348 | 0.251 | 0.166 | 0.278 | 0.418 | 0.303 | 0.200 | 0.336 |
| 0.25..... | 0.465 | 0.343 | 0.243 | 0.375 | 0.544 | 0.401 | 0.284 | 0.438 |
| 0.3 ..... | 0.581 | 0.443 | 0.323 | 0.479 | 0.667 | 0.509 | 0.371 | 0.551 |
| 0.35..... | 0.703 | 0.543 | 0.391 | 0.583 | 0.794 | 0.615 | 0.443 | 0.659 |
| 0.4 ..... | 0.821 | 0.626 | 0.468 | 0.669 | 0.920 | 0.702 | 0.524 | 0.750 |
| 0.45..... | 0.918 | 0.717 | 0.543 | 0.764 | 1.02 | 0.796 | 0.602 | 0.848 |
| 0.5 ..... | 1.02 | 0.803 | 0.630 | 0.852 | 1.12 | 0.884 | 0.693 | 0.937 |
| 0.6 ..... | 1.20 | 0.974 | 0.756 | 1.03 | 1.30 | 1.06 | 0.818 | 1.11 |
| 0.8 ..... | 1.47 | 1.20 | 0.948 | 1.26 | 1.54 | 1.25 | 0.987 | 1.31 |
| 1 ..... | 1.58 | 1.30 | 1.06 | 1.36 | 1.58 | 1.30 | 1.06 | 1.36 |

NOTE.—$t_0$ in Gyr.

[a] Mean of the $\pm 2\ \sigma$ entries of cols. (6) and (9) of Tables 9–12.

[b] For the open-bubble inflation model, accounting only for fluctuations generated during the evolution inside the bubble (RP94).

[c] For the flat-space scale-invariant spectrum open model (W83).

did not analyze the DMR data using $C_\ell$'s for these models, and in this case the perturbations are normalized to the $Q_{\mathrm{rms\text{-}PS}}$ values from the $t_0 \simeq 10.5$ Gyr, $\Omega_B h^2 = 0.0055$ analyses. (As discussed above, shifts in $h$ and $\Omega_B h^2$ do not greatly alter the inferred normalization amplitude.)

Columns (6) and (9) of Tables 9–12 give the $2\ \sigma$ range of $(\delta M/M)[8\ h^{-1}\ \mathrm{Mpc}]$. These were determined using the $P(k)$ derived from numerical integration of the perturbation equations. For about two dozen cases, these rms mass fluctuations determined using the two independent numerical integration codes were compared and found to be in excellent agreement. (At fixed $Q_{\mathrm{rms\text{-}PS}}$, they differ by $\sim 0.002\%$–$0.5\%$ depending on model parameter values, with the typical difference being $\sim 0.1\%$. We emphasize that this is mostly a reflection of currently achievable numerical accuracy.)

To usually better than $\sim 3\%$ accuracy, for $0.2 \leq \Omega_0 \leq 1$, the $2\ \sigma$ $(\delta M/M)[8\ h^{-1}\ \mathrm{Mpc}]$ entries of columns (6) and (9) of Tables 9–12 may be summarized by the fitting formulae listed in Table 14. These fitting formulae are more accurate than expressions for $(\delta M/M)[8\ h^{-1}\ \mathrm{Mpc}]$ derived at the same cosmological parameter values using an analytic approximation to the transfer function and the normalization of equations (8)–(11).

For open models, as discussed below, it proves most convenient to characterize the peculiar velocity perturbation by the parameter

$$\beta_I = \frac{\Omega_0^{0.6}}{b_{IRAS}} = 1.3\Omega_0^{0.6}\,\frac{\delta M}{M}\,(8\ h^{-1}\ \mathrm{Mpc})\,, \qquad (14)$$

where $b_{IRAS}$ is the linear bias factor for *IRAS* galaxies (see, e.g., Peacock & Dodds 1994). The $2\ \sigma$ range of $\beta_I$ are listed in columns (7) and (10) of Tables 9–12.

Table 13 compares the $(\delta M/M)[8\ h^{-1}\ \mathrm{Mpc}]$ values for spectra of types (1)–(3) above. Clearly, there is no significant observational difference between the predictions for the different spectra. In what follows, for the open-bubble inflation model, we concentrate on the type (1) spectrum above.

Again, the ranges in Tables 9–14 are those determined from the maximal $2\ \sigma$ $Q_{\mathrm{rms\text{-}PS}}$ range. Table 15 lists "central DMR-normalized" values for $(\delta M/M)[8\ h^{-1}\ \mathrm{Mpc}]$, defined as the mean of the maximal $\pm 2\ \sigma$ entries of Tables 9–12. (The mean of the $\pm 2\ \sigma$ fitting formulae of Table 14 may be used to interpolate between the entries of Table 15.) We again emphasize that it is incorrect to draw conclusions about model viability based solely on these "central" values—for the purpose of constraining model parameter values by, e.g., comparing numerical simulation results to observational data one must make use of computations at a few different values of the normalization selected to span the $\pm 2\ \sigma$ ranges of Tables 9–12.

## 5. CURRENT OBSERVATIONAL CONSTRAINTS ON DMR-NORMALIZED MODELS

The DMR likelihoods do not meaningfully exclude any part of the $(\Omega_0,\ h,\ \Omega_B h^2)$ parameter space for the models considered here. In this section we combine current observational constraints on global cosmological parameters with the DMR-normalized model predictions to place constraints on the range of allowed model parameter values. It is important to bear in mind that some measures of observational cosmology remain uncertain; thus, our analysis here must be viewed as tentative and subject to revision as the observational situation approaches equilibrium. To constrain our model parameter values, we have employed the most robust of the current observational constraints. Tables 9–12 list some observational predictions for the models considered here, and the boldface entries are those that are inconsistent with current observational data at the $2\ \sigma$ significance level.

### 5.1. *Observational Constraints Used*

For each cosmographic or large-scale parameter, we have generally chosen to use constraints from a single set of observations or from a single analysis. We generally use the most recent analyses since we assume that they incorporate a better understanding of the uncertainties, especially those due to systematics. The specific constraints we use are sum-

marized below, where we compare them to those derived from other analyses.

The model predictions depend on the age of the universe $t_0$. To reconcile the models with the high measured values of the Hubble parameter $h$, we have chosen to focus on $t_0 \simeq 10.5$, 12, and 13.5 Gyr, which are near the lower end of the ages now under discussion. For instance, Jimenez et al. (1996) find that the oldest globular clusters have ages $\sim$11.5–15.5 Gyr (also see Salaris, Degl'Innocenti, & Weiss 1997; Renzini et al. 1996) and that it is very unlikely that the oldest clusters are younger than 9.7 Gyr.

The value of $\Omega_0$ is another input parameter for our computations. As summarized by Peebles (1993, § 20), on scales $\lesssim 10\,h^{-1}$ Mpc, a variety of different observational measurements indicate that $\Omega_0$ is low. For instance, virial analyses of X-ray cluster data indicate $\Omega_0 = 0.24$, with a 2 $\sigma$ range: $0.04 < \Omega_0 < 0.44$ (Carlberg et al. 1996—we have added their 1 $\sigma$ statistical and systematic uncertainties in quadrature and doubled to get the 2 $\sigma$ uncertainty). In a CDM model in which structure forms at a relatively high redshift (as is observed), these local estimates of $\Omega_0$ do constrain the global value of $\Omega_0$ (since, in this case, it is inconceivable that the pressureless CDM is much more homogeneously distributed than is the observed baryonic mass). We hence adopt a 2 $\sigma$ upper limit of $\Omega_0 < 0.6$ to constrain the CDM models we consider here. (This large upper limit allows for the possibility that the models might be moderately biased.) The boldface entries in column (1) of Tables 9–12 indicate those $\Omega_0$ values inconsistent with this constraint.

Column (2) of Tables 9–12 gives the value of the Hubble parameter $h$ that corresponds to the chosen values of $\Omega_0$ and $t_0$. Current observational data favors a larger $h$ (see, e.g., Kennicutt, Freedman, & Mould 1995; Baum et al. 1995; van den Bergh 1995; Sandage et al. 1996; Ruiz-Lapuente 1996; Branch et al. 1996; Riess, Press, & Kirshner 1996; but also see Schaefer 1996). For the purpose of our analysis here we adopt the *HST* value $h = 0.69 \pm 0.08$ (1 $\sigma$ uncertainty; Tanvir et al. 1995); doubling the uncertainty, the 2 $\sigma$ range is $0.53 \leq h \leq 0.85$. The boldface entries in column (2) of Tables 9–12 indicates those model parameter values which predict an $h$ inconsistent with this range.

Comparison of the standard nucleosynthesis theoretical predictions for the primordial light-element abundances to what is determined by extrapolation of the observed abundances to primordial values leads to constraints on $\Omega_B h^2$. It has usually been argued that $^4$He and $^7$Li allow for the most straightforward extrapolation from the locally observed abundances to the primordial values (see, e.g., Dar 1995; Fields & Olive 1996; Fields et al. 1996, hereafter FKOT). The observed $^4$He and $^7$Li abundances then suggest $\Omega_B h^2 = 0.0066$, and a conservative assessment of the uncertainties indicate a 2 $\sigma$ range: $0.0051 < \Omega_B h^2 < 0.016$ (FKOT; also see Copi et al. 1995; Sarkar 1996).

Observational constraints on the primordial deuterium (D) abundance should, in principle, allow for a tightening of the allowed $\Omega_B h^2$ range. There are now a number of different estimates of the primordial D abundance, and since the field is still in its infancy, it is, perhaps, not surprising that the different estimates are somewhat discrepant. Songaila et al. (1994), Carswell et al. (1994), and Rugers & Hogan (1996a, 1996b) use observations of three high-redshift absorption clouds to argue for a high primordial D abundance and so a low $\Omega_B h^2$. Tytler, Fan, & Burles (1996) and Burles & Tytler (1998) study two absorption clouds and argue for a low primordial D abundance and so a high $\Omega_B h^2$. Carswell et al. (1996) and Wampler et al. (1996) examine other absorption clouds but are not able to constrain $\Omega_B h^2$ strongly. While the error bars on $\Omega_B h^2$ determined from these D abundance observations are somewhat asymmetric, to use these results to qualitatively pick the $\Omega_B h^2$ values we wish to examine we assume that the errors are Gaussian (and where needed add all uncertainties in quadrature to get the 2 $\sigma$ uncertainties). The large D abundance observations suggest $\Omega_B h^2 = 0.0062$ with a 2 $\sigma$ range: $0.0046 < \Omega_B h^2 < 0.0078$ (Rugers & Hogan 1996a). When these large D abundances are combined with the observed $^4$He and $^7$Li abundances, they indicate $\Omega_B h^2 = 0.0064$, with a 2 $\sigma$ range: $0.0055 < \Omega_B h^2 < 0.0087$ (FKOT). The large D abundances are consistent with the standard interpretation of the $^4$He and $^7$Li abundances, and with the standard model of particle physics (with three massless neutrino species); they do, however, seem to require a modification in galactic chemical evolution models to be consistent with local determinations of the D and $^3$He abundances (see, e.g., FKOT; Cardall & Fuller 1996). The low D abundance observations favor $\Omega_B h^2 = 0.024$ with a 2 $\sigma$ range: $0.018 < \Omega_B h^2 < 0.030$ (Burles & Tytler 1998). The low D abundance observations seem to be more easily accommodated in modifications of the standard model of particle physics, i.e., they are difficult to reconcile with exactly three massless neutrino species; alternatively, they might indicate a gross, as yet unaccounted for, uncertainty in the observed $^4$He abundance (Burles & Tytler 1998; Cardall & Fuller 1996). The low D abundance is approximately consistent with locally observed D abundances but probably requires some modification in the usual galactic chemical evolution model for $^7$Li (Burles & Tytler 1998; Cardall & Fuller 1996).

To accommodate the range of $\Omega_B h^2$ now under discussion, we compute model predictions for $\Omega_B h^2 = 0.0055$ (Table 9), 0.007 (Table 12), 0.0125 (Table 10), and 0.0205 (Table 11). We shall find that this uncertainty in $\Omega_B h^2$ precludes determination of robust constraints on model parameter values. Fortunately, recent improvements in observational capabilities should eventually lead to a tightening of the constraints on $\Omega_B h^2$ and so allow for tighter constraints on the other cosmological parameters.

Column (3) of Tables 9–12 gives the cosmological baryonic-mass fraction for the models we consider here. The cluster baryonic-mass fraction is the sum of the cluster galactic-mass and gas-mass fractions. Assuming that the White et al. (1993) 1 $\sigma$ uncertainties on the cluster total, galactic, and gas masses are Gaussian and adding them in quadrature, we find for the 2 $\sigma$ range of the cluster baryonic-mass fraction:

$$\frac{M_B}{M_{\rm total}} = (1 \pm 0.55)\left(0.009 + \frac{0.05}{h^{1.5}}\right). \qquad (15)$$

Elbaz, Arnaud, & Böhringer (1995), White & Fabian (1995), David, Jones, & Forman (1995), Markevitch et al. (1996), and Buote & Canizares (1996) find similar (or larger) gas-mass fractions. Note that Elbaz et al. (1995) and White & Fabian (1995) find that the gas-mass error bars are somewhat asymmetric; this non-Gaussianity is ignored here. Assuming that the cluster baryonic-mass fraction is an unbiased estimate of the cosmological baryonic-mass fraction, we may use equation (15) to constrain the cosmo-

logical parameters. The boldface entries in column (3) of Tables 9–12 indicates those model parameter values that predict a cosmological baryonic-mass fraction inconsistent with the range of equation (15).

Viana & Liddle (1996; hereafter VL) have reanalyzed the combined galaxy $P(k)$ data of Peacock & Dodds (1994), ignoring some of the smaller scale data in which nonlinear effects might be somewhat larger than previously suspected. Using an analytic approximation to the $P(k)$, they estimate that the scaling parameter (eq. [13])[20] $S = 0.23$, with a 2 $\sigma$ range,

$$0.20 \leq S \leq 0.27 \, . \tag{16}$$

This estimate is consistent with earlier ones.[21] It might be of interest to determine whether the wiggles in $P(k)$ due to the pressure in the photon-baryon fluid (see Fig. 21) can significantly affect the determination of $S$, especially in large $\Omega_B/\Omega_0$ models. [These wiggles are not well described by the analytic approximation to $P(k)$.] The boldface entries in column (4) of Tables 9–12 indicate those model parameter values that predict a scaling parameter value inconsistent with the range of equation (16).

To determine the value of the linear bias parameter $b$,

$$\frac{\delta N}{N}(8\ h^{-1}\ \mathrm{Mpc}) = b\,\frac{\delta M}{M}(8\ h^{-1}\ \mathrm{Mpc}) \, , \tag{17}$$

where $\delta N/N$ is the rms fractional perturbation in galaxy number, we adopt the APM value (Maddox, Efstathiou, & Sutherland 1996) of $(\delta N/N)[8\ h^{-1}\ \mathrm{Mpc}] = 0.96$, with 2 $\sigma$ range:

$$0.75 < \frac{\delta N}{N}(8\ h^{-1}\ \mathrm{Mpc}) < 1.2 \, , \tag{18}$$

where we have added the uncertainty due to the assumed cosmological model and due to the assumed evolution in quadrature with the statistical 1 $\sigma$ uncertainty (Maddox et al. 1996, eq. [43]), and doubled to get the 2 $\sigma$ uncertainty. The range of equation (18) is consistent with that determined from eqs. (7.33) and (7.73) of Peebles (1993).

The local abundance of rich clusters, as a function of their X-ray temperature, provides a tight constraint on $(\delta M/M)[8\ h^{-1}\ \mathrm{Mpc}]$. Eke, Cole, & Frenk (1996; hereafter ECF) (and S. Cole 1996, private communication) find for the open model at 2 $\sigma$

$$\frac{\delta M}{M}(8\ h^{-1}\ \mathrm{Mpc}) = (0.52 \pm 0.08)\Omega_0^{-0.46+0.10\Omega_0} \, , \tag{19}$$

where we have assumed that the ECF uncertainties are Gaussian.[22] The constraints of equation (19) are consistent with, but more restrictive than, those derived by VL.[23] This is because ECF use observational data over a larger range in X-ray temperature to constrain $\delta M/M$ and also use $N$-body computations at $\Omega_0 = 0.3$ and 1 to calibrate the Press-Schechter model (which is used in their determination of the constraints). Furthermore, ECF also make use of hydrodynamical simulations of a handful of individual clusters in the fiducial CDM model ($\Omega_0 = 1$) to calibrate the relation between the gas temperature and the cluster mass and then use this calibrated relation for the computations at all values of $\Omega_0$. The initial conditions for all the simulations were set using the analytical approximation to $P(k)$, so again it might be of interest to see whether the wiggles in the numerically integrated $P(k)$ could significantly affect the determination of the constraints of equation (19). Kitayama & Suto (1996) use X-ray cluster data, and a method that allows for the fact that clusters need not have formed at the redshift at which they are observed, to constrain directly the value of $\Omega_0$ for CDM cosmogonies normalized by the DMR 2 year data. Their conclusions are in reasonable accord with what would be found by using equation (19) (derived assuming that observed clusters are at their redshifts of formation). However, Kitayama & Suto (1996) note that evolution from the redshift of formation to the redshift of observation can affect the conclusions, so a more careful comparison of these two results is warranted. The boldface entries in columns (6) and (9) of Tables 9–12 indicate those model parameter values whose predictions are inconsistent with the constraints of equation (19).[24]

From large-scale peculiar velocity observational data, Zaroubi et al. (1997) estimate $(\delta M/M)[8\ h^{-1}\ \mathrm{Mpc}] = (0.85 \pm 0.2)\Omega_0^{-0.6}$ (2 $\sigma$). It might be significant that the large-scale peculiar velocity observational data constraint is somewhat discordant with (higher than) the cluster temperature function constraint.

Since $J_3$ is less sensitive to smaller length scales (compared to $(\delta M/M)[8\ h^{-1}\ \mathrm{Mpc}]$), observational constraints on $J_3$ are more reliably contrasted with the linear theory predictions. However, since $J_3$ is sensitive to larger length scales, the observational constraints on $J_3$ are significantly less restrictive than the $\pm 8\%$ (1 $\sigma$) constraints of equation (19), and so we do not record the predicted values of $J_3$ here.

Observational constraints on the mass power spectrum determined from large-scale peculiar velocity observations provide another constraint on the mass fluctuations. Kolatt & Dekel (1997) find at the 1 $\sigma$ level

$$h^3 P(k/h = 0.1\ \mathrm{Mpc}^{-1}) = (4.6 \pm 2.3) \times 10^3 \Omega_0^{-1.2}\ \mathrm{Mpc}^3 \, , \tag{20}$$

where the 1 $\sigma$ uncertainty also accounts for sample variance (T. Kolatt 1996, private communication). Since the uncer-

[20] VL actually set $2h = 1$ in the exponent of eq. (13), so the numerical values of their constraint on $S$ should be reduced slightly. We ignore this small effect here.

[21] LLRV used results from an earlier analysis which favored larger values of $S$ than eq. (16)—this is one reason why LLRV favor a higher $\Omega_0$ for the open-bubble inflation model than do GRSB.

[22] Note that the constraint of eq. (19) is derived for a fixed $S$ and that in general it depends weakly on the value of $S$ (and so on the value of $h$ and $\Omega_0$)—see Fig. 13 of ECF. In our preliminary analysis here, we ignore this mild dependence on $h$ and $\Omega_B$. Also note that the constraint of eq. (19) is approximately that required for consistency with the observed cluster correlation function.

[23] VL favor $(\delta M/M)[8\ h^{-1}\ \mathrm{Mpc}] = 0.60$ for fiducial CDM, which is at the $+2\,\sigma$ limit of eq. (19). (As discussed in ECF, this is because VL normalize to the cluster temperature function at 7 keV, where there is a rise in the temperature function.) This is one reason why LLRV favor a higher value of $\Omega_0$ for the open-bubble inflation model than did GRSB.

[24] Given the $\sim \pm 8\%$ (1 $\sigma$) uncertainty of eq. (19), approximate analyses based on using the analytic BBKS approximation to the transfer function should make use of the more accurate parameterization of eq. (13) (rather than that with $2h = 1$ in the exponent), as this gives $(\delta M/M)[8\ h^{-1}\ \mathrm{Mpc}]$ to better than $\sim 5\%$ in the observationally viable part of parameter space (provided use is made of the numerically determined values of $A$).

tainties associated with the constraint of equation (19) are more restrictive than those associated with the constraint of equation (20), we do not tabulate predictions for this quantity here. However, comparison may be made to the predicted linear theory mass power spectra of Figure 21, bearing in mind the $\sim \pm 4.6$ (2 $\sigma$) uncertainty of equation (20) (the uncertainty is approximately Gaussian; T. Kolatt 1996, private communication),[25] and the uncertainty in the DMR normalization (not shown in Fig. 21).

Columns (7) and (10) of Tables 9–12 give the DMR-normalized model predictions for $\beta_I$ (eq. [14]). Cole, Fisher, & Weinberg (1995) measure the anisotropy of the redshift space power spectrum of the *IRAS* 1.2 Jy survey and conclude $\beta_I = 0.52$ with a 2 $\sigma$ c.l. range:

$$0.24 \leq \beta_I \leq 0.80 , \tag{21}$$

where we have doubled the error bars of equation (5.1) of Cole et al. (1995) to get the 2 $\sigma$ range. Cole et al. (1995, Table 1) compare the estimate of equation (21) to other estimates of $\beta_I$, and, at 2 $\sigma$, all estimates of $\beta_I$ are consistent. It should be noted that the model predictions of $\beta_I$ (eq. [14]) in Tables 9–12 assume that for *IRAS* galaxies $(\delta N/N)[8\ h^{-1}$ Mpc$] = 1/1.3$ holds exactly, i.e., they ignore the uncertainty in the rms fractional perturbation in *IRAS* galaxy number, which is presumably of the order of that in equation (18). As the constraints from the deduced $\beta_I$ values, equation (21), are not yet as restrictive as those from other large-scale structure measures, we do not pursue this issue in our analysis here. The boldface entries in columns (7) and (10) of Tables 9–12 indicate those model parameter values whose predictions are inconsistent with the constraints of eq. (21).

### 5.2. *Constraints on Model Parameter Values*

The boldface entries in Tables 9–12 summarize the current constraints imposed by the observational data discussed in the previous section on the model parameter values for the open-bubble inflation model (spectra of type [1] above) and for the flat-space scale-invariant spectrum open model (type [4] above). The current observational constraints on the models are not dissimilar, but this is mostly a reflection of the uncertainty on the constraints themselves since the model predictions are fairly different.

In the following discussion of the preferred part of model parameter space, we focus on the open-bubble inflation model (RP94). Note from Table 13 that the large-scale structure predictions of the open-bubble inflation model do not depend on perturbations generated in the first epoch of inflation (BGT; YST) and also do not depend significantly on the contribution from the non–square-integrable basis function (YST).

Table 9 corresponds to the part of parameter space with "maximized" small-scale power in matter fluctuations. This is accomplished by picking a low $t_0 \simeq 10.5$ Gyr (and so large $h$) and by picking a low $\Omega_B h^2 = 0.0055$ (this is the lower 2 $\sigma$ limit from standard nucleosynthesis and the observed $^4$He, $^7$Li, and high D abundances; FKOT). The tightest constraints on the model parameter values come from the matter power spectrum observational data constraints on the shape parameter $S$ (Table 9, col. [4]) and from the cluster X-ray temperature function observational data constraints on $(\delta M/M)[8\ h^{-1}$ Mpc] (col. [6]). Note that for $\Omega_0 = 0.3$, the predicted upper 2 $\sigma$ value of $(\delta M/M)[8\ h^{-1}$ Mpc$] = 0.69$, while ECF conclude that at 2 $\sigma$, the observational data require that this be at least 0.74, so an $\Omega_0 = 0.3$ case fails this test. The constraints on $\beta_I$ (col. [7]) are not as restrictive as those on $(\delta M/M)[8\ h^{-1}$ Mpc]. For these values of $t_0$ and $\Omega_B h^2$, the cosmological baryonic-mass fraction at $\Omega_0 = 0.3$ is predicted to be 0.033 (col. [3]), while at 2 $\sigma$ White et al. (1993) require that this be at least 0.039 (at $h = 0.75$), so again this $\Omega_0 = 0.3$ model just fails this test. Given the observational uncertainties, it might be possible to make minor adjustments to model parameter values so that an $\Omega_0 \sim 0.3$–$0.35$ model with $t_0 \sim 10.5$ Gyr and $\Omega_B h^2 \sim 0.0055$ is just consistent with the observational data. However, it is clear that current observational data do not favor an open model with $\Omega_B h^2 \simeq 0.0055$—the observed cluster $(\delta M/M)[8\ h^{-1}$ Mpc] favors a larger $\Omega_0$ while the observed cluster baryonic-mass fraction favors a smaller $\Omega_0$, and so are in conflict.

Table 10 gives the predictions for the $t_0 \simeq 12$ Gyr, $\Omega_B h^2 = 0.0125$ models. This value of $\Omega_B h^2$ is consistent with the 2 $\sigma$ range determined from standard nucleosynthesis and the observed $^4$He and $^7$Li abundances: $0.0051 < \Omega_B h^2 < 0.016$ (FKOT; also see Copi et al. 1995; Sarkar 1996). It is, however, somewhat difficult to reconcile $\Omega_B h^2 = 0.0125$ with the 2 $\sigma$ range derived from the observed $^4$He, $^7$Li, and current high D abundances $0.0055 < \Omega_B h^2 < 0.0087$ (FKOT), or with that from the current observed low D abundances $0.018 < \Omega_B h^2 < 0.030$ (Burles & Tytler 1998). In any case, the observed D abundances are still under discussion and must be viewed as preliminary. In this case, open-bubble inflation models with $0.35 < \Omega_0 \lesssim 0.5$ are consistent with the observational constraints. The current central observational data values for $S$ and $\beta_I$ favor $\Omega_0 \sim 0.4$, while that for the cluster baryonic-mass fraction prefers $\Omega_0 \sim 0.3$, and that for $(\delta M/M)[8\ h^{-1}$ Mpc] favors $\Omega_0 \sim 0.45$, so in this case the agreement between predictions and observational data is fairly impressive (although the Tanvir et al. 1995 central $h$ value favors $\Omega_0 \sim 0.2$). Note that in this case models with $\Omega_0 \gtrsim 0.6$ are quite inconsistent with the data.

Table 11 gives the predictions for $t_0 \simeq 13.5$ Gyr, $\Omega_B h^2 = 0.205$ models. This baryonic-mass density value is consistent with that determined from the current observed low D abundances but is difficult to reconcile with the current standard nucleosynthesis interpretation of the observed $^4$He and $^7$Li abundances (Cardall & Fuller 1996). The larger value of $\Omega_B h^2$ (and smaller value of $h$) has now lowered small-scale power in mass fluctuations somewhat significantly, opening up the allowed $\Omega_0$ range to larger values. Models with $0.4 < \Omega_0 < 0.6$ are consistent with the observational data, although the higher $\Omega_0$ part of the range is starting to conflict with what is determined from the small-scale dynamical estimates, and the models do require a somewhat low $h$ (but not yet inconsistently so at the 2 $\sigma$ significance level—while the Tanvir et al. 1995 central $h$ value requires $\Omega_0 < 0.1$, at 2 $\sigma$ the $h$ constraint only requires $\Omega_0 \lesssim 0.6$). The central observational values for $S$, the cluster baryonic-mass fraction, $(\delta M/M)[8\ h^{-1}$ Mpc], and $\beta_I$ favor $\Omega_0 \sim 0.5$, so the agreement with observational data is fairly impressive and could even be improved by reducing $t_0$ a little to raise $h$.

[25] Thus at the higher, $\sim 2\ \sigma$, significance level, eq. (20) provides a strong upper limit on $P(k/h = 0.1\ \mathrm{Mpc}^{-1})$, especially at larger $\Omega_0$ because of the $\Omega_0$ dependence.

Table 12 gives the predictions for another part of model parameter space. Here we show $\Omega_B h^2 = 0.007$ models (at $t_0 \simeq 12$ Gyr), consistent with the central value of $\Omega_B h^2$ determined from standard nucleosynthesis using the observed $^4$He, $^7$Li, and high D abundances (FKOT). The larger value of $\Omega_B h^2$ (compared to Table 9) eases the cluster baryonic-mass fraction constraint, which now requires only $\Omega_0 < 0.4$. The increase in $\Omega_B h^2$ also decreases the mass fluctuation amplitude, which makes it more difficult to argue for $\Omega_0 = 0.3$; however, models with $0.35 < \Omega_0 < 0.4$ seem to be consistent with the observational constraints when $\Omega_B h^2 \sim 0.007$ and $t_0 \sim 12$ Gyr. It is interesting that in this case the central observational data values we consider for $S$, for $(\delta M/M)[8\ h^{-1}$ Mpc], and for $\beta_I$ prefer $\Omega_0 \sim 0.4$; however, that for the cluster baryonic-mass fraction (as well as that for $h$) favors $\Omega_0 \sim 0.2$ (although at 2 $\sigma$ the cluster baryonic-mass fraction constraint only requires $\Omega_0 < 0.4$). Hence, while $\Omega_0 \sim 0.35$–$0.4$ open-bubble inflation models with $\Omega_B h^2 \sim 0.007$ and $t_0 \sim 12$ Gyr are quite consistent with the observational constraints, in this case the agreement between predictions and observations is not spectacular. Note that in this case models with $\Omega_0 \gtrsim 0.5$–$0.6$ are quite inconsistent with the observational data.

In summary, open-bubble inflation models based on the CDM picture (RP94; BGT; YST) are reasonably consistent with current observational data provided $0.3 < \Omega_0 \lesssim 0.6$. The flat-space scale-invariant spectrum open model (W83) is also reasonably compatible with current observational constraints for a similar range of $\Omega_0$. The uncertainty in current estimates of $\Omega_B h^2$ is one of the major reasons that such a large range in $\Omega_0$ is consistent with current observational constraints.

Our previous analysis of the DMR 2 year data led us to conclude that only those open-bubble inflation models near the lower end of the above range ($\Omega_0 \sim 0.3$–$0.4$) were consistent with the majority of observations (GRSB). The increase in the allowed range to higher $\Omega_0$ values $\sim 0.5$–$0.6$ can be ascribed to a number of small effects. Specifically, these are (1) the slight downward shift in the central value of the DMR 4 year normalization relative to the 2 year one (G96); (2) use of the full 2 $\sigma$ range of normalizations allowed by the DMR data analysis (instead of the 1 $\sigma$ range allowed by the galactic-frame quadrupole-excluded DMR 2 year data set used previously); (3) use of the 2 $\sigma$ range of the small-scale dynamical estimates of $\Omega_0$ instead of the 1 $\sigma$ range used in our earlier analysis; (4) our consideration of a range of $\Omega_B h^2$ values here (in GRSB we focused on $\Omega_B h^2 = 0.0125$); and (5) our consideration of a range of $t_0$ values here (in GRSB we concentrated on $t_0 \simeq 12$ Gyr). We emphasize, however, that the part of parameter space with $\Omega_0 \sim 0.5$–$0.6$ is favored only if $\Omega_B h^2$ is large ($>0.02$), $h$ is low ($<0.55$), and the small-scale dynamical estimates of $\Omega_0$ turn out to be biased somewhat low.

### 5.3. *Indications from Additional Observational Constraints*

The observational results we have used to constrain model parameter values in the previous sections are the most robust currently available. In this section, we summarize several of the more tentative constraints from more recent observations.

In our analysis of the DMR 2 year data normalized models, we compared model predictions for the rms value of the smoothed peculiar velocity field to results from the analysis of observational data (Bertschinger et al. 1990). We do not do so again here since, given the uncertainties, the conclusions drawn in GRSB are not significantly modified. In particular, comparison of the appropriate quantities implies that we can treat the old 1 $\sigma$ upper limits essentially as 2 $\sigma$ upper limits for the four-year analysis.

In GRSB we used $\beta_I$ determined by Nusser & Davis (1994), $0.2 < \beta_I < 1.0$ (2 $\sigma$), to constrain the allowed range of models to $0.2 < \Omega_0 \lesssim 0.6$. Here we use the Cole et al. (1995) estimate, $0.24 < \beta_I < 0.80$ (2 $\sigma$), which, for the models of Table 10, requires $\Omega_0 > 0.25$. This value is just below the lower limit ($\Omega_0 \gtrsim 0.3$) derived from the Bertschinger et al. (1990) results in GRSB. We hence conclude that the large-scale flow results of Bertschinger et al. (1990) indicates a lower 2 $\sigma$ limit on $\Omega_0$ that is about $\Delta\Omega_0 \sim 0.05$ higher than that suggested by the redshift-space distortion analysis of Cole et al. (1995).[26] However, we strongly emphasize that the central value of the large-scale flow results of Bertschinger et al. (1990) does favor a significantly larger value of $\Omega_0$ than the rest of the data we have considered here. Furthermore, as discussed in detail in GRSB, there is some uncertainty in how to interpret properly large-scale velocity data in the open models, particularly given the large sample variance associated with the measurement of a single bulk velocity (Bond 1996; also see LLRV). A more careful analysis, as well as more observational data, is undoubtedly needed before it will be possible to conclude robustly that the large-scale velocity data do indeed force one to consider significantly larger values of $\Omega_0$ than is favored by the rest of the observational constraints (and hence rule out the models considered here).

It might be significant that on comparing the mass power spectrum deduced from a refined set of peculiar velocity observations to the galaxy power spectrum determined from the APM survey, Kolatt & Dekel (1997) estimate that for the optically selected APM galaxies $\beta = 0.80$ with a 2 $\sigma$ range,

$$0.60 < \beta < 1.0\ . \tag{22}$$

(Note that it has been argued that systematic uncertainties preclude a believable determination of $\beta_I$ from a comparison of the observed large-scale peculiar velocity field to the *IRAS* 1.2 Jy galaxy distribution; Davis, Nusser, & Willick 1996.) This range is consistent with other estimates now under discussion. The Stromlo-APM comparison of Loveday et al. (1996) indicates $\beta \simeq 0.48$, with a 2 $\sigma$ upper limit of 0.75, while Baugh (1996) concludes that $\beta < 1.0$ (2 $\sigma$), and Ratcliffe et al. (1996) argue for $\beta = 0.55 \pm 0.12$. Using the APM range for $(\delta N/N)[8\ h^{-1}$ Mpc], equation (18), the Kolatt & Dekel (1997) estimate of $\beta$, equation (22), may be converted to an estimate of $\delta M/M$, and at 2 $\sigma$,

$$\frac{\delta M}{M}(8\ h^{-1}\ \mathrm{Mpc}) = (0.45\text{–}1.2)\Omega_0^{-0.6}\ . \tag{23}$$

It is interesting that at $\Omega_0 = 1$, the lower part of this range is consistent with that determined from the cluster X-ray temperature function data, equation (19), although at lower $\Omega_0$, equation (23) indicates a larger value then does equation (19) because of the steeper rise to low $\Omega_0$.

[26] Note that the lower limit from the Bertschinger et al. (1990) analysis is not as restrictive as that set by the cluster X-ray temperature function data constraints on $(\delta M/M)[8\ h^{-1}$ Mpc].

Zaroubi et al. (1997) have constrained model parameter values by comparing large-scale flow observations to that predicted in the DMR 2 year data normalized open-bubble inflation model. They conclude that the open-bubble inflation model provides a good description of the large-scale flow observations if, at $2\sigma$,

$$0.31 < \Omega_0 h < 0.44 . \quad (24)$$

From Table 12 we see that an open-bubble inflation model with $\Omega_0 = 0.45$ and $h = 0.62$ provides a good fit to all the observational data considered in § 5.1. For $h = 0.62$, Zaroubi et al. (1997) conclude that at $2\sigma\,\Omega_0 > 0.5$ (eq. [24]), just above our value of $\Omega_0 = 0.45$. Since the Zaroubi et al. (1997) analysis does not account for the uncertainty in the DMR normalization (T. Kolatt 1996, private communication), it is still unclear if the constraints from the large-scale flow observations are in conflict with those determined from the other data considered here (and so rule out the open-bubble inflation model). It might also be significant that on somewhat smaller length scales, there is support for a smaller value of $\Omega_0$ from large-scale velocity field data (Shaya, Peebles, & Tully 1995).

The cluster peculiar velocity function provides an alternate mechanism for probing the peculiar velocity field (see, e.g., Croft & Efstathiou 1994; Moscardini et al. 1996; Bahcall & Oh 1996). Bahcall & Oh (1996) conclude that current observational data is well described by an $\Omega_0 = 0.3$ flat-$\Lambda$ model with $h = 0.67$ and $(\delta M/M)[8\ h^{-1}\ \mathrm{Mpc}] = 0.67$. This normalization is somewhat smaller than that indicated by the DMR data (see, e.g., Ratra et al. 1997). While Bahcall & Oh (1996) did not compare the cluster peculiar velocity function data to the predictions of the open-bubble inflation model, approximate estimates indicate that these data are consistent with the open-bubble inflation model predictions for the range of $\Omega_0$ favored by the other data we consider in §§ 5.1 and 5.2—see the $(\delta M/M)[8\ h^{-1}\ \mathrm{Mpc}]$ values for the allowed models in Tables 9–12. Bahcall & Oh (1996) also note that it is difficult, if not impossible, to reconcile the cluster peculiar velocity observations with what is predicted in high density models like fiducial CDM and MDM.

At fixed $(\delta M/M)[8\ h^{-1}\ \mathrm{Mpc}]$, low-density cosmogonies form structure earlier than high-density ones. Thus, observations of structure at high redshift may be used to constrain the matter density. As benchmarks, we note that scaling from the results of the numerical simulations of Cen & Ostriker (1993), in a open model with $(\delta M/M)[8\ h^{-1}\ \mathrm{Mpc}] = 0.8$ galaxy formation peaks at a redshift $z_g \simeq 2.3$ when $\Omega_0 = 0.45$ and at $z_g \simeq 2.5$ when $\Omega_0 = 0.4$. Thus, the open-bubble inflation model is not in conflict with observational indications that the giant elliptical luminosity function at $z \sim 1$ is similar to that at the present (see, e.g., Lilly et al. 1995; Glazebrook et al. 1995; Im et al. 1996), nor is it in conflict with observational evidence for massive galactic disks at $z \sim 1$ (Vogt et al. 1996). These models can also accommodate observational evidence of massive star-forming galaxies at $z \sim 1.5$ (Cowie, Hu, & Songaila 1995), as well as the significant peak at $z \sim 2.2$ in the number of galaxies as a function of (photometric) redshift found in the Hubble Deep Field (Gwyn & Hartwick 1996), and it is not inconceivable that objects like the $z = 2.7$ "protogalaxy" candidate[27] (Yee et al. 1996; Ellingson et al. 1996) can be produced in these models. It is, however, at present unclear whether the open-bubble inflation model can accommodate a substantial population of massive star-forming galaxies at $z \sim 3$–$3.5$ (Steidel et al. 1996; Giavalisco, Steidel, & Macchetto 1996), and if there are many more examples of massive damped Ly$\alpha$ systems[28] like the one at $z = 4.4$ (see, e.g., Lu et al. 1996; Wampler et al. 1996; Fontana et al. 1996), then, depending on the masses, these might be a serious problem for the open-bubble inflation model. On the other hand, the recent discovery of galaxy groups at $z \sim 2.4$ (see, e.g., Francis et al. 1996; Pascarelle et al. 1996) probably do not pose a serious threat for the open-bubble inflation model, while massive clusters at $z \sim 0.5$–$1$ (see, e.g., Luppino & Gioia 1995; Pelló et al. 1996) can easily be accommodated in the model. It should be noted that in adiabatic $\Omega_0 = 1$ models normalized to fit the present small-scale observations, e.g., fiducial CDM (with a normalization inconsistent with that from the DMR), or MDM, or tilted CDM (without a cosmological constant), it is quite difficult, if not impossible, to accommodate the above observational indications of early structure formation (see, e.g., Ma & Bertschinger 1994; Ostriker & Cen 1996).

With the recent improvements in observational capabilities, neoclassical cosmological tests hold great promise for constraining the world model. It might be significant that current constraints from these tests are consistent with that region of the open-bubble inflation model parameter space that is favored by the large-scale structure constraints. These tests include the *HST* elliptical galaxy number counts test (Driver et al. 1996), an early application of the apparent magnitude-redshift test using Type Ia supernovae (Perlmutter et al. 1996), as well as analyses of the rate of gravitational lensing of quasars by foreground galaxies (see, e.g., Torres & Waga 1996; Kochanek 1996). It should be noted that these tests are also consistent with $\Omega_0 = 1$ models and plausibly with a time-variable cosmological "constant"–dominated spatially flat model (see, e.g., Ratra & Quillen 1992; Torres & Waga 1996), but they do put pressure on the flat-$\Lambda$ CDM model.

Smaller scale CMB spatial anisotropy measurements will eventually significantly constrain the allowed range of model parameter values. Figure 22 compares the $1\sigma$ range of CMB spatial anisotropy predictions for a few representative open-bubble inflation (as well as flat-space scale-invariant spectrum open) models to available CMB spatial anisotropy observational data. From a preliminary comparison of the predictions of DMR 2 year data normalized open-bubble inflation models to available CMB anisotropy observational data, Ratra et al. (1997) concluded that the range of parameter space for the open-bubble inflation model that was favored by the other observational data was also consistent with the small-scale CMB anisotropy data. This result was quantified by GRS, who also considered open-bubble inflation models normalized to the $\pm 1\ \sigma$ values of the DMR 2 year data (and hence considered open-bubble inflation models normalized at close to the DMR 4

[27] Note that if the velocity dispersion of the nearby foreground cluster has actually been significantly underestimated, the striking properties of this object could mostly be a consequence of gravitational lensing, and it would seem to be more reasonably interpreted as a massive star-forming galaxy (Williams & Lewis 1996).

[28] These have many of the properties expected of young galaxies (Wolfe 1993; Djorgovski et al. 1996, and references therein).

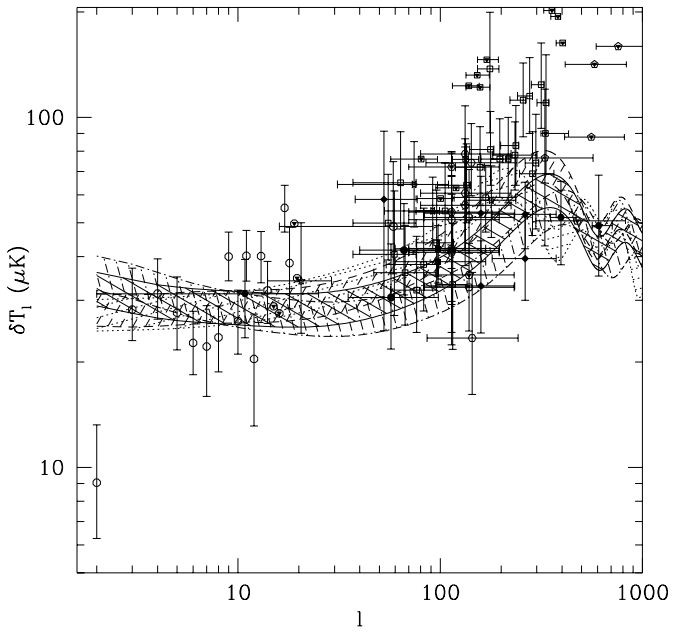


FIG. 22*a*

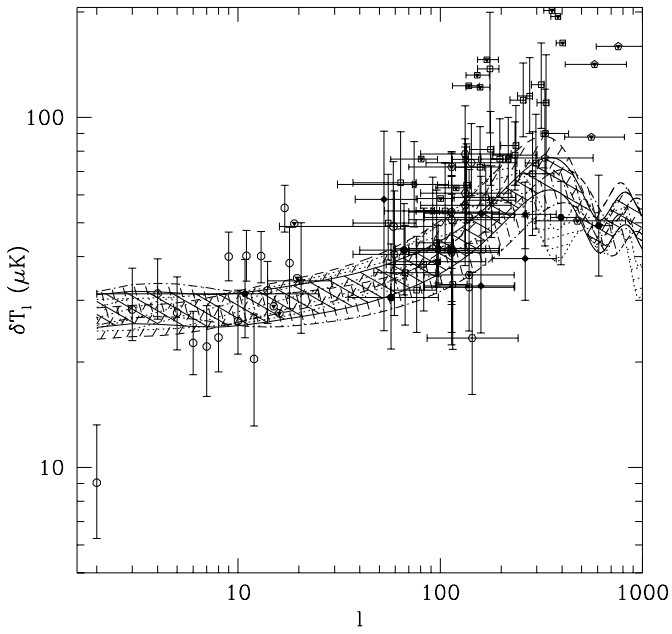


FIG. 22*b*

FIG. 22.—CMB anisotropy band temperature predictions and observational results, as a function of multipole $\ell$, to $\ell = 1000$. The four pairs of wavy curves (in different line styles) demarcating the boundaries of the four partially overlapping wavy hatched regions (hatched with straight lines in different line styles) in panel (*a*) are DMR-normalized open-bubble inflation model (RP94) predictions for what would be seen by a series of ideal, Kronecker-delta window function, experiments (see Ratra et al. 1997 for details). Panel (*b*) shows DMR-normalized CMB anisotropy spectra with the same cosmological parameters for the flat-space scale-invariant spectrum open model (W83). The model-parameter values are $\Omega_0 = 0.3$, $h = 0.7$, $\Omega_B h^2 = 0.0075$, $t_0 = 11.3$ Gyr (*dot-dashed lines*); $\Omega_0 = 0.4$, $h = 0.65$, $\Omega_B h^2 = 0.0125$, $t_0 = 11.7$ Gyr (*solid lines*); $\Omega_0 = 0.5$, $h = 0.55$, $\Omega_B h^2 = 0.0175$, $t_0 = 13.4$ Gyr (*dashed lines*); and, $\Omega_0 = 1$, $h = 0.5$, $\Omega_B h^2 = 0.0125$, $t_0 = 13.0$ Gyr (*dotted lines*)—for more details on these models, see Ratra et al. (1997). For each pair of model prediction demarcation curves, the lower one is normalized to the lower 1 $\sigma$ $Q_{\rm rms\text{-}PS}$ value determined from the analysis of the galactic coordinate maps accounting for the high-latitude Galactic emission correction and including the $\ell = 2$ moment in the analysis, and the upper one is normalized to the upper 1 $\sigma$ $Q_{\rm rms\text{-}PS}$ value determined from the analysis of the ecliptic coordinate maps ignoring the Galactic emission correction and excluding the $\ell = 2$ moment from the analysis. Among the open-bubble inflation models of panel (*a*), the $\Omega_0 = 0.4$ model is close to what is favored by the analysis of Table 10, and the $\Omega_0 = 0.5$ model is close to that preferred from the analysis of Table 11. The $\Omega_0 = 0.3$ model is on the edge of the allowed region from the analysis of Table 12, and the $\Omega_0 = 1$ fiducial CDM model is incompatible with cosmographic and large-scale structure observations. A large fraction of the smaller scale observational data in these plots are tabulated in Ratra et al. (1997). Note that, as discussed in this paper, some of the data points are from reanalyses of the observational data. There are 69 detections and 22 2 $\sigma$ upper limits shown. Since most of the smaller scale data points are derived assuming a flat bandpower CMB anisotropy angular spectrum, which is more accurate for narrower (in $\ell$) window functions, we have shown the observational results from the narrowest windows available. The data shown are from the DMR galactic frame maps ignoring the Galactic emission correction (Górski 1997; *open octagons* with $\ell \leq 20$); from FIRS (Ganga et al. 1994, as analyzed by Bond 1995; *solid pentagon*); Tenerife (Hancock et al. 1997a; *open five-point star*); Bartol (Piccirillo et al. 1997; *solid diamond*, note that atmospheric contamination may be an issue); SK93, individual-chop SK94 Ka and Q, and individual-chop SK95 cap and ring (Netterfield et al. 1997; *open squares*); SP94 Ka and Q (Gundersen et al. 1995; the points plotted here are from the flat bandpower analysis of Ganga et al. 1997, *solid circles*); BAM 2-beam (Tucker et al. 1997, at $\ell_{\rm eff} = 58.2$ with $\ell_{e^{-0.5}}$ spanning 16 to 92, and accounting for the 20% calibration uncertainty; *open circle*); Python-G, -L, and -S (see, e.g., Platt et al. 1997; *open six-point stars*); ARGO (see, e.g., Masi et al. 1996, both the Hercules and Aries + Taurus scans are shown—note that the Aries + Taurus scan has a larger calibration uncertainty of 10%; *solid squares*); MAX3, individual-channel MAX4, and MAX5 (see, e.g., Tanaka et al. 1996, including the MAX5 MUP 2 $\sigma$ upper limit $\delta T_\ell < 35$ $\mu$K at $\ell_{\rm eff} = 139$, Lim et al. 1996; *open hexagons*); MSAM92 and MSAM94 (see, e.g., Inman et al. 1997; *open diamonds*); WDH1–3 and WDI, II (see, e.g., Griffin et al. 1998; *open pentagons*); and CAT (Scott et al. 1996—CAT1 at $\ell_{\rm eff} = 396$ with $\ell_{e^{-0.5}}$ spanning 351 to 471, and CAT2 at $\ell_{\rm eff} = 608$ with $\ell_{e^{-0.5}}$ spanning 565 to 710, both accounting for calibration uncertainty of 5%; *solid hexagons*). Detections have vertical 1 $\sigma$ error bars. Solid inverted triangles inserted inside the appropriate symbols correspond to nondetections and are placed at the upper 2 $\sigma$ limits. Vertical error bars are not shown for nondetections. As discussed in Ratra et al. (1997), all $\delta T_\ell$ (vertical) error bars also account for the calibration uncertainty (but in an approximate manner, except for the SP94 Ka and Q results from Ganga et al. 1997—see Ganga et al. 1997 for a discussion of this issue). The observational data points are placed at the $\ell$-value at which the corresponding window function is most sensitive (this ignores the fact that the sensitivity of the experiment is also dependent on the assumed form of the sky-anisotropy signal and so gives a somewhat misleading impression of the multipoles to which the experiment is sensitive—see Ganga et al. 1997 for a discussion of this issue). Excluding the DMR points at $\ell \leq 20$, the horizontal lines on the observational data points represent the $\ell$-space width of the corresponding window function (again ignoring the form of the sky-anisotropy signal). Note that from an analysis of a large fraction of the data (corresponding to detections of CMB anisotropy) shown in these figures, GRS (Figs. 5 and 6) conclude that all the models shown in panel (*a*), including the fiducial CDM one, are consistent with the CMB anisotropy data.

year data value; see Figs. 5 and 6 of GRS). GRS discovered that (given the uncertainties associated with the smaller scale measurements) the 1 $\sigma$ uncertainty in the value of the DMR normalization precludes determination of robust constraints on model parameter values, although the range of model parameter space for the open-bubble inflation model favored by the analysis here was found to be consistent with the smaller scale CMB anisotropy observations, and $\Omega_0 \sim 0.1$ open-bubble inflation models were not favored by the smaller scale CMB anisotropy observational

data (GRS, Figs. 5 and 6).[29] A detailed analysis of the UCSB South Pole 1994 CMB anisotropy data (Gundersen et al. 1995) by Ganga et al. (1997) reaches a similar conclusion: at 1 $\sigma$ (assuming a Gaussian marginal probability distribution), the data favor open-bubble inflation models with $\Omega_0 < 0.5$, while at 2 $\sigma$, the UCSB South Pole 1994 data are consistent with the predictions of the open-bubble, flat-$\Lambda$, and fiducial CDM inflation models.

## 6. DISCUSSION AND CONCLUSION

We have compared the DMR 53 and 90 GHz sky maps to a variety of open model CMB anisotropy angular spectra in order to infer the normalization of these open cosmogonical models. Our analysis explicitly quantifies the small shifts in the inferred normalization amplitudes due to (1) the small differences between the galactic- and ecliptic-coordinate sky maps; (2) the inclusion or exclusion of the $\ell = 2$ moment in the analysis; and (3) the faint high-latitude Galactic emission treatment. We have defined a maximal 2 $\sigma$ uncertainty range based on the extremal solutions of the normalization fits, and a maximal 1 $\sigma$ uncertainty range may be defined in a similar manner. For this maximal 1 $\sigma$ $Q_{\rm rms\text{-}PS}$ range, the fractional 1 $\sigma$ uncertainty, at fixed $\Omega_B$ and $h$ (but depending on the assumed CMB anisotropy angular spectrum and model parameter values), ranges between $\sim 10\%$ and $\sim 12\%$.[30] (Compare this to the $\sim 8\%$, 1 $\sigma$, uncertainty of eq. [19].) Since part of this uncertainty is due to the small systematic shifts, the maximal 2 $\sigma$ fractional uncertainty is smaller than twice the maximal 1 $\sigma$ fractional uncertainty. For the largest possible 2 $\sigma$ $Q_{\rm rms\text{-}PS}$ range defined above, the fractional uncertainty varies between $\sim 16\%$ and $\sim 19\%$. Note that this accounts for intrinsic noise, cosmic variance, and effects (1)–(3) above. Other systematic effects, e.g., the calibration uncertainty (Kogut et al. 1996) or the beamwidth uncertainty (Wright et al. 1994), are much smaller than the effects we have accounted for here. It has also been shown that there is negligible non-CMB contribution to the DMR data sets from known extragalactic astrophysical foregrounds (Banday et al. 1996).

By analyzing the DMR maps using CMB anisotropy spectra at fixed $\Omega_0$ but different $h$ and $\Omega_B$, we have also explicitly quantified the small shifts in the inferred normalization amplitude due to shifts in $h$ and $\Omega_B$. Although these shifts do depend on the value of $\Omega_0$ and the assumed model power spectrum, given the other uncertainties, it is reasonable to ignore these small shifts when normalizing the models considered in this work.

We have analyzed the open-bubble inflation model, accounting only for the fluctuations generated during the evolution inside the bubble (RP94), including the effects of the fluctuations generated in the first epoch of spatially flat inflation (BGT; YST) and finally accounting for the contribution from a non–square-integrable basis function (YST). For observationally viable open-bubble models, the observable predictions do not depend significantly on the latter two sources of anisotropy. The observable predictions of the open-bubble inflation scenario seem to be robust—it seems that only those fluctuations generated during the evolution inside the bubble need to be accounted for.

As discussed in the Introduction, a variety of more specific realizations of the open-bubble inflation scenario have recently come under scrutiny. These are based on specific assumptions about the vacuum state prior to open-bubble nucleation. In these specific realizations of the open-bubble inflation scenario, there are a number of additional mechanisms for stress-energy perturbation generation (in addition to those in the models considered here), including those that come from fluctuations in the bubble wall, as well as effects associated with the nucleation of a nonzero size bubble. While current analyses suggest that such effects also do not add a significant amount to the fluctuations generated during the evolution inside the bubble, it is important to continue to pursue such investigations—both to examine more carefully the robustness of the open-bubble inflation scenario predictions, as well as to try to find a reasonable particle physics based realization of the open-bubble inflation scenario.

As has been previously noted for other CMB anisotropy angular spectra (G96), the various different DMR data sets lead to slightly different $Q_{\rm rms\text{-}PS}$ normalization amplitudes, but well within the statistical uncertainty. This total range is slightly reduced if one considers results from analyses either ignoring or including the quadrupole moment.

The DMR data alone can not be used to constrain $\Omega_0$ over range $0.1 \leq \Omega_0 \leq 1$ in a statistically meaningful fashion for the open models considered here. However, it is reasonable to conclude that when the quadrupole moment is excluded from the analysis, the $\Omega_0 \sim 0.4$ model CMB anisotropy spectral shape is most consistent with the DMR data, while the quadrupole-included analysis favors $\Omega_0 \sim 0.7$ (for the open-bubble inflation model in the range $0.1 \leq \Omega_0 \leq 1$).

Current cosmographic observations, in conjunction with current large-scale structure observations compared to the predictions of the DMR-normalized open-bubble inflation model derived here, favor $0.3 < \Omega_0 \lesssim 0.6$. The large allowed range is partially a consequence of the current uncertainty in $\Omega_B$. This range is consistent with the value weakly favored ($\Omega_0 \sim 0.4$) by a quadrupole-excluded analysis of the DMR data alone. It might also be significant that mild bias is indicated both by the need to reconcile these larger values of $\Omega_0$ with what is determined from small-scale dynamical estimates, as well as to reconcile the smaller DMR-normalized $(\delta M/M)[8\ h^{-1}\ {\rm Mpc}]$ values (for this favored range of $\Omega_0$) with the larger observed galaxy number fluctuations (e.g., eq. [18]).

In common with the low-density flat-$\Lambda$ CDM model, we

[29] The recent analysis of Hancock et al. (1997b) is generally consistent with these results. They conclude that $\Omega_0 \sim 0.7$ is favored, but even at 1 $\sigma$, $0.3 \leq \Omega_0 \leq 1.7$ is allowed—this broad range is consistent with the conclusion of GRS that it is not yet possible to constrain meaningfully cosmological parameter values from the CMB anisotropy data alone. Note also that Hancock et al. (1997b) do not consider the effects of the systematic shifts between the various DMR data sets and also exclude a number of data points, e.g., the four MSAM points and the MAX3 MUP point (which is consistent with the recent MAX5 MUP result; Lim et al. 1996), which do not disfavor a lower value of $\Omega_0$ for the open-bubble inflation model (Ratra et al. 1997; GRS).

[30] Note that the quoted 1 $\sigma$ (statistical and systematic) uncertainty of BW (footnote 4; also see Bunn, Liddle, & White 1996), 7.6%, is smaller than the DMR 4 year data 1 $\sigma$ uncertainty estimated in, e.g., G96, Wright et al. (1996), and here. This is because we explicitly estimate the effect of all known systematic uncertainties for each assumed CMB anisotropy angular spectrum and account for them, in the most conservative manner possible, as small shifts. (In particular: we do not just account for the small systematic difference between the galactic- and ecliptic-frame maps; we do not assume that any of the small systematic differences lead to model-independent systematic shifts in the inferred $Q_{\rm rms\text{-}PS}$ values; and we do not add the systematic shifts in quadrature with the statistical uncertainty.) Since our accounting of the uncertainties is the most conservative possible, our conclusions about model viability are the most robust possible.

have established that in the low-density open-bubble CDM model, one may adjust the value of $\Omega_0$ to accommodate a large fraction of present observational constraints. For a broad class of these models, with adiabatic Gaussian initial energy-density perturbations, this focuses attention on values of $\Omega_0$ that are larger than the range of values for $\Omega_B$ inferred from the observed light-element abundances in conjunction with standard nucleosynthesis theory. Whether this additional CDM is nonbaryonic or is simply baryonic material that does not take part in standard nucleosynthesis remains a major outstanding puzzle for these models.

In conclusion, the open-bubble inflation model with $0.3 < \Omega_0 \lesssim 0.6$ is most consistent with current observations.

We acknowledge the efforts of those contributing to the *COBE*-DMR. *COBE* is supported by the Office of Space Sciences of NASA Headquarters. We also acknowledge the advice and assistance of C. Baugh, S. Cole, J. Garriga, T. Kolatt, C. Park, L. Piccirillo, G. Rocha, G. Tucker, D. Weinberg, and K. Yamamoto. B. R. acknowledges support from NSF grant EPS-9550487 with matching support from the state of Kansas and from a K*STAR First award. R. S. is supported in part by a PPARC grant and KBN grant 2P30401607.

REFERENCES

Abbott, L. F., & Schaefer, R. K. 1986, ApJ, 308, 546
Bahcall, N. A., & Oh, S. P. 1996, ApJ, 462, L49
Banday, A. J., et al. 1996, ApJ, 468, L85
———. 1997, ApJ, 475, 393
Banks, T., et al. 1995, Phys. Rev. D, 52, 3548
Bardeen, J. M., Bond, J. R., Kaiser, N., & Szalay, A. S. 1986, ApJ, 304, 15 (BBKS)
Baugh, C. M. 1996, MNRAS, 280, 267
Baugh, C. M., & Efstathiou, G. 1993, MNRAS, 265, 145
Baum, W. A., et al. 1995, AJ, 110, 2537
Bennett, C. L., et al. 1994, ApJ, 436, 423
———. 1996, ApJ, 464, L1
Bertschinger, E., et al. 1990, ApJ, 364, 370
Bond, J. R. 1995, Phys. Rev. Lett., 74, 4369
———. 1996, in Cosmology and Large Scale Structure, ed. R. Schaeffer, J. Silk, M. Spiro, & J. Zinn-Justin (Amsterdam: Elsevier), 469
Branch, D., Fisher, A., Baron, E., & Nugent, P. 1996, ApJ, 470, L7
Bucher, M., Goldhaber, A. S., & Turok, N. 1995, Phys. Rev. D, 52, 3314 (BGT)
Bucher, M., & Turok, N. 1995, Phys. Rev. D, 52, 5538 (BT)
Bunn, E. F., Liddle, A. R., & White, M. 1996, Phys. Rev. D, 54, R5917
Bunn, E. F., & White, M. 1997, ApJ, 480, 6 (BW)
Buote, D. A., & Canizares, C. R. 1996, ApJ, 457, 565
Burles, S., & Tytler, D. 1998, Science, submitted
Cardall, C. Y., & Fuller, G. M. 1996, ApJ, 472, 435
Carlberg, R. G., et al. 1996, ApJ, 462, 32
Carswell, R. F., et al. 1994, MNRAS, 268, L1
———. 1996, MNRAS, 278, 506
Cayón, L., et al. 1996, MNRAS, 279, 1095
Cen, R., & Ostriker, J. P. 1993, ApJ, 414, 407
Chaboyer, B., Demarque, P., Kernan, P. J., & Krauss, L. M. 1996, Science, 271, 957
Cohn, J. D. 1996, Phys. Rev. D, 54, 7215
Cole, S., Fisher, K. B., & Weinberg, D. H. 1995, MNRAS, 275, 515
Copi, C. J., Schramm, D. N., & Turner, M. S. 1995, Phys. Rev. Lett., 75, 3981
Cowie, L. L., Hu, E. M., & Songaila, A. 1995, Nature, 377, 603
Croft, R. A. C., & Efstathiou, G. 1994, MNRAS, 268, L23
da Costa, L. N., et al. 1994, ApJ, 437, L1
Dar, A. 1995, ApJ, 449, 550
David, L. P., Jones, C., & Forman, W. 1995, ApJ, 445, 578
Davis, M., Nusser, A., & Willick, J. A. 1996, ApJ, 473, 22
Djorgovski, S. G., Pahre, M. A., Bechtold, J., & Elston, R. 1996, Nature, 382, 234
Driver, S. P., Windhorst, R. A., Phillipps, S., & Bristow, P. D. 1996, ApJ, 461, 525
Eke, V. R., Cole, S., & Frenk, C. S. 1996, MNRAS, 282, 263 (ECF)
Elbaz, D., Arnaud, M., & Böhringer, H. 1995, A&A, 293, 337
Ellingson, E., Yee, H. K. C., Bechtold, J., & Elston, R. 1996, ApJ, 466, L71
Fields, B. D., Kainulainen, K., Olive, K. A., & Thomas, D. 1996, New Astron., 1, 77 (FKOT)
Fields, B. D., & Olive, K. A. 1996, Phys. Lett. B, 368, 103
Fischler, W., Ratra, B., & Susskind, L. 1985, Nucl. Phys. B, 259, 730
Fontana, A., et al. 1996, MNRAS, 279, L27
Francis, P. J., et al. 1996, ApJ, 457, 490
Ganga, K., Page, L., Cheng, E., & Meyer, S. 1994, ApJ, 432, L15
Ganga, K., Ratra, B., Gundersen, J. O., & Sugiyama, N. 1997, ApJ, 484, 7
Ganga, K., Ratra, B., & Sugiyama, N. 1996, ApJ, 461, L61 (GRS)
García-Bellido, J. 1996, Phys. Rev. D, 54, 2473
Garriga, J. 1996, Phys. Rev. D, 54, 4764
Gaztañaga, E. 1995, ApJ, 454, 561
Giavalisco, M., Steidel, C. C., & Macchetto, F. D. 1996, ApJ, 470, 189
Glazebrook, K., Peacock, J. A., Miller, L., & Collins, C. A. 1995, MNRAS, 275, 169
Górski, K. M. 1994, ApJ, 430, L85
———. 1997, in Microwave Background Anisotropies, ed. F. R. Bouchet, R. Gispert, B. Guideron, & J. Tran Thanh Van (Gif-sur-Yvette: Editions Frontieres), 77
Górski, K. M., et al. 1994, ApJ, 430, L89
———. 1996, ApJ, 464, L11 (G96)
Górski, K. M., Ratra, B., Sugiyama, N., & Banday, A. J. 1995, ApJ, 444, L65 (GRSB)
Gott, J. R., III. 1982, Nature, 295, 304
Griffin, G. S., Nguyên, H. T., Peterson, J. B., & Tucker, G. S. 1998, in preparation
Gouda, N., Sugiyama, N., & Sasaki, M. 1991, Prog. Theo. Phys., 85, 1023
Gundersen, J. O., et al. 1995, ApJ, 443, L57
Guth, A. 1981, Phys. Rev. D, 23, 347
Guth, A. H., & Weinberg, E. J. 1983, Nucl. Phys. B, 212, 321
Gwyn, S. D. J., & Hartwick, F. D. A. 1996, ApJ, 468, L77
Hamazaki, T., Sasaki, M., Tanaka, T., & Yamamoto, K. 1996, Phys. Rev. D, 53, 2045
Hancock, S., et al. 1997a, MNRAS, 289, 505
Hancock, S., Rocha, G., Lasenby, A. N., & Gutiérrez, C. M. 1997b, MNRAS, in press
Harrison, E. R. 1970, Phys. Rev. D, 1, 2726
Haslam, C. G. T., et al. 1981, A&A, 100, 209
Hu, W., & Sugiyama, N. 1994, Phys. Rev. D, 50, 627
———. 1995, Phys. Rev. D, 51, 2599
Im, M., Griffiths, R. E., Ratnatunga, K. J., & Sarajedini, V. L. 1996, ApJ, 461, L79
Inman, C. A., et al. 1997, ApJ, 478, L1
Jimenez, R., et al. 1996, MNRAS, 282, 926
Kamionkowski, M., Ratra, B., Spergel, D. N., & Sugiyama, N. 1994, ApJ, 434, L1
Kamionkowski, M., & Spergel, D. N. 1994, ApJ, 432, 7
Kazanas, D. 1980, ApJ, 241, L59
Kennicutt, R. C., Jr., Freedman, W. L., & Mould, J. R. 1995, AJ, 110, 1476
Kitayama, T., & Suto, Y. 1996, ApJ, 469, 480
Kochanek, C. S. 1996, ApJ, 466, 638
Kogut, A., et al. 1996, ApJ, 470, 653
Kolatt, T., & Dekel, A. 1997, ApJ, 479, 592
Liddle, A. R., Lyth, D. H., Roberts, D., & Viana, P. T. P. 1996a, MNRAS, 278, 644 (LLRV)
Liddle, A. R., Lyth, D. H., Viana, P. T. P., & White, M. 1996b, MNRAS, 282, 281
Lilly, S. J., et al. 1995, ApJ, 455, 108
Lim, M. A., et al. 1996, ApJ, 469, L69
Linde, A. 1995, Phys. Lett. B, 351, 99
Linde, A., & Mezhlumian, A. 1995, Phys. Rev. D, 52, 6789
Loveday, J., Efstathiou, G., Maddox, S. J., & Peterson, B. A. 1996, ApJ, 468, 1
Lu, L., Sargent, W. L. W., Womble, D. S., & Barlow, T. A. 1996, ApJ, 457, L1
Luppino, G. A., & Gioia, I. M. 1995, ApJ, 445, L77
Lyth, D. H., & Woszczyna, A. 1995, Phys. Rev. D, 52, 3338
Ma, C.-P., & Bertschinger, E. 1994, ApJ, 434, L5
Maddox, S. J., Efstathiou, G., & Sutherland, W. J. 1996, MNRAS, 283, 1227
Markevitch, M., et al. 1996, ApJ, 456, 437
Masi, S., et al. 1996, ApJ, 463, L47
Moscardini, L., et al. 1996, MNRAS, 282, 384
Netterfield, C. B., et al. 1997, ApJ, 474, 47
Nusser, A., & Davis, M. 1994, ApJ, 421, L1
Ostriker, J. P., & Cen, R. 1996, ApJ, 464, 27
Ostriker, J. P., & Steinhardt, P. J. 1995, Nature, 377, 600
Pascarelle, S. M., et al. 1996, ApJ, 456, L21
Peacock, J. A., & Dodds, S. J. 1994, MNRAS, 267, 1020
Peebles, P. J. E. 1984, ApJ, 284, 439
———. 1993, Principles of Physical Cosmology (Princeton: Princeton Univ. Press)
Peebles, P. J. E., & Yu, J. T. 1970, ApJ, 162, 815
Pelló, R., et al. 1996, A&A, 314, 73
Perlmutter, S., et al. 1996, in Thermonuclear Supernovae, ed. P. Ruiz-Lapuente, R. Canal, & J. Isern (Dordrecht: Kluwer), 749
Piccirillo, L., et al. 1997, ApJ, 475, L77

Platt, S. R., et al. 1997, ApJ, 475, L1
Ratcliffe, A., et al. 1996, MNRAS, 281, L47
Ratra, B. 1991, Phys. Lett. B, 260, 21
Ratra, B., & Peebles, P. J. E. 1994, ApJ, 432, L5 (RP94)
———. 1995, Phys. Rev. D, 52, 1837 (RP95)
Ratra, B., & Quillen, A. 1992, MNRAS, 259, 738
Ratra, B., Sugiyama, N., Banday, A. J., & Górski, K. M. 1997, ApJ, 481, 22
Reach, W. T., Franz, B. A., Kelsall, T., & Weiland, J. L. 1995, in Unveiling the Cosmic Infrared Background, ed. E. Dwek (New York: AIP), 37
Renzini, A., et al. 1996, ApJ, 465, L23
Riess, A. G., Press, W. H., & Kirshner, R. P. 1996, ApJ, 473, 88
Rugers, M., & Hogan, C. J. 1996a, ApJ, 459, L1
———. 1996b, AJ, 111, 2135
Ruiz-Lapuente, P. 1996, ApJ, 465, L83
Salaris, M., Degl'Innocenti, S., & Weiss, A. 1997, ApJ, 479, 665
Sandage, A., et al. 1996, ApJ, 460, L15
Sarkar, S. 1996, Rep. Prog. Phys., 59, 1493
Sasaki, M., & Tanaka, T. 1996, Phys. Rev. D, 54, R4705
Sato, K. 1981a, Phys. Lett. B, 99, 66
———. 1981b, MNRAS, 195, 467
Schaefer, B. E. 1996, ApJ, 460, L19
Scott, P. F., et al. 1996, ApJ, 461, L1
Shaya, E. J., Peebles, P. J. E., & Tully, R. B. 1995, ApJ, 454, 15
Smoot, G., et al. 1992, ApJ, 396, L1
Songaila, A., Cowie, L. L., Hogan, C. J., & Rugers, M. 1994, Nature, 368, 599
Steidel, C. C., et al. 1996, ApJ, 462, L17
Stompor, R. 1994, A&A, 287, 693
———. 1997, in Microwave Background Anisotropies, ed. F. R. Bouchet, R. Gispert, B. Guideron, & J. Tran Thanh Van (Gif-sur-Yvette: Editions Frontieres), 91
Stompor, R., Górski, K. M., & Banday, A. J. 1995, MNRAS, 277, 1225
Sugiyama, N. 1995, ApJS, 100, 281
Sugiyama, N., & Gouda, N. 1992, Prog. Theo. Phys., 88, 803
Sugiyama, N., & Silk, J. 1994, Phys. Rev. Lett., 73, 509
Tadros, H., & Efstathiou, G. 1995, MNRAS, 276, L45
Tanaka, S. T., et al. 1996, ApJ, 468, L81
Tanvir, N. R., Shanks, T., Ferguson, H. C., & Robinson, D. R. T. 1995, Nature, 377, 27
Torres, L. F. B., & Waga, I. 1996, MNRAS, 279, 712
Tucker, G. S., et al. 1997, ApJ, 475, L73
Tytler, D., Fan, X.-M., & Burles, S. 1996, Nature, 381, 207
van den Bergh, S. 1995, Science, 270, 1942
Viana, P. T. P., & Liddle, A. R. 1996, MNRAS, 281, 323 (VL)
Vogt, N. P., et al. 1996, ApJ, 465, L15
Wampler, E. J., et al. 1996, A&A, 316, 33
White, D. A., & Fabian, A. C. 1995, MNRAS, 273, 72
White, S. D. M., Navarro, J. F., Evrard, A. E., & Frenk, C. S. 1993, Nature, 366, 429
Williams, L. L. R., & Lewis, G. F. 1996, MNRAS, 281, L35
Wilson, M. L. 1983, ApJ, 273, 2 (W83)
Wolfe, A. M. 1993, Ann. NY Acad. Sci., 688, 281
Wright, E. L., et al. 1994, ApJ, 420, 1
———. 1996, ApJ, 464, L21
Yamamoto, K., & Bunn, E. F. 1996, ApJ, 464, 8 (YB)
Yamamoto, K., Sasaki, M., & Tanaka, T. 1995, ApJ, 455, 412 (YST)
———. 1996, Phys. Rev. D, 54, 5031
Yee, H. K. C., et al. 1996, AJ, 111, 1783
Zaroubi, S., Dekel, A., Hoffman, Y., & Kolatt, T. 1997, ApJ, in press
Zeldovich, Ya. B. 1972, MNRAS, 160, 1P